WIRELESS POWER TRANSFER TO BIOMEDICAL IMPLANTS

RANGARAJAN JEGADEESAN
(B.E, Electronics and Communications Engineering, Anna Varsity)

A THESIS SUBMITTED FOR THE DEGREE OF
DOCTOR OF PHILOSOPHY

DEPARTMENT OF ELECTRICAL AND COMPUTER ENGINEERING

NATIONAL UNIVERSITY OF SINGAPORE
AUGUST 2013

DECLARATION

I hereby declare that this thesis is my original work and it has been written by me in its entirety.

I have duly acknowledged all the sources of information which have been used in the thesis.

This thesis has also not been submitted for any degree in any university previously

Rangarajan Jegadeesan

15 Aug, 2013

Acknowledgement

I have been blessed with many novel souls who have helped me complete my dissertation. No amount of thanking would do justice to the help and guidance they have provided me over the last four years. I still want to thank them from my heart, for without them my PhD would have lasted for eternity.

I would like to thank my supervisor Dr. Guo Yong Xin for investing faith in me and provide an excellent opportunity to work in his group. His guidance and help over the last four years have stood pillar to my research. He has come out of his way to help me in many occasions outside office hours and I see in him a true well-wisher. My deepest gratitude to him for his influence on me, which has undoubtedly made me a better person, let alone better researcher.

Dr. Je Minkyu has provided me excellent support and guidance in numerous occasions and helped me a great deal with the opportunity to work at Institute of Microelectronics, Agency for Science Technology and Research (A*STAR). I am very thankful to him for his supervision and advice.

I am grateful to Mr. Sing Cheng-Hiong, Madam Guo Lin, Madam Lee Siew and all my lab members who have provided invaluable contribution to my work in this dissertation. Special thanks to Mr. Duan Zhu for his insightful thoughts and discussions which helped me carry out significant experiments. I owe much to Dr. Yen Shih-Cheng, Dr. Nitish V. Thakor and Dr. Eberhart Zrenner for their help to carry out experiments in cadaver head and rat.

I stand humbled by my innumerable friends who have provided enormous support, motivation and most importantly their time-share during my PhD. I am extremely grateful and feel honoured to have shared my best moments during my PhD with ever-lively Dharmesh and Aanand.

I dedicate this thesis to my loving parents, sister, uncle, aunt and cousins who have shaped my life all these years with their unconditional love, moral support, encouragement and wise words.

List of Publications

1. **R. Jegadeesan**, Y. X. Guo, "A study on the inductive power links for implantable biomedical devices", *IEEE International symposium on Antennas and Propagation*, 2010 vol., no., pp.1-4, 11-17 July 2010.
2. Y.X. Guo, Z. Duan, **R. Jegadeesan**, "Inductive wireless power transmission for implantable devices", *IEEE International Workshop on Antenna Technology*, 2011, vol. no., pp.445, 448, 7-9 March 2011.
3. **R. Jegadeesan**, Y.X. Guo, "Evaluation and optimization of high frequency wireless power links," *IEEE International Symposium on Antennas and Propagation (APSURSI)*, 2011, vol., no.,pp.400,403, 3-8 July 2011.
4. **R. Jegadeesan**, Y.X. Guo, M. Je, "Overcoming coil misalignment using magnetic fields of induced currents in wireless power transmission," *IEEE MTT-S International Microwave Symposium Digest (MTT)*, 2012 , vol., no., pp.1,3, 17-22 June 2012.
5. **R. Jegadeesan**, Y.X. Guo, M. Je, "Computing mutual inductance between spatially misaligned coils for wireless power transmission," *IEEE International Symposium on Antennas and Propagation (APSURSI)*, 2012, vol., no., pp.1,2, 8-14 July 2012.
6. Y.X. Guo; **R. Jegadeesan**, "Efficient Inductive Power Transfer for biomedical applications," *IEEE International Workshop on Electromagnetics, Applications and Student Innovation*, 2012, vol. no., pp.1, 2, 6-9 Aug. 2012.
7. **R. Jegadeesan**, Y.X. Guo, "Topology Selection and Efficiency Improvement of Inductive Power Links," *IEEE Transactions on Antennas and Propagation*, vol. 60, no.10, pp.4846, 4854, Oct.2012.
8. **R. Jegadeesan**, Y.X. Guo, X. Rui-Feng, M. Je, "An efficient wireless power link for neural implant," *IEEE International Symposium on Radio-Frequency Integration Technology (RFIT)*, 2012, vol. no., pp.122,124, 21-23 Nov. 2012.
9. **R. Jegadeesan**, Y.X. Guo, M. Je, "Electric Near-Field Coupling for Wireless Power Transfer in Biomedical applications", *IEEE MTT-S*

International Workshop on RF and Wireless Technologies for Biomedical and Health care Applications, Dec.9-11, 2013.

10. **R. Jegadeesan**, Y. X. Guo, M. Je, "Localization of Intermediate coil in a 3-Coil Inductive Power Transfer Link" submitted to *IEEE Transactions on Antennas and Propagation, Nov 4, 2013*

Table of Contents

Abstract

Wireless Power transfer using electric and magnetic near-fields have found their use in a plethora of applications, biomedical implants being one of them. The stringent regulation on size and safety imposed by the biomedical implants necessitates a highly efficient power transfer link design. The added challenges of misalignment and motion artifact very common in biomedical implants need to be addressed as well.

In this dissertation, we present a detailed analysis of near –field (inductive and capacitive) wireless power transfer links and evaluate them for use in biomedical implants. We propose new techniques to improve the power transfer efficiency of transcutaneous links and overcome the challenges posed by the implant application.

We compare and contrast the different resonant topologies in inductive power links and provide selection criteria to choose the right topology based on the link parameters. Power link optimization for maximum power transfer efficiency has been proposed based on the right choice of topology, optimal load and optimal frequency of operation.

We have proposed and evaluated a novel idea to overcome the challenges of misalignment and motion artifacts, very relevant in biomedical implants using passive intermediate coils. Theoretical models for computing power transfer efficiency of misaligned links have been developed and the method to choose the proper placement of the intermediate coil has been presented both qualitatively and quantitatively with experimental results agreeing well with developed models.

Capacitive power transfer links as an attractive alternative to the traditional inductively coupled link for transcutaneous powering of biomedical implants has been proposed. With complete theoretical models and corroborating experimental results in rats, our proposed method of using capacitive coupled links makes a strong claim for its use in biomedical applications.

List of Tables

List of Figures

List of Abbreviations

WPT – Wireless Power Transmission

IPT – Inductive Power Transmission

CPT – Capacitive Power Transmission

RPT – Radiative Power Transmission

PTE – Power Transfer Efficiency

TX coil – Transmitting coil

RX coil – Receiving coil

IX coil – Intermediate coil

TX – Transmitter

RX – Receiver

RF – Radio Frequency

RFID – Radio Frequency Identification

SAR – Specific Absorption Rate

HFSS – High Frequency Structural Simulator

NI – Neural Implant

ADS – Advanced Design System

SS – Series-Series Topology

SP – Series-Parallel Topology

PP – Parallel-Parallel Topology

PS- Parallel-Series Topology

Chapter 1: Introduction

1.1 Introduction to Wireless Power Transmission

Transmission of electric power from one device to another without the use of a direct conductive medium such as wires is termed as Wireless Power Transmission (WPT). WPT can be achieved by creating electric, magnetic or electromagnetic coupling between a device and its counterpart. The device from which the power is transmitted is called the Transmitter (TX) and the device which receives this power and supplies it to the payload is called the Receiver (RX).

1.2 Wireless Power Transmission Methods

Various methods exist through which WPT can be achieved, though the prominent methods are Inductive Power Transmission (IPT), Capacitive Power Transmission (CPT) and Radiated Power Transmission (RPT). The three methods differ in the type of coupling between the TX and RX. IPT uses inductive coupling (mutual inductance between TX and RX), CPT uses capacitive coupling (capacitance between the TX and RX) and RPT uses radiation to transmit power from TX to RX.

1.2.1 Inductive Power Transmission (IPT)

Inductive power Transmission is by far the most prominent method used today to transmit power wirelessly over short distances (few tens of mm). IPT uses the mutual inductance (inductive coupling) between two inductors to transmit power from one to another. Inductive coupling is a well-studied phenomenon and was first proposed by Tesla [1] and has subsequently found use in industrial, robotic and biomedical applications. In IPT, both the TX and RX are inductors. The TX is excited using a time varying current which produces a varying magnetic field. The receiving coil (RX) when placed in this varying magnetic field develops an electric potential across its terminals as per Faraday's law of electromagnetic induction. This electromotive force induced in RX powers the load connected to it thereby enabling wireless power

transmission from TX to RX. Since the power transfer is carried out due to the mutual inductance between the two coils, this type of coupling is termed as inductive coupling. This is a near-field coupling method as there is no radiative component. A simple image of an inductively coupled link is shown in Figure 1-1.

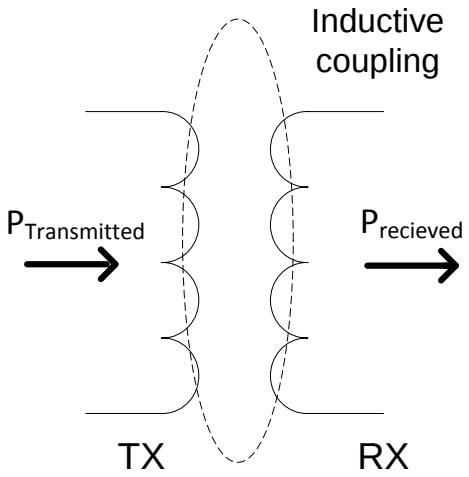

Figure 1-1 Inductive Coupling Scheme

1.2.2 Capacitive Power Transmission (CPT)

Wireless power transmission using capacitive coupling is the simplest method to transfer power wirelessly. It needs fewer components than an IPT system due to the fact that same currents flow through the transmitting and receiving side, thereby eliminating the need for separating tuning circuits at the transmitting side and receiving side. However, wireless power transfer using CPT finds its use in very few applications due its very short range (<10 mm). It is used in very few applications for harnessing specific benefits such as wireless power transfer through metallic interfaces. The CPT uses the capacitive coupling between the TX and RX to transmit power wirelessly. Both TX and RX are metal structures (mostly planar) which together form a capacitor. By using a pair of TX and RX the CPT can be achieved using the scheme shown in Figure 1-2. When TX is powered, the currents are coupled to the RX through the capacitor formed by TX and RX. Two pairs of TX and RX are needed to complete the power transfer loop as can be seen in Figure

1-2. Similar to the IPT method, the CPT uses near-field coupling and the radiation is very minimal, if not absent.

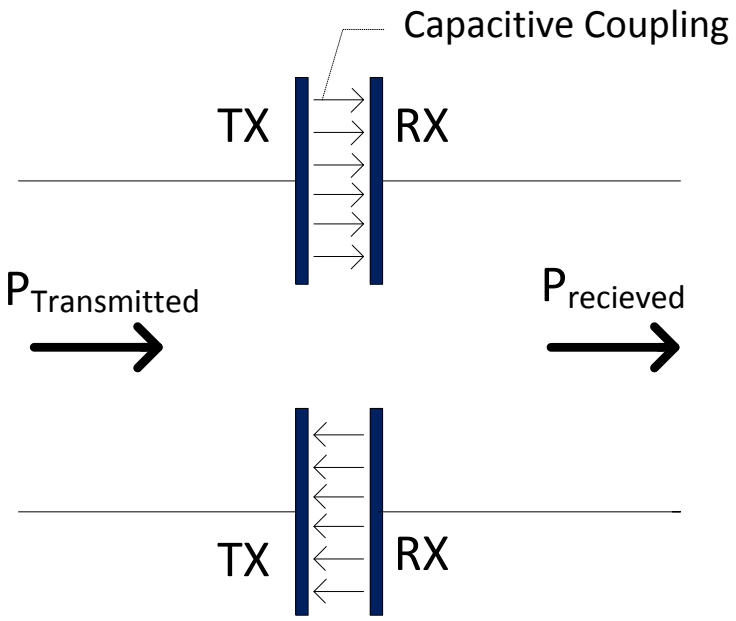

Figure 1-2 Capacitive coupling scheme

1.2.3 Radiative Power Transmission (RPT)

Wireless Power Transmission through radiated waves is known as Radiative Power Transmission (RPT) and it is implemented by simply using a transmitting antenna (TX) and a receiving antenna (RX). The radiations from TX are absorbed by the RX and the power is rectified and fed to the load. Since the radiations travel in all directions and are absorbed by the surroundings, it is the most inefficient method to transfer power wirelessly. The safety standards on levels of power transmission also limit the power transfer capability. However, the longer range provided by the RPT helps power remote devices wirelessly and is used in a few satellite and military applications [10], [14], [18] and [21]. The RPT scheme is shown in Figure 1-3. Both TX and RX are antennas (rectangular patch is shown as example in Figure 1-3) and power radiated from TX is received by RX and is rectified to power the payload. Since electromagnetic wave carries the energy from TX to RX, larger ranges of power transfer are possible than can be achieved using IPT and CPT. RPT is predominantly a far field method as the power is carried via the radiated fields.

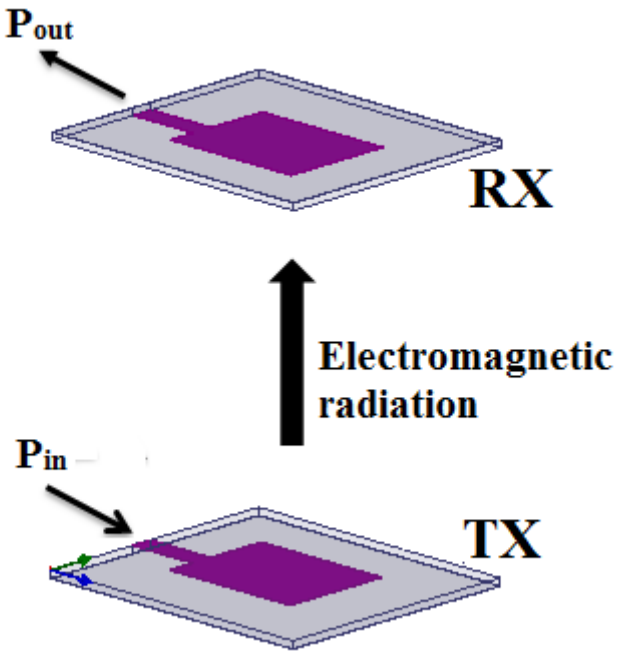

Figure 1-3 Radiative Power Transmission Scheme

1.3 Suitability of WPT schemes to Biomedical implants

Biomedical implants are artificial devices implanted into humans to perform vital functions thereby monitoring or sometimes even replacing faulty organs in the body. Such devices are permanently sealed in biocompatible cases and are powered using rechargeable batteries. Due to the irreplaceable nature of the battery and practical limitations on using wires through skin and tissues, wireless power transfer is used to charge the battery from outside the body and is known as transcutaneous power transmission. Thus powering implants wirelessly provides an aesthetic and convenient means to safely power the implant devices and improves the overall reliability of the device. All the three aforementioned power transfer methods (IPT, CPT and WPT) can be used to power the implant devices. However not all of them are efficient and suitable to the biomedical implant application.

The proper choice of wireless powering method for the biomedical implant application is vital. A look at the field patterns generated by TX provides us important cues about the suitability of the WPT method to the biomedical implant application.

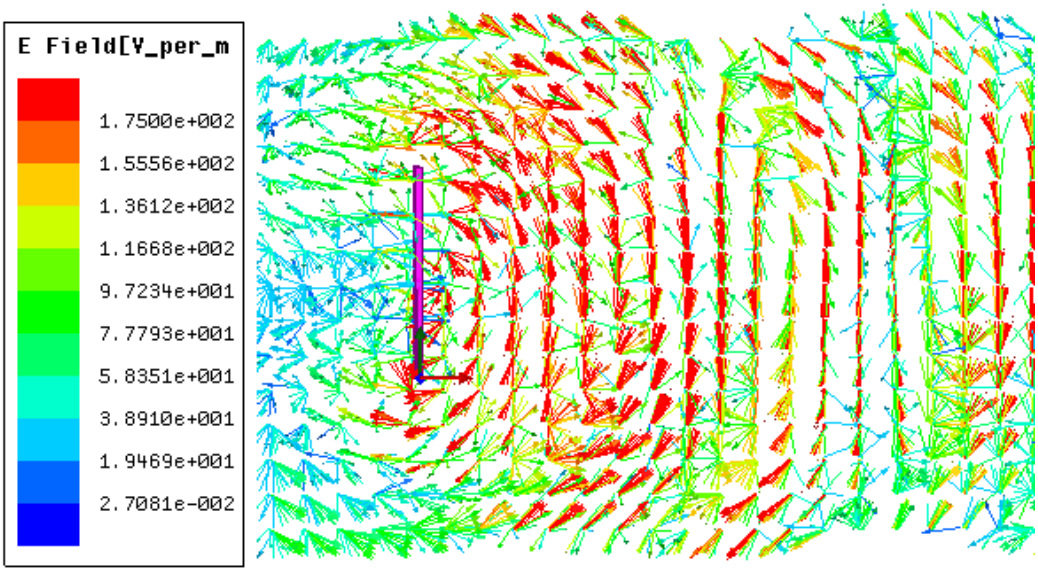

Figure 1-4 Electric Field generated by a patch antenna (12.45 mm X 16 mm, Rogers5880 substrate, 0.8mm thick), when excited at 4.5 GHz and phase = 0.

(The plane of the patch is normal to the plane of the paper.)

First let us consider an RPT system using a patch antenna similar to the one shown in Figure 1-3. The electric field generated by the patch antenna (12.45 mm X 16 mm, 0.8mm thick Rogers's 5880 substrate) with a strip line feed when excited at 4.5 GHz is shown in Figure 1-4. The fields were simulated using High Frequency Signal Simulator (HFSS Version.12). As can be seen, the radiated energy spreads in many directions as the wave travels farther from TX and the wave-front expands out. The radiated energy also leaves the source (TX) irrespective to whether RX is present or not. Hence the portion of power received by the RX is much lesser than the power transmitted at TX making it an inefficient power transfer. Nevertheless, it presents a way to transfer power wirelessly over large separations.

Secondly, let us consider an IPT system with square planar single turn inductors replacing the TX and RX shown in Figure 1-1. The magnetic field generated by a single turn square planar inductor (8mm sides, 0.8mm trace width) on a 0.8mm thick FR4 PCB, when excited at 400 MHz is shown in Figure 1-5.

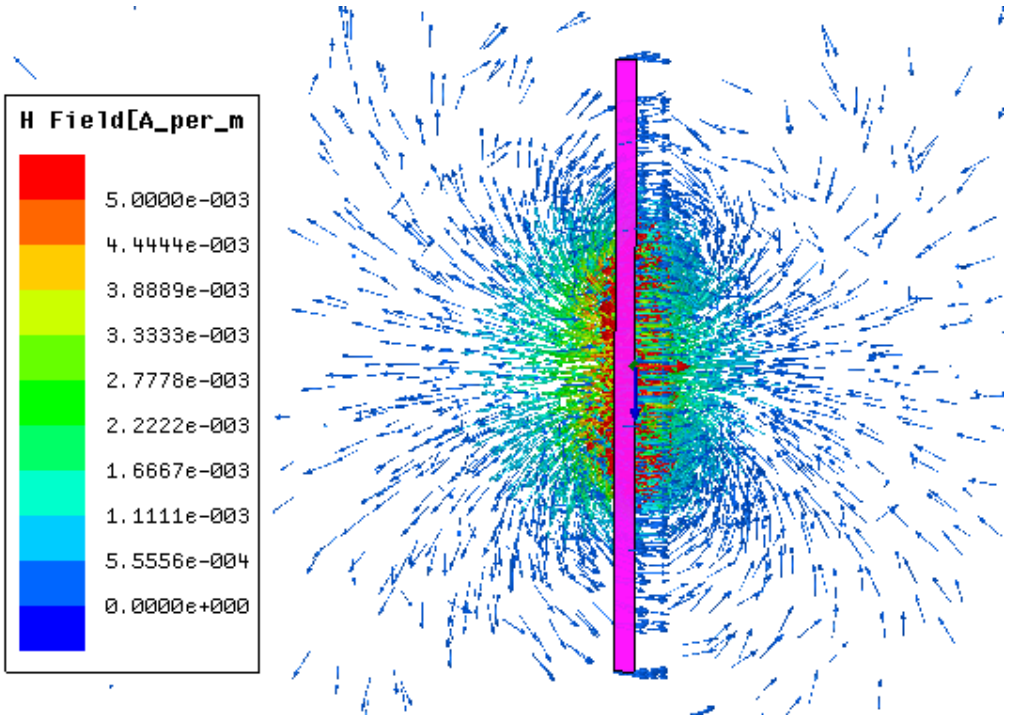

Figure 1-5 Magnetic field generated by a single turn square planar inductor(10mm sides, 0.2mm trace width, 0.8mm thick FR4 substrate) when excited at 400MHz, phase = 0.

(The plane of the coil is normal to the plane of the paper.)

As can be seen, the magnetic field lines are very much confined to the space close to the coil. It has to be mentioned here that the magnetic energy associated with TX stays with it as long as RX is absent. Excluding the coil losses in TX, there is no power wastage in the IPT system as long as RX is absent. When RX is introduced into the magnetic field generated by TX, only then energy is tapped from it. Thus it is more efficient to transfer power using IPT. However due to the confined fields, the RX has to be close to TX to have efficient power transfer and thus the range of operation is limited.

Now let us consider a CPT system with square planar patches replacing the capacitance plates (TX) shown in Figure 1-2. The electric field generated by a pair of 10mmX10mm square patches lying side by side on the same 0.8mm thick FR4 substrate (lateral separation is 5mm) when fed with a 500 MHz signal is shown in Figure 1-6 (Simulated using HFSS Version.12).

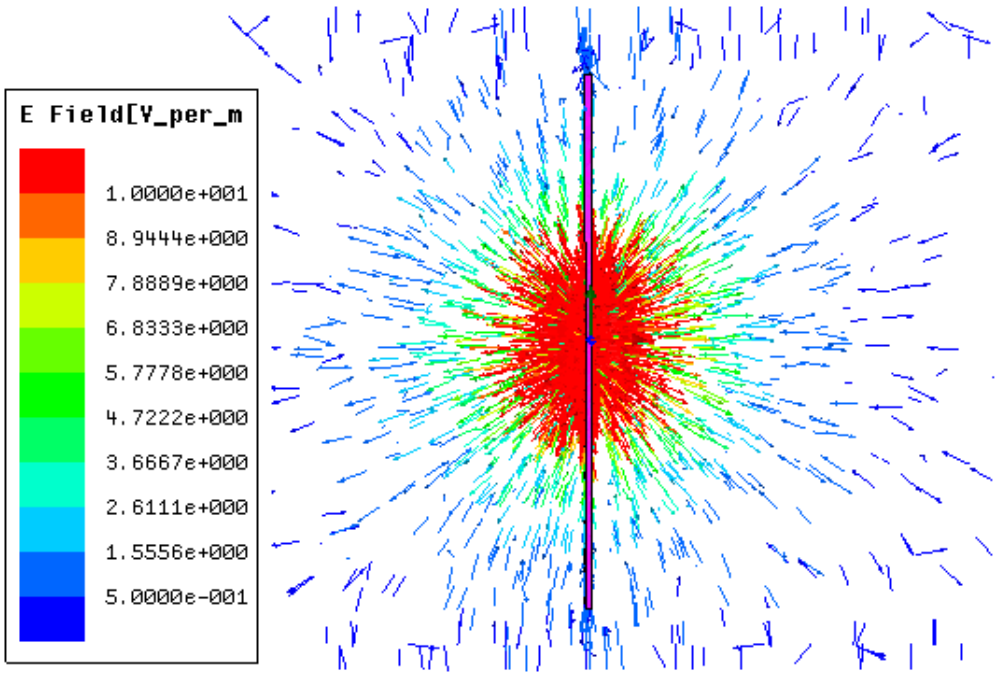

Figure 1-6 Electric field generated by a pair of square patches (10mm X 10mm) built on a 0.8mm thick FR4 substrate , fed by a 500 MHz source, phase=0.

(The plane of the patches is normal to the plane of the paper.)

As can be seen, the fields are very much confined to the patches and the electric energy stays with the source unless another pair of plates (RX) is brought to tap the energy. Thus CPT presents itself as an efficient means of power transfer albeit one limitation that the range has to be very small (due to the confined fields) for seamless operation.

Having looked at the three different power transfer methods, we can gauge the suitability of these methods to biomedical implants based on the application requirements. Most implant devices need power transfer across skin, fat and few tissues with a total range not exceeding few tens of millimetres as have been considered in [39]-[52], [58]-[76] and [80]-[87]. The implant device has a stringent size restriction and demands a small form-factor power transfer system. The losses in the power transfer system cause undesired heating of tissues and lesser battery life (at the TX side), thereby strongly demanding good Power Transfer Efficiency (PTE).

Though RPT can be implemented in a very small form factor, the very low efficiency of power transfer makes it unsuitable for the use in biomedical implants. The design of efficient, high speed (GHz) rectifiers with large power handling capability (100mW) in a small package is another challenging task that adds to the already very low efficiency of power transfer in RPT thereby ruling out its use in biomedical implants. Few works have been reported on using RPT in biomedical implants [94] however with less power transfer capability and has been neglected ever since in favour of the near field IPT method. For small separations, the near- field power transfer method IPT is better posed to transfer power efficiently than the far-field power transfer method RPT. The higher efficiency of power transfer, reasonably small size implementation and lower frequency of operation (when compared with RPT) easily matches the requirements of the biomedical implant application and has been the number one choice for transcutaneous power transmission. The CPT method has not been used in bio-medical implants due to its large area requirement (to get sufficient capacitance) to transfer power without breaching the SAR limits [38] and very short range. However we propose to use CPT for specific biomedical applications with small work around in this dissertation. Going forward, in this thesis we focus on the IPT and CPT methods.

1.4 Background on WPT for biomedical implants

Biomedical implants such as cochlear, retinal, neural and artificial hearts are mostly powered using transcutaneous transformers which use the principle of inductive coupling. The requirements and limitations enforced on the design of WPT links vary with the type of the implant application it addresses. Hence specific design approaches are used for each type of implants.

1.4.1 Early works

Radiative power transfer was one of the foremost methods practically demonstrated in transmitting power wirelessly as shown in early works [1]-[6]. Most of these works were built upon the early idea proposed by Tesla [1]. Later works [7]-[17] on wireless power transmission were mainly limited to

military, aerospace and satellite applications which served as the primary platform for research and development. The commercial use of RPT, even though proposed in [17] for domestic power transmission, was not pragmatic as hazardous levels of power were needed to be radiated using giant antennas. The RPT method evolved a great deal with the invention of integrated circuits and started finding some commercial applications with low levels of power transmission requirement, the biomedical implant being one of them. Power rectifiers were integrated along with the antennas to form a hybrid device known as rectennas, which can directly provide rectified power from incident RF waves [18-31]. Even on- chip antennas were reported in [32] for WPT at 94 GHz. Ambient EM waves (from cell phone towers and TV broadcast signals) could also be used to harvest energy as has been shown in [33-36]. However the power levels obtained using ambient energy harvesting are too low to be able to be used for powering implants. Even very recent work [37] has reported the use of rectennas in implantable applications, however the power transfer capability was limited to 5mW in order to satisfy the SAR regulatory level of 1.6 W/Kg proposed by ANSI/IEEE [38]. Such low power transfer capability has limited the use of RPT in implantable devices. Thus most of the existing works on transcutaneous powering of implants have used IPT as a very capable and reliable substitute to RPT. The very first works on transcutaneous power transmission using IPT was in the early 1960s with main focus on power transfer feasibility across a tissue barrier [39]-[40]. The research was furthered by integrating data transfer to the existing transcutaneous power link thereby providing a completely wireless implanted device [41]. Further research on the use of IPT for transcutaneous powering was done and analysis on resonant tuning, increased power transfer capability, coil miniaturization, usage of magnetic core, transmitter power control, wide band transfer and coupling insensitive power transfer were carried out by various groups from 1965 to 1990 and have been reported in [42] – [52]. These works also benefited other industrial applications such as contactless powering, decentralized manufacturing and electric vehicle charging and have been reported in [53] – [57]. The use of IPT links in three biomedical implant applications namely cardio implant, cochlear implant and neural implant is discussed below.

1.4.2 Cardio implants

Cardio implants are the very first biomedical implant devices that were used in humans to provide vital cardio-vascular functions such as cardiac resynchronisation, heart beat stimulation (artificial pacemaker), cardiac monitoring and defibrillation. Due to the implanted nature of these devices, they are powered in a transcutaneous fashion. Ventricular assist systems and artificial hearts were driven using motors that were powered wirelessly through IPT and were first developed in Pennsylvania State University [58]. Since the motors consume lot of power, the implanted device required more than 20W of power for pumping blood artificially. Such huge power transfer was achieved using very large coils which were also required to overcome the coil misalignment issue. This work was improved by [59] with a pair of concave and convex shaped coils that align to each other mechanically. The possibility of using series resonance in IPT was evaluated in [60] to better the power transfer efficiency. Further improvements on the power transfer front were achieved using coil geometry modification in [61], [64] & [66]. The effect of near-by metals on the IPT system for the cardiac implant is studied and detailed in [62]. Further leakage compensation technique [65] and magnetic core usage ([63] & [68]) were reported for improving IPT in cardiac implant applications. Analysis of currents and heating of the nearby tissues due to the use of IPT for artificial heart systems were reported in [67] and [69]. Dual transmission of power and data for artificial heart was reported in recent work [70] with a total power transfer of 40.8W with series compensation of the transmitting and receiving coils. Ventricular assist device which consumes lesser power (8W) than an artificial heart has been shown to be powered using IPT with a use of high quality factor resonators that improve the power transfer efficiency drastically in [71] and this work remains the bench mark for the wireless power transmission in a cardiac implant device.

1.4.3 Cochlear implants

Cochlear implants help restore hearing ability in humans who suffer from profound deafness by stimulating the acoustic nerve. These devices are implanted deep inside the cochlea and there can as many as 24 electrodes [72]

which are placed on the acoustic nerve. By proper stimulation of the electrodes, a rudimentary perception of speech and music can be achieved. The sound from the environment is picked up by a microphone which then feeds the speech processing engine that drives the electrodes with appropriate signals which will be carried by the acoustic nerve to the brain, where the perception of speech produced. The earliest works [72]-[73] on powering such implanted cochlear stimulator device wirelessly were reported in early 1980s. Up to 4 electrodes were powered in a transcutaneous fashion using resonant tuned inductive coupling and it paved way for complete isolation of the implant device. An improved version of the cochlear implant with transcutaneous transfer of both power and data was demonstrated in [75] using inductive coupling, which by now has become the main stream method for powering implants. The power consumption required by the implant was reported at 45mW with complete wireless data and stimulation functionality. With advancement in CMOS technology and circuits, later works [76-77] redesigned the stimulators and power rectifier units to reduce the overall power consumption of the implant device, thereby reducing the burden on inductive power link and extending the battery life at the external power transmission unit. Recent work [78] provides a glimpse into the use of MEMS based energy harvesters to power cochlear implants. Latest works on cochlear implants [79] and [80] have further focussed on reducing the power consumption on the stimulator by using energy recycling and improving the overall design of the implant using redesigned electrode placement respectively with power levels less than 15mW required for proper operation of the device.

1.4.4 Neural implants

Neural implants are used to stimulate nerves, record nerve/brain signals and control neural prosthesis. Neural implant devices are classified into two types, the recording type and the stimulating type. The neural recording systems acquire the complex action potential generated by the nerves and they mainly comprise of a neural electrode to pick up and a low noise amplifier to amplify the signals. The neural stimulating system will comprise of the stimulating

electrodes and a charge balanced current driver to drive current to the electrodes and consumers more power than a recording system. The earliest neural implant devices to adopt the IPT based wireless power transmission systems are reported in [81] and [82]. Improvements were made in the electrode, amplifier design and back channel telemetry to reduce the overall power consumption of the implant device [83] - [85]. The various aspects of inductively powering neural implant devices were first analysed and a design guide for transcutaneous powering of implant devices for neural implant was first reported in [86]. A completely new approach to harvest energy from the chemical processes in human body is reported in [87]. However the power harvested is not sufficient enough to power a complete neural implant with back channel telemetry. The first demonstration of a completely implanted multi-channel neural stimulator with transcutaneous power and data transfer is presented in [88]. The power consumption was less than 50 mW at the implant side to drive 64 electrode sites with data signals transferred at the rate of 2.5Mb/s. The power consumption for the neural recording system was further lowered by use of ultra-low power neural amplifiers, impedance modulation based telemetry, selective spike transmission, analog/digital data compression and time multiplexing of operational amplifiers as shown in [89]-[90] and [92] . The effect of packaging the neural recording device and long term stability and longevity of the implant device in tissue environment is studied and detailed in [91] & [93]. Integrating the implant antenna on the flexible substrate for transcutaneous power transmission in neural implant is reported in [94] with on chip RF- DC conversion at 400MHz. The power transfer capability in this method was limited to 21 mW due to the inefficiency inherent in RPT. Recent works are looking at passive antennas implanted on the nerve with back scattering signals carrying the nerve potentials [95]. Though no animal testing results are available, a case for such neural recording systems has been made. A completely low power neural recording system with wireless power transfer has been reported in [96] and consumes power as low as 6mW. This work remains as the bench mark for neural recording systems till date.

Similarly IPT for retinal implants have also been reported in many works [97]-[100]. Recent work [101] has reported the usage of four coils for wireless power transfer to the retinal implant. Summarising, from the existing literature it is well documented that the IPT links are predominantly used in biomedical implant applications for transcutaneous powering. The power requirement and size of the implant devices are shown in Table 1-1

Implant	Operating Power	Range	Implant coil dimension	method
Cardio	15mW – 20W*	10mm - 25mm	<400 mm^2	IPT
Cochlear	<15mW	10mm - 25mm	<100 mm^2	IPT
Neural	<20mW	5mm - 25mm	<100 mm^2	IPT
Retinal	<50mW	20mm - 25mm	<64 mm^2	IPT

Table 1-1 Summary of the biomedical implant requirements from existing works [39] – [101]

1.5 Research Objective

Almost all of the biomedical implants today use inductively coupled links to transfer power wirelessly. Out of the many works that report IPT for biomedical implant application [39]-[52] and [58]-[101], only a hand few of them ([41], [49], [51], [61], [70], [73] and [101]) have focussed on optimizing the power link. Recent works on IPT link optimisation [110], [111] and [122] have focussed on maximising the quality factor of the coils at a given frequency of operation and using high Q coils to overcome the loading of TX coil. Since there is the option to choose the topology of IPT link, its frequency of operation and matching load, we see that the optimization carried out in these works have definite scope for improvement. The PTE which is the key metric in IPT links can be definitely improved if further optimizations are

carried and we proceed in that direction to obtain key results that will be presented in this thesis. The other main issues with coil misalignment [129] and motion artifacts which are unavoidable in biomedical implants have not been addressed in a satisfactory fashion. Works like [59] resort to mechanical design to overcome misalignment at the cost of space and aesthetics. We focus on addressing these two key issues for better usability of IPT in biomedical implants. Hence we adhere to two key objectives shown below.

A. To improve the PTE of inductively coupled WPT links and overcome the challenges posed by the biomedical implant application.

B. To analyse and propose alternative method (CPT) for efficiently powering biomedical implants.

1.6 Original Contributions

The original contributions that will be presented in this dissertation are listed below

A. Complete analysis of the IPT links with series and parallel resonant topologies and accurate closed form expressions for PTE (both resonant and non-resonant) are derived and verified experimentally. The Concept of boundary frequency that separates the series and parallel resonant topologies in IPT has been identified, presented and verified experimentally

B. Proposal has been made to use optimal load and frequency to achieve the ultimate limit on PTE. The closed form expressions for optimal load and maximum PTE are derived and verified experimentally. Step by step procedure to maximize the PTE between two coils is presented with an example.

C. Proposal has been made to use a passive intermediate coil to overcome the issue of coil misalignment and motion artifact in transcutaneous power links used for biomedical implants. Complete modelling of the IPT link with intermediate coil is presented with closed form expression for PTE which is verified experimentally

D. Numerical method for computing the mutual inductance between two coils that have both linear and angular misalignment is developed. A method to position the intermediate coil optimally for PTE improvement based on the root locus charts is shown.

E. Proposal to use CPT links for beneath-the-skin implant application is made. Modeling of CPT links with closed form expressions for PTE based on physical link dimensions and inclusion of tissue losses has been done. The presented results are verified experimentally.

1.7 Organisation of the Thesis

Chapter 1 gives a brief overview of the wireless power transfer methods, their suitability for use in biomedical implants and the scope & objectives of the work that will be presented in this thesis. Chapter 2 provides a complete analysis of the IPT method and presents ways to maximize the PTE. Newer link designs using the research findings are compared with existing works. Chapter 3 presents a novel IPT link design method to overcome misalignment and motion artifact issues which contribute to the poor performance of transcutaneous power links with a theoretical model that is verified using experimental results. Chapter 4 discusses the CPT method and proposes its possible use in biomedical implant. Chapter 5 concludes the research work presented in this thesis and the suggestions for furthering this research has been made.

Chapter 2: Maximizing efficiency of inductive power transfer links

2.1 Introduction to WPT using inductive power transmission

Inductive power transfer is being used in numerous applications for transferring power wirelessly as has been discussed earlier. Biomedical applications such as cochlear, neural, cardiac and retinal implants use inductive coupling for transferring power wirelessly and numerous works [39-99] have reported their use. Electric vehicles [56] & [102], industrial systems [53], [55] & [103], lighting [104] and robotics [54] are other domains where inductive power transfer has become a common phenomenon. In applications such as biomedical implants, the inductive links are loosely coupled owing to the large separation between the coils and the presence of tissues. The sizes of the coils are limited by the strict form factor requirements for medical implants. However in applications such as wireless chargers for mobile devices, the devices are placed on a charging pad/console to provide better coupling. Also the size constraints are liberal as compared with biomedical implants.

Inductive links are thus designed for a variety of applications each with a different set of requirements (both physical and electrical) and the design of such inductive power links requires diligent analysis and optimization that caters to specific application needs. To be specific, the biomedical implant application demands far more stringent norms on the design of the power transfer link that the design has to be meticulously thought out. In this chapter we present the design methodology behind efficient wireless power transfer based on a detailed analysis.

The main parameter that quantifies an inductive power link is its PTE and it is one of the main design objectives. The efficiency can be improved by using magnetic resonant technique in the receiving coil and was first proposed by Tesla [1]. From the plethora of existing literatures on design and optimization of wireless inductive power links, we find that almost all of them use the shunt

resonant technique to transfer power efficiently and most of the design and optimization efforts have been directed towards this method.

The shunt resonant method provides a larger voltage swing that aids the rectifier circuitry. The series resonant method provides more current than voltage and hence places more design constraint on the rectifier circuitry. This justifies the predominant use of shunt resonant method. Matching networks can be used to overcome this drawback in series resonant circuit. However, it brings extra cost, space and power loss in the network. It is difficult to afford space for matching networks in applications such as biomedical implants which have stringent size norms though there are many other applications where additional space is not a real issue. If at all the series resonant method has to be adopted for biomedical implants, it should present some valiant advantages over the shunt method to trade for the cost and space requirements.

We analyse the series and shunt resonant methods generically to draw comparison between the two and identify any such advantages. We identified that the power transfer efficiency of both the methods bettered each other in a range of frequencies in which the link is operated. In fact there is a frequency boundary between the two methods where each one is dominant. We call this frequency the cross over frequency (f_c) and is shown to be

$$f_c = \frac{R_l}{2\pi L_s}\left(\sqrt{1 - \frac{k^2 L_p R_s}{L_s R_p}}\right) \qquad \textbf{(2.1)}$$

Where R_l is the load, L_s/L_p is the secondary/primary inductance, R_s/R_p are the effective loss resistance of the secondary/primary coils. The series resonant method has a better power transfer efficiency than its shunt counterpart when the frequency of operation is above f_c and vice versa. The predominant use of low frequency of operation (at most in the MHz range) in wireless power transfer has been favouring the shunt resonant method consistent with its ubiquitous use. With recent advancements in the study of biomedical implants,

it has been proved that it is safer and more efficient to transfer power at the sub GHz to low GHz range [105-106] and it opens up the possibility of using series resonant method as it can provide a better PTE than its shunt counterpart at high frequencies. In fact the series resonant method has some inherent advantages like better response to fluctuations in coupling coefficient and the ability to operate with smaller loads (suitable for RF circuits matched to 50 ohm) as will be shown later from the analysis.

At this juncture, there are now the possibilities of two methods which can be used for WPT using inductive coupling, each with this own advantages and disadvantages. There is a clear need to identify which method to resort to, given an application requirement. This should be seen in the light of the fact that the load, frequency of operation, and the size of the coils are different for various applications, not to mention the varied methods of inductor realization. We address this problem by devising a method to identify the apt resonant method based on a detailed analysis. We resort to analysing the inductive links using an equivalent circuit model of inductors thereby making the results applicable to most inductor realizations and is explained in later section. We use the results of our analysis to identify which method (or topology as we will refer to from here on) to use for a given power link (frequency of operation, load and coils are given) based on the efficiency of operation. We identify the frequency range in which each topology can be used and verify it experimentally using a set of planar coils fabricated on a PCB. We also address the misconception behind the use of resonant tuning in the context of wireless power links and identify its limitations. The reasoning behind the anomaly in certain cases where resonant tuning is not optimal has been provided both theoretically and verified using simulations from HFSS & ADS.

We further our research to identifying the optimal load and optimal frequency of operation for a given link thereby answering the ultimate question, "Given a pair of coils and their orientation in space, is there a maximum efficiency of power transfer from one coil structure to another across all loads, frequency of operation and types of resonance. If so how can it be achieved?" This result can go a long way in improving the efficiency of existing and new power

transfer links by adopting the concept of optimal load, optimal frequency of operation and dominant type of resonant tuning. We show using an example how to arrive at the maximum efficiency of power transfer and verify the results using simulation results from HFSS.

2.2 Inductive Power Transfer Topologies

Inductive coupled links use mutual inductance between the primary and secondary coils to transfer power.

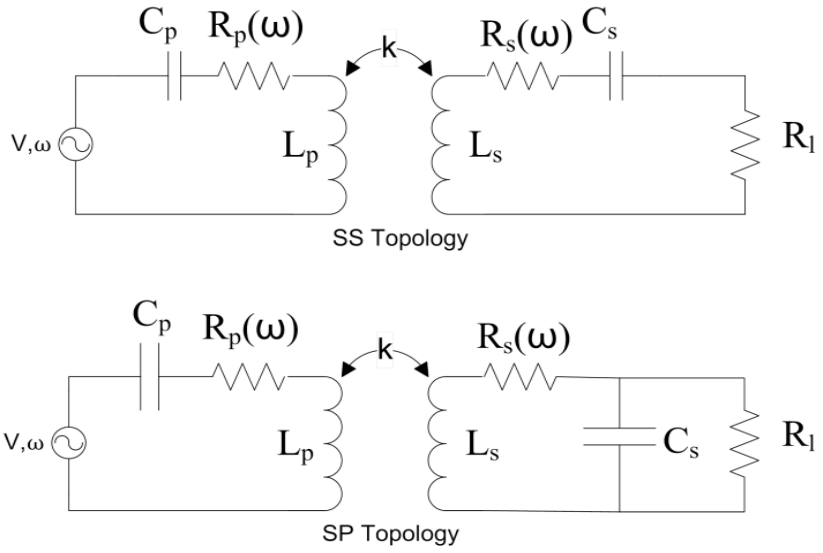

Figure 2-1 The SS and SP topologies used in IPT

The efficiency of the power transfer and the magnitude of the power transferred to the load can be improved using resonant tuning [107-113] and matching techniques [108] at the primary and secondary respectively. Based on the type of resonance (series/parallel) used in the secondary side and the type of compensation (series/parallel) used in the primary side, four different topologies can be formulated. For convenience, the four topologies can be represented as SS/SP/PS/PP, where the first alphabet denotes the type of compensation in the primary side and the second alphabet denotes the type of resonance used in the secondary side. It should also be mentioned that the type of resonance in the secondary alone influences the power transfer efficiency irrespective of the type of the primary compensation used and has been shown in our previous work [114]. Hence we will analyse the SS and SP topology

alone as shown in Figure 2-1 and the results also apply to PS and PP topology respectively.

2.3 Power Transfer Efficiency of Inductively coupled link

The power transferred from the primary side is dissipated in the primary and secondary coil and the rest of the power is delivered to the load. The ratio of power delivered to the load to the total power input to the primary coil is defined as the Power Transfer Efficiency (PTE). In [107-108], transformer topologies are compared without considering the effect of secondary coil loss in the effective loading of primary side. Thus the result pertain only to transformers and does not hold true for either applications that use coils with low quality factors or when the load is sufficiently small.

$$Z_r^{SS} = \frac{\omega^4 k^2 L_p L_s C_s^2 (R_s(\omega) + R_l)}{\omega^2 C_s^2 (R_s(\omega) + R_l)^2 + (1 - \omega^2 L_s C_s)^2} + j\frac{(1 - \omega^2 L_s C_s)\omega^3 k^2 L_p L_s C_s}{\omega^2 C_s^2 (R_s(\omega) + R_l)^2 + (1 - \omega^2 L_s C_s)^2} \quad \textbf{(2.2)}$$

The power transfer efficiency can be computed by modelling the secondary side as an equivalent load for the primary side and using the principle of power sharing. The secondary side can be modelled as reflected impedance on the primary side for the purpose of our analysis. The secondary impedance as reflected to the primary side can be shown as in (2.2) and (2.3).

$$Z_r^{SP} = \frac{\omega^2 k^2 L_s L_p [R_l + R_s(\omega) + \omega^2 R_l^2 C_s^2 R_s(\omega)]}{[R_s(\omega) + R_l(1 - \omega^2 L_s C_s)]^2 + [\omega L_s + \omega R_l C_s R_s(\omega)]^2} + j\frac{\omega^3 k^2 L_s L_p [C_s R_l^2 (1 - \omega^2 L_s C_s) - L_s]}{[R_s(\omega) + R_l(1 - \omega^2 L_s C_s)]^2 + [\omega L_s + \omega R_l C_s R_s(\omega)]^2} \quad \textbf{(2.3)}$$

Based on the principle of power sharing, the total PTE of the two topologies can be computed as

$$\eta_t^{SS} = \left\{1 + \frac{R_s(\omega)}{R_l} + \frac{R_p(\omega)}{k^2 L_p R_l}\left\{L_s + \left[\frac{\left(R_l + R_s(\omega)\right)^2}{L_s} - \frac{2}{C_s}\right]\frac{1}{\omega^2} + \left(\frac{1}{L_s C_s^2}\right)\frac{1}{\omega^4}\right\}\right\}^{-1} \quad \textbf{(2.4)}$$

$$\eta_t^{SP} = \left\{1 + \frac{R_s(\omega)}{R_l} + \omega^2 R_l\, R_s(\omega) C_s^2 + \frac{R_p(\omega)}{k^2 L_p L_s R_l}\left\{\left[\frac{(1 - \omega^2 L_s C_s) R_l + R_s(\omega)}{\omega}\right]^2 + \left[L_s + R_l\, C_s R_s(\omega)\right]^2\right\}\right\}^{-1} \quad \textbf{(2.5)}$$

For now we will assume the fact that resonance maximizes efficiency of inductive power links as followed in [109-113] and derive the efficiency expression under resonance conditions. We will validate this assumption and in fact identify cases where this assumption fails in the next section. We can show that under resonant tuning conditions, the efficiency expressions reduce to

$$\eta_{t,max}^{SS} = \frac{1}{1 + \frac{R_s(\omega)}{R_l} + \frac{R_p(\omega)\left(R_l + R_s(\omega)\right)^2}{k^2 L_p L_s \omega^2 R_l}} \quad \textbf{(2.6)}$$

$$\eta_{t,max}^{SP} = \left\{1 + \frac{R_s(\omega)}{R_l} + \frac{R_l\, R_s(\omega)}{L_s^2 \omega^2} + \frac{R_p(\omega)}{k^2 L_p L_s R_l}\left\{\left[\frac{R_s(\omega)}{\omega}\right]^2 + \left[L_s + \frac{R_l\, R_s(\omega)}{L_s \omega^2}\right]^2\right\}\right\}^{-1} \quad \textbf{(2.7)}$$

2.4 Experimental Verification

We chose to fabricate square planar inductors (Figure 2-2) on PCB to verify the efficiency expressions experimentally as it is cheapest and quickest way to realize inductors. The geometry of the fabricated inductors is shown in Table 2-1.

	Primary Coil	Secondary Coil
Number of turns	20	11
Internal diameter	10 mm	10 mm
External diameter	49 mm	20.4 mm
Width of trace	0.5 mm	0.2 mm
Pitch of the spiral	1 mm	0.5 mm
L effective	12.8 µH	2.84 µH
R effective	4.47 Ω	2.80 Ω
Q Factor	53.9	19.11
Coupling (k)	0.173	

Table 2-1 Geometry and measured parameters (at 3MHz) of the coil used to validate the analysis

The values of the effective inductance and series resistance of the coils were extracted from the measured one-port S parameter using the network analyzer (HP8753D). The two coils were then stacked together and separated by a distance of 10 mm using spacers as shown in Figure 2-3. The coupling coefficient was measured using the two-port S parameters obtained from the aligned coil system. The values of the parameters extracted from measurement

at 3MHz are also provided in Table 2-1. The efficiency expressions were computed using MATLAB for the measured parameters for frequencies from 1 MHz to 7 MHz and two different loads (50 ohm, 100 ohm) using (2.6) & (2.7). The efficiency values in (2.6) & (2.7) were actually evaluated by substituting the measured parameters (Self-inductance, resistance and mutual inductance) of the coil which were obtained using a network analyzer (HP8753D) as shown in Table 2-1. To verify the calculated efficiencies experimentally, the same set up shown in Figure 2-3 was used and the primary side was powered using an analog signal generator (Agilent E8257D) and the secondary side was connected to an oscilloscope (HP 54616C). The power drawn from the source and power delivered to the load were measured at tuned resonant frequencies from 1 MHz to 7 MHz after accounting for the input reflection at the primary side.

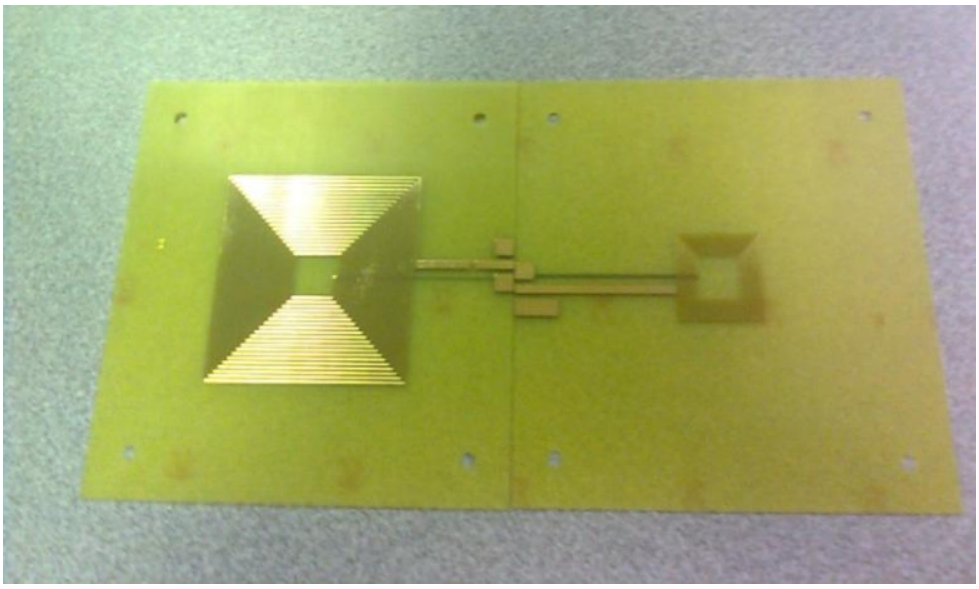

Figure 2-2 The square planar inductors fabricated on PCB used in the experimental verification of the PTE of IPT system

The efficiency was then computed as a ratio of received power to the transmitted power. The experiment was repeated for two different loads (50 ohm and 100 ohm). The computed efficiency (specified as MATLAB) is compared with the measured efficiency values. From the graphs shown in Figure 2-4 and Figure 2-5, it can be seen that the results agree well with each other. The very accurate prediction of the efficiency is due to the usage of

measured values of the coils in evaluating (2.6) & (2.7) which were in-turn derived without making approximations.

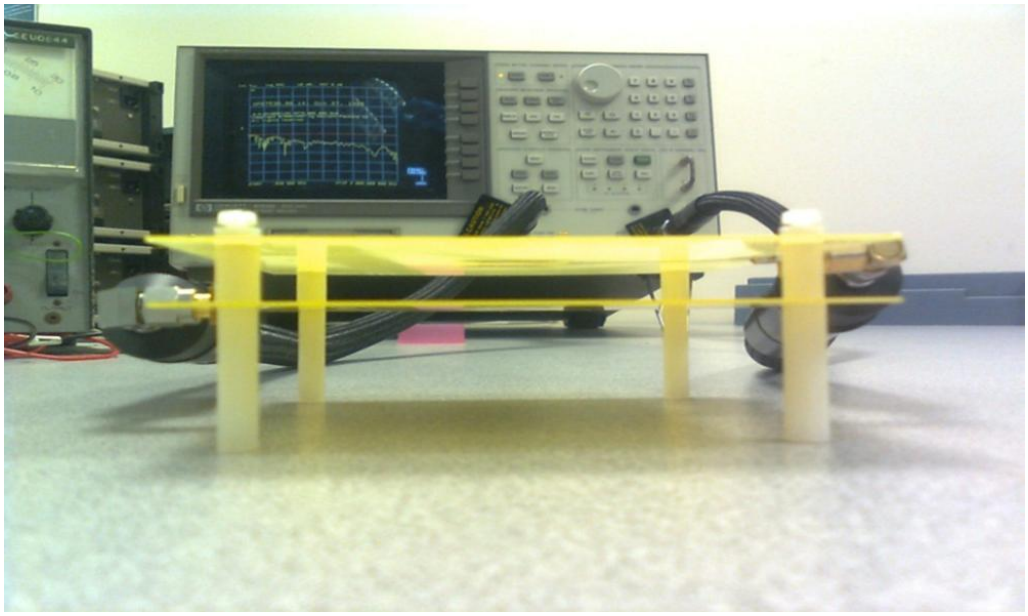

Figure 2-3 Experimental set up used for PTE measurement.

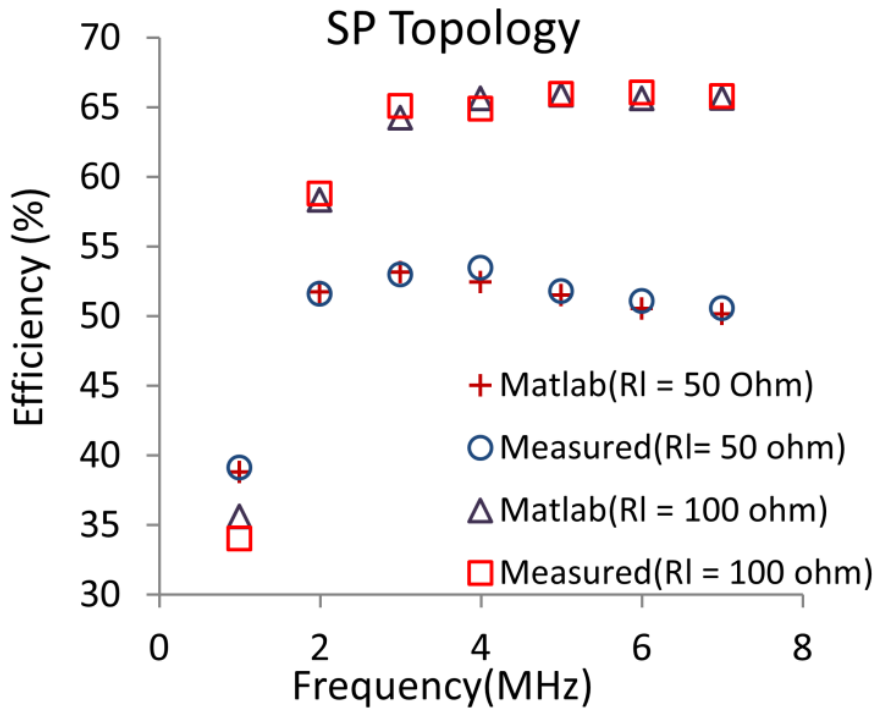

Figure 2-4 Comparison of power transfer efficiency between measurements and calculation for SP topology

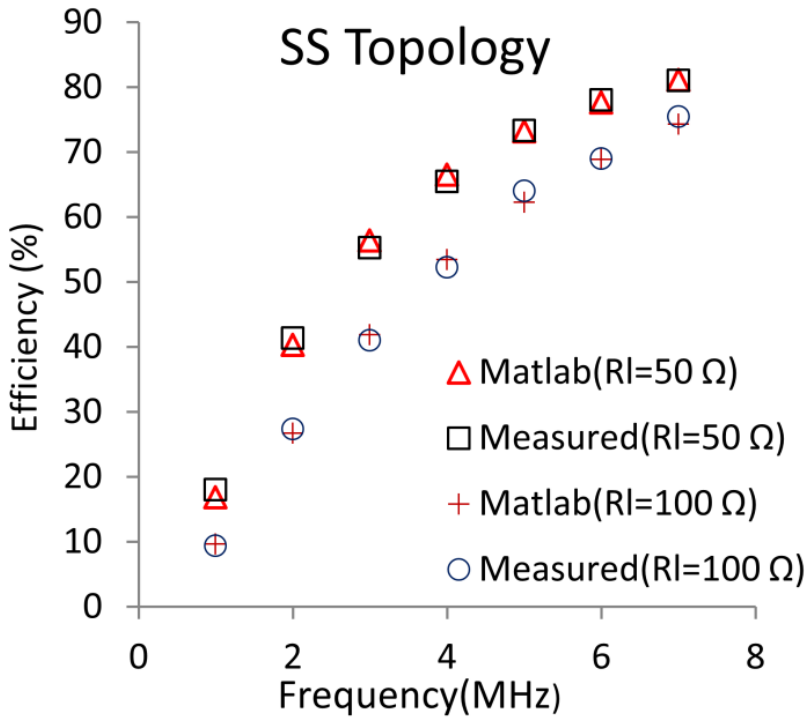

Figure 2-5 Comparison of efficiency between measurements and calculation for SS topology tuned for maximum efficiency

2.5 Limitations of Resonant Tuning

We go back to the topic of resonant tuning which we used to maximize the efficiency in the previous section. The use of resonant tuning has been misunderstood in the context of inductive power links. Many prior works [109-113] take for granted that resonance is an absolute necessity to maximize power efficiency. In fact this assumption is valid for almost all wireless power links and might never fail for most applications. Though it can be considered as a parasitic case in the context of wireless power links, it is nevertheless required to point out the possibility of a non-resonant link operating more efficiently than the resonant one when the coupling is very strong and the parallel resonant topology is used.

We explain this anomaly by referring to (2.2) and (2.3) for the reflected impedance of the secondary side on the primary side of the link. We see that for SS topology the imaginary part of the reflected impedance is zero at resonance irrespective of the coupling coefficient. This is not true with the SP topology as it presents a capacitive load to the primary side at resonance and it

vanishes only under low coupling conditions (typically k<0.25). Thus the SP topology under strong coupling conditions requires a coupling dependent tuning method and resonance does not clearly maximize the power transfer efficiency.

To explain this mathematically and identify the criterion for maximum efficiency in this scenario, we maximize the efficiency expressions with respective to the secondary capacitor Cs. We obtain the capacitances that maximize the efficiency for the SS and SP topology as follows

$$C_S^{SS} = \frac{1}{\omega^2 L_s} \tag{2.8}$$

$$C_S^{SP} = \frac{1}{\omega R_s(\omega)\left(k^2 Q_p + Q_s + Q_s^{-1}\right)} \tag{2.9}$$

Where Q_p and Q_s are the quality factors of the primary and secondary coils at the frequency of operation defined by

$$Q_p = \frac{\omega L_p}{R_p} \tag{2.10}$$

$$Q_s = \frac{\omega L_s}{R_s} \tag{2.11}$$

It is clearly evident from (2.8) and (2.9) that SS topology has maximum efficiency at resonance irrespective of the nature of coupling and the SP topology has maximum efficiency when the secondary side is non-resonating. When the coupling becomes weak, the expression in (2.9) reduces to the resonance mode of operation.

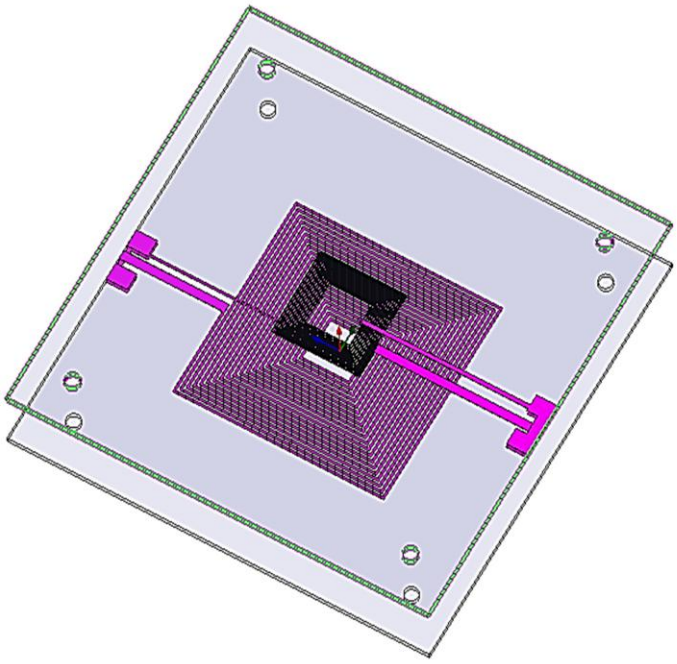

Figure 2-6 Simulation set in HFSS

We simulated two planar spiral inductors as shown in Figure 2-6 using HFSS. We extracted the inductance and resistance of the coils at different frequencies and fed them into ADS (circuit model) which carried out the efficiency calculations for the two choices of tuning capacitors as given in (2.8) and (2.9) to obtain the graph shown in Figure 2-7. It can be seen from Figure 2-7 that non resonant tuning method as proposed by (2.9) has a better efficiency than the shunt resonant tuning method. The improvement in efficiency from shunt resonant to shunt non resonant mode is significant only when the coupling is strong ($k > 0.25$). Most of the inductive power transfer links have coupling coefficients typically less than 0.25 and hence for all practical purposes we can assume that the resonant tuning will maximize efficiency which justifies the ubiquitous use of resonant tuning in today's power links. Thus it is required to keep in mind for future applications that the non-resonant tuning will be able to provide better efficiency than the resonant tuning method for tightly coupled circuits.

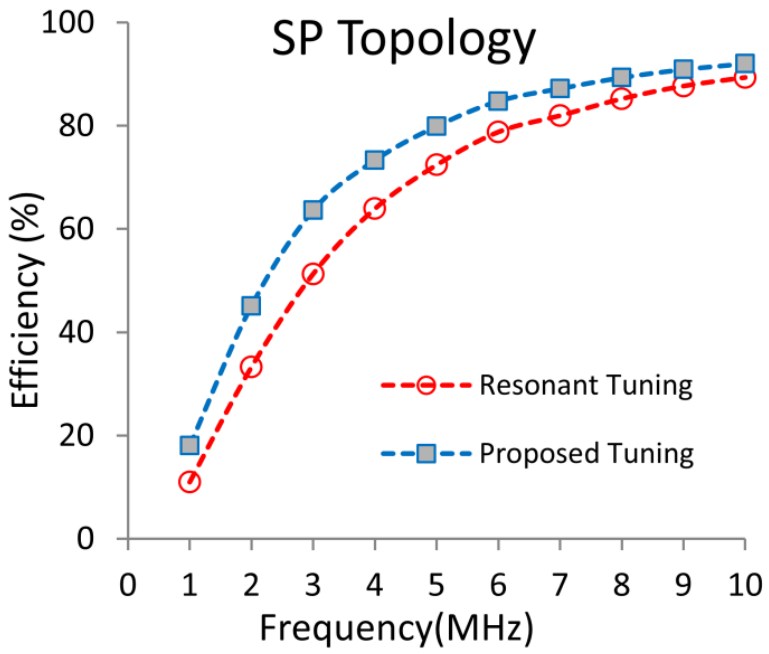

Figure 2-7 Comparison of efficiencies obtained using resonant tuning and the proposed tuning method simulated using HFSS and ADS.

2.6 Topology Selection for fixed load

For a given application, there is a need to identify which topology operates more efficiently. We compare the efficiencies of the series and parallel resonant power transfer methods in this section to identify under what conditions does one method out performs the other. We infer the following from the analysis. The efficiency increases sharply with frequency for the SS topology. This is justified from (2.6 as the dominant term in the denominator reduces as the square of frequency. For the SP topology, the efficiency has a local maximum with respect to frequency and hence the efficiency dies down at higher frequencies. From these two inferences, we conjuncture the existence of frequency boundary between the topologies, that specifies which topology outperforms the other at a particular frequency of interest.

2.7 Cross over Frequency (f_c)

By comparing the maximum efficiency of the SS and SP topology for the same choice of coils, it can be shown that the frequency at which both the topologies have the same efficiency is given by

$$f_c = \frac{R_l}{2\pi L_s}\left(\sqrt{1 - \frac{k^2 L_p R_s}{L_s R_p}}\right)$$

(2.12)

We call this the cross over frequency (f_c). When the operating frequency is larger than the cross over frequency (f_c), the SS topology provides a higher efficiency than the SP topology and vice versa. It is to be noted that the R_p and R_s that are used in (2.12 are frequency dependent quantities. However the ratio of R_p and R_s does not change much with frequency and hence the ratio can be theoretically evaluated at any standard frequency and substituted in (2.12) to find the cross over frequency.

$$f_c = \frac{R_l}{2\pi L_s}$$

(2.13)

Thus we can infer from (2.12) that series resonant method is more efficient for smaller loads and high frequency of operation whereas parallel resonant method works well for larger loads and low frequency of operation. When the inductive link is loosely coupled (k<<1), the cross over frequency reduces to the expression provided in [107]. The cross over frequency in (2.12) applies only to a special case of loosely coupled coils and is not independent of the coupling coefficient *k* as claimed in that literature. In order to verify (2.12), the two fabricated planar square spiral coils shown in Figure 2-2 were characterized to obtain their inductance, series resistance and coupling at a fixed separation of 10 mm. We then made measurements on efficiency after using proper tuning circuits at the secondary side by following the same procedure as has been mentioned in previous section. The frequency was swept from 1 MHz to 8 MHz for two different loads (50 ohm and 100 ohm) to obtain the cross over frequency. The cross over frequency was then obtained by modelling the inductive link in HFSS and the abstracted parameters are fed into its equivalent circuit model in ADS to obtain the simulated efficiencies. The cross-over frequency was then calculated using the theoretical model [115-117] for inductors on PCB using MATLAB. Figure 2-8 shows the

comparison of cross over frequencies for two different loads. It can be seen the results correlate well with each other.

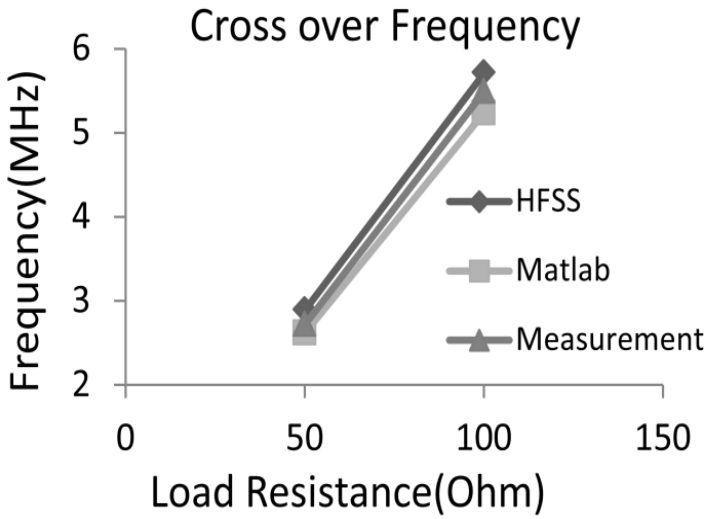

Figure 2-8 Experimental verification of the expression for cross over frequency for two different loads

Thus given a pair of inductors, the most efficient topology can be chosen by computing the cross over frequency and comparing it with the frequency of operation. The predominant use of low frequency of operation in implants had favoured the SP topology and hence the SS topology has not been considered so far as a viable method to transfer power in earlier works. With the push towards high frequency operation in wireless power links, it is imperative that SS topology can provide better efficient links in the foreseeable future. Also from (2.6), we can see that for the SS topology with smaller loads the dominant term in the denominator is the second term and hence the efficiency fluctuations with respect to changes in coupling coefficient are smaller than its parallel counterpart.

2.8 Optimal load

The concept of cross over frequency was presented in the previous section and it is noticeable that the choice of topology depends on the load impedance used. In application where the load impedance is fixed and matching networks cannot be implemented (due to cost/space constraints), the cross over frequency presents a very simple method to identify the dominant topology.

However in applications where there is freedom to choose a load, the topology selection problem becomes difficult as we can choose a load in favour of either topologies and hence left with the question of which topology to use under any loading conditions. We address this scenario as follows. The efficiency is a function of load impedance as is evident from (2.6) and (2.7). This raises a question, whether the efficiency can be furthered by proper choice (if allowed to be chosen) of an optimal load. In applications where the load can be chosen or matched to maximize the power transfer efficiency, we strive to find out the optimal load for both the topologies and we compare the efficiency between the two topologies under optimal loading conditions. The optimal load for the series and shunt resonant topologies can be computed as

$$R_{l,opt}^{SS} = R_s(\omega)\sqrt{1 + k^2 Q_p Q_s} \tag{2.14}$$

$$R_{l,opt}^{SP} = R_s(\omega)Q_s^2\sqrt{\frac{1 + k^2(\frac{Q_p}{Q_s})}{1 + k^2 Q_p Q_s}} \tag{2.15}$$

Surprisingly, the efficiency expressions for the optimized load for both the topologies take the same form as shown in (2.16).

$$\eta = \left(1 + \frac{1}{r} + \frac{1}{k^2 Q_p Q_s}(2 + r + r^{-1})\right)^{-1} \tag{2.16}$$

The values of r for the two topologies are given in (2.17) and (2.18). We used the simulation setup similar to the one in Figure 2-6 however with a separation of 10 mm between the coils and extracted its equivalent circuit parameters.

$$r_{ss} = \sqrt{1 + k^2 Q_p Q_s} \quad (17)$$

(2.17)

$$r_{sp} = \sqrt{\frac{1 + k^2 Q_p Q_s}{1 + k^2 (\frac{Q_p}{Q_s})}} \quad (18)$$

(2.18)

These were used to compute the power transfer efficiency using the experimentally verified expression in (2.6) and (2.7) for loads varying from $1/5^{th}$ to 2.5 times of optimal load and for frequencies ranging from 4 to 10 MHz. The maximum efficiency operating points for the above curves were then theoretically computed using ((2.16) - (2.18)) by using the extracted parameter values from HFSS (shown as ((16) + HFSS) are plotted in Figure 2-9 and Figure 2-10 .

The maximum efficiency points corresponding to optimized loads for each frequency matches well with corresponding computed values from (2.16) as can be seen from graphs. It can be seen from the graphs that the optimal load increases with frequency for a given pair of coils for both the topologies. However if we keep increasing the frequency of operation, the efficiency will drop to zero near the self-resonant frequency of the coil. It should also be noted that the efficiency is relatively stable with changes in the load when the frequency of operation is high and hence we infer that the high frequency wireless links are relatively robust to load variations than its low frequency counter parts.

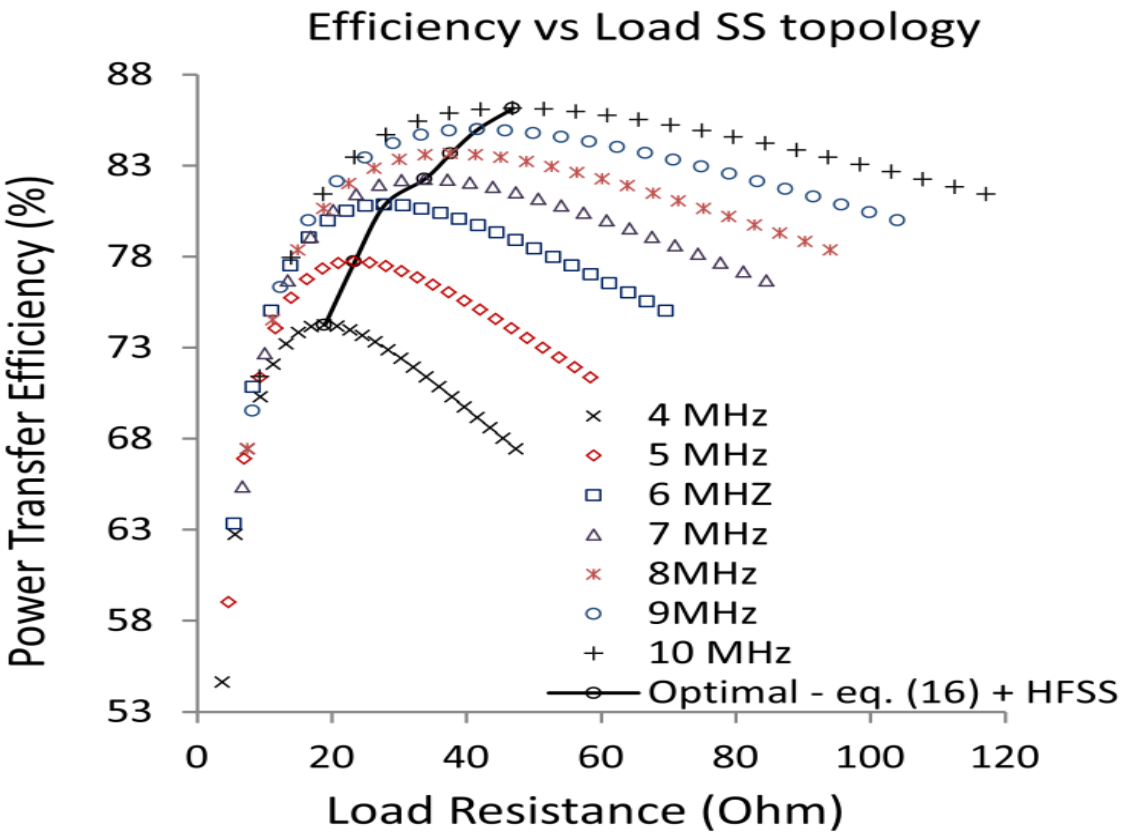

Figure 2-9 Graph of Efficiency versus Load for the SS topology

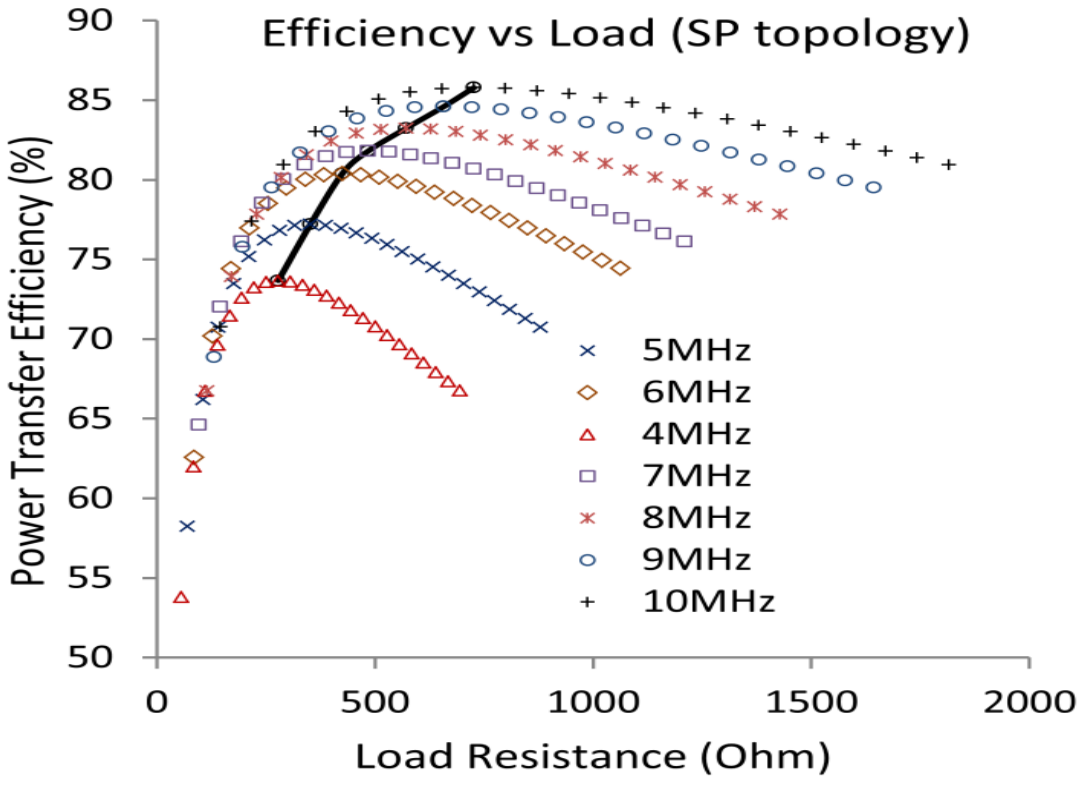

Figure 2-10.Graph of Efficiency versus Load for the SS topology

Having obtained optimized loads for both the topologies, we compare their efficiencies under optimal loading conditions. We now compute the factor T defined as

$$T = \eta_{ss}^{-1} - \eta_{sp}^{-1}$$

(2.19)

It can be shown that T < 0 for all frequencies of operation leading to an important result that, "With optimized loads, the SS topology always outperforms the SP topology." However for weakly coupled the efficiencies of the series and shunt resonant topologies under optimal loading conditions are almost the same with the former slightly higher than the latter.

$$T = \left(\frac{r_{ss} - r_{sp}}{r_{ss} r_{sp}}\right)\left(\frac{r_{ss} r_{sp} - 1}{r_{ss}^2 - 1} - 1\right)$$

(2.20)

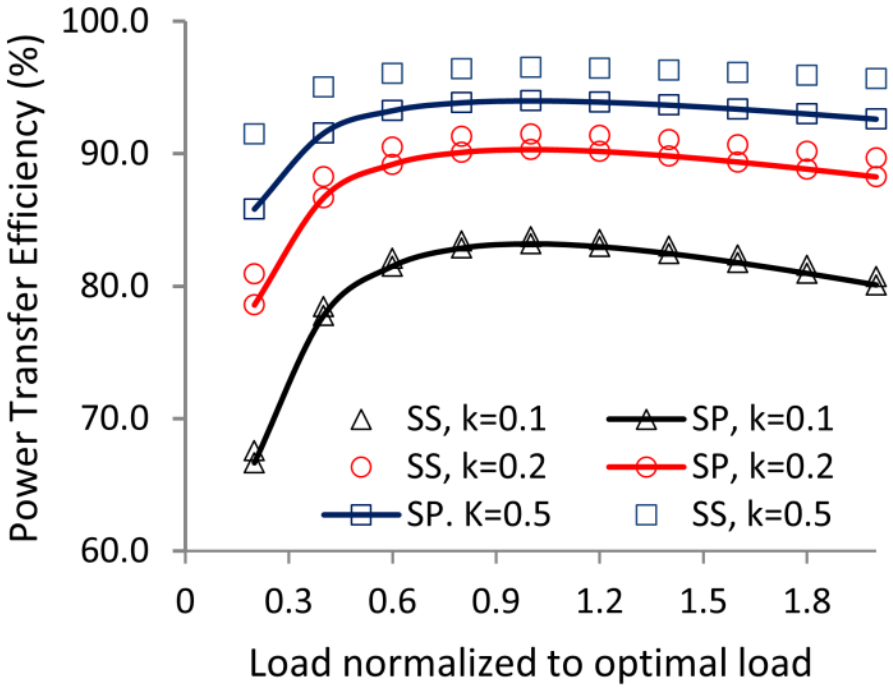

Figure 2-11 Power transfer efficiency versus load (normalized to optimal load)

To verify this important result, we simulate the efficiencies for the same pair of coils under different coupling conditions in HFSS and the results are shown in Figure 2-11. For weakly coupled links with optimized loads both the series

and shunt resonant topologies have nearly equal efficiencies and as coupling increases the dominance of the series resonant topology is very prominent as evident from the graph in Figure 2-11, which shows the efficiencies for various loads under different coupling conditions.

Thus given a link with a freedom to choose the load, SS topology needs to be selected for strongly coupled coils and for weakly coupled links both the topologies operate at the same efficiency and the topology needs to be chosen based on the specific advantages suitable for a particular application.

2.9 Optimal Frequency of Operation

With all the analysis in place, we try to answer whether there is an optimal frequency of power transfer between two coils with an optimal load and dominant topology. The optimal frequency of operation however depends on the type of fabrication used to realize the inductor and hence no generic closed form expression for optimal frequency of operation can be provided. We proceed as follows. First we know from earlier sections that the SS topology is more efficient than SP topology. Thus the optimal frequency of operation is that frequency which maximizes the power transfer efficiency of SS topology. From (2.16), using basic algebra we can show that maximizing the PTE is equal to maximizing the objective function g shown below. If g is maximized, the efficiency in (2.16) is also maximized for a given coupling between the coils.

$$g(f) = Qp(f)Qs(f) \tag{2.21}$$

Thus the optimal frequency of operation reduces to that frequency which maximizes the product of quality factors of the coils. The quality factors of the coils can be obtained by evaluating the inductance and resistance of the coils at different frequencies using the appropriate theoretical model for the inductors. For square planar inductors the closed form expressions can be used from [115, ((2)], [116, ((5)], [117, ((6-8)] and [118, ch.4.10.1].

All the aforementioned work makes use of the inductor parameter values (inductance and self-resistance) and mutual inductances which were either measured using a network analyzer or simulated using HFSS. However theoretical modelling of the coils for square planar PCB realization can also be used to obtain the inductor parameters and we refer to [115, ((2)], [116, ((5)], [117, ((6-8)] and [118, ch.4.10.1] for a completely theoretical approach.

The models are accurate for operating frequencies away from the self-resonant frequency of the coil and since the wireless power transfer links operate away from the self-resonant frequency of the coil(so that Q factor is large), the models are applicable. The accuracy of the aforementioned models of inductors resulted in an error < 5% for the wireless power transfer efficiency, which can be acceptable for engineering applications.

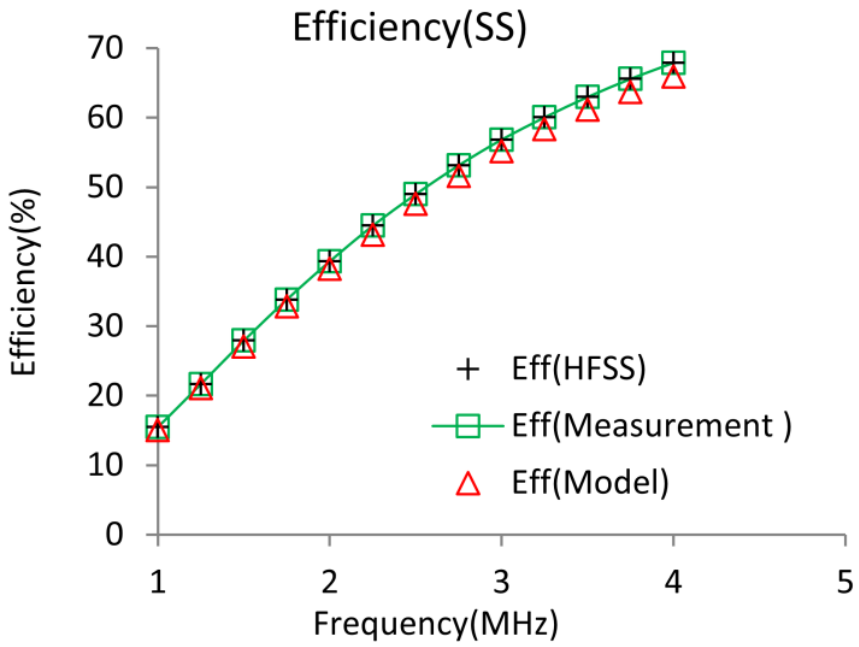

Figure 2-12 Comparison of Efficiency values by evaluating (6) using inductor parameters from models and measurement

The comparison between the results obtained using models and using the measured values of the coil parameters has been done by evaluating (2.6) and (2.7) as shown in Figure 2-12 and Figure 2-13. The coils used for this comparison study were 16 turn square planar inductors fabricated on a FR4 PCB, with an internal diameter of 7mm and an external diameter of 25.4mm.

The pitch of the inductor spiral was 0.6mm and the trace width of the coil was 0.2mm. The primary and secondary coils are assumed to be identical and separated by a distance of 10mm.

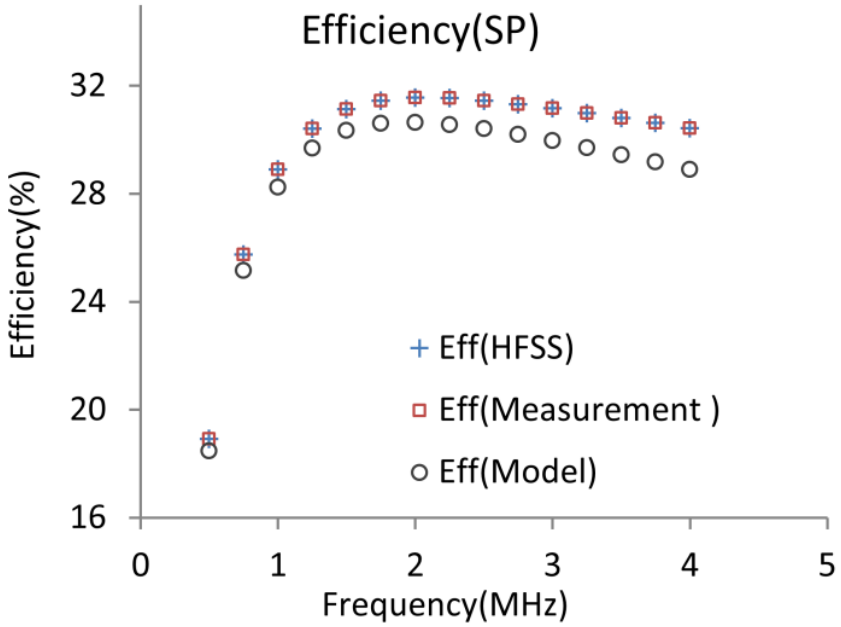

Figure 2-13 Comparison of Efficiency values by evaluating (6) using inductor parameters from models and measurement

2.10 Ultimate limit on Power Transfer Efficiency

Given a pair of coils and their orientation in space, it is now possible using ((2.14) to (2.21)) to calculate the maximum efficiency of operation from one coil to another across all loads, topology and frequency of operation. To demonstrate this, we consider a pair of identical single turn square spiral inductors built on a FR4 substrate (Figure 2-14) with external size of 3 mm and has a one ounce (35 um thickness) copper trace with width of 200 um separated from each other by an axial distance of 7 mm. To arrive at the ultimate limit on power transfer efficiency, we follow the four steps shown below.

Step 1: Identify the optimal frequency of operation

The models for the inductors in Figure 2-14 are extracted from our earlier work [119]. The function *g(f)* in (2.21) is maximized to obtain the optimal operation frequency as 3.01GHz.

Step 2: Topology identification

Since small single turn inductors have very low inductance and since their separation is larger than their dimensions, the coupling is very weak and based on our inference in VI, both SS and SP topology would operate at the same efficiency. Hence we can choose either of the topologies, and we will proceed with the use of SS topology.

Step 3: Optimal Load.

The optimal load at 3.01 GHz for SS topology is then computed using (2.17) as 2.1 ohm.

Step 4: The maximum efficiency

The maximum efficiency is then simply computed from (2.16) as 35.67%. The resonating capacitance for the SS topology is computed for 3.01 GHz as 0.37pF.

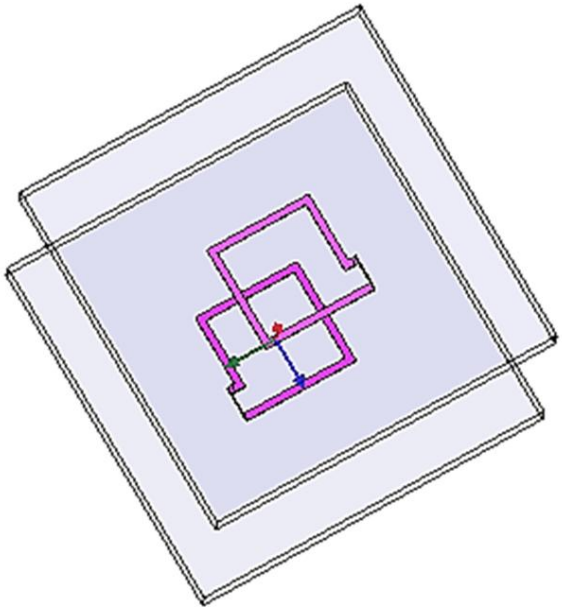

Figure 2-14 Example structure chosen for Efficiency maximization

The maximum efficiency versus frequency curve was then simulated using HFSS and ADS as for this link structure and is shown in Figure 2-15. It can be seen that the optimal frequency of operation obtained by maximizing the function (2.21) is in the vicinity of 3 GHz and it coincides with the maximal efficiency obtained using simulations, thereby verifying the result (2.21).

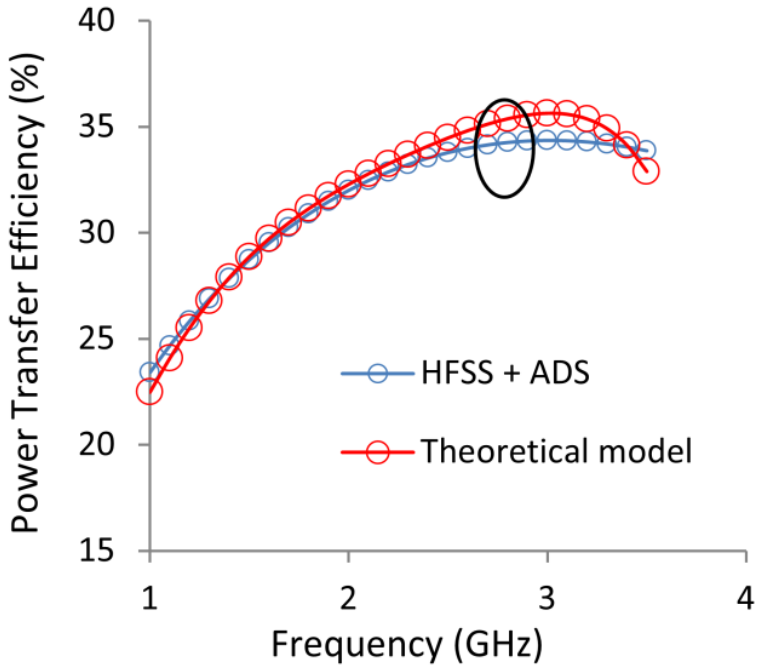

Figure 2-15 Optimal frequency of power transfer, comparison between theoretical prediction and HFSS simulations

We now summarize that, for the structure given in Figure 2-14, the most efficient (35.67%) way to transfer power from one coil structure to another is to connect a series resonating capacitor of 0.37 pF to either coils and terminating or matching the receiving coil to 2.1 ohm and operating the link at a frequency of 3.01 GHz.

2.11 Application to Biomedical Implants

In this chapter we will showcase the results on the performance of wireless power transfer links built by applying our findings in this chapter and compare them with existing works. We will consider neural implant application and build IPT links for them and compare them with existing state of the art links. The Neural implants can be classified into two main types. There are ones used for recording neural data from brain and there are others used to record

data from/stimulate nerves directly and we will call them Neural Implant-1 (NI-1) and Neural Implant -2 (NI-2) respectively. The NI-1 allows more area (300 mm^2) as the implant is placed over the skull beneath the scalp. For NI-2 application, the size constraint is stringent as the limbs where the implants are housed do not have such large area and the size is limited to 100 mm^2. The concept of wirelessly powering the neural implant (NI-1) is shown in Figure 2-16

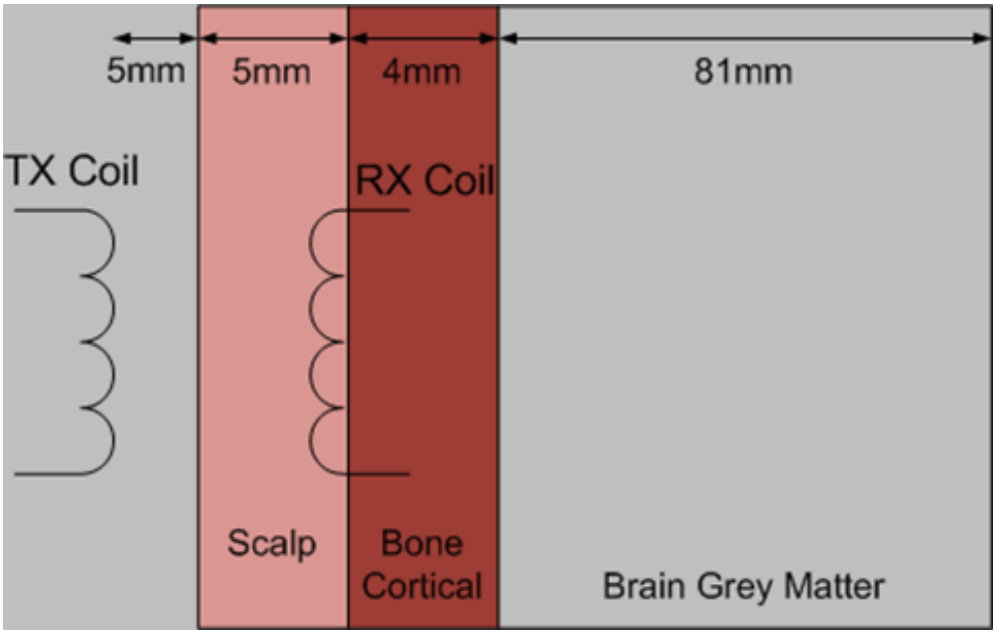

Figure 2-16 The IPT link used in neural implants.

The optimal link design for the neural implants NI-1 and NI-2 were carried out based on our findings in earlier section. The PTE results are compared with best case results from existing literature on IPT link optimization [111] & [122]. The PTE were simulated using HFSS with appropriate tissue models. It can be clearly seen from Table 2-2 that topology selection, frequency and load optimization based on our findings have improved the PTE of IPT links significantly. For the case of NI-2 implant it can be seen the power transfer efficiency can be bettered with a coil 36% smaller in size to the one reported in [111]. For the case of NI-1 implant it can be seen that the PTE can be bettered [122] (even with the tissues losses accounted) with a 34% smaller implanted coil.

	Link Design and Specifications (for 10mm Separation)	PTE (%)
Our Approach	<u>NI – 1 design (Implant coil)</u> Dimension= 250mm^2, planar Trace width = 0.2 mm Pitch = 0.5 mm No of turns = 12 Frequency of operation = 10 MHz Optimal load used (19 ohm) Method: Series resonant topology Tissue Losses Included : **Yes**	82%
	<u>NI-2 design: (Implant Coil)</u> Implant coil 2= 64 mm^2,planar Trace width = 0.1 mm Pitch = 0.2 mm No of turns = 13 Frequency of operation = 21 MHz Optimal load used (11 ohm) Method : Series resonant topology Tissue Losses Included: **Yes**	52.6 %
U.M. Jow & M. Ghovanloo [111]	<u>NI-1 design:</u> Not Available	
	<u>NI-2 design: (Implant Coil)</u> Implant coil = 100mm^2,planar Trace width = 0.2 mm Pitch = 0.35mm Frequency of operation = 13.56 MHz Load = 500 Ohm Method: Parallel resonant topology Tissue Losses Included: **Yes**	51.8%
A.K. RamRakhyani, S. Mirabbasi, C. Mu [122]	<u>NI-1 design: (Implant Coil)</u> Implant coil = 380mm^2, wire wound. Trace width = 0.1 mm Pitch = 0.2mm Frequency of operation = 13.56 MHz Load = 5.6 Ohm Method: four coil topology Tissue losses included : **NO**	< 80%
	<u>NI-2 design:</u> Not Available	

Table 2-2 Comparison of IPT link designs for the neural implant application

2.12 Experimental results in tissue environment

The testing of PTE using pork meat was carried out separately using IPT links described in Table 2-1 with a 10mm separation between the TX and RX at 3MHz. The power transfer efficiency measured (57.6%) was close to the simulation results (59%) obtained using dry fat tissue models in HFSS. The experimental set up for PTE measurement with pork meat is as shown in Figure 2-17.

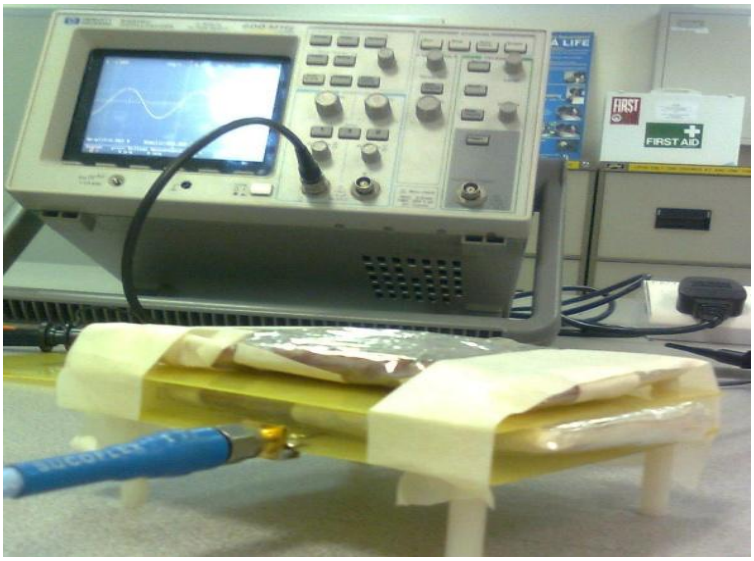

Figure 2-17 PTE measurement with pork meat

Figure 2-18 The cadaver head experiment for transcutaneous power transfer.

The RX coil designed for NI-2 implant as shown in Table 2-2 was tested in a cadaver head at the National University Hospital, whilst operating at 10MHz with a separation of 15 mm between the implant coil and transmitting coil as

shown in Figure 2-18. The power transfer efficiency was measured at 40% under normal conditions and during worst case misalignment (25mm separation, 45 degree angular misalignment) was measured at 16%. The experiment was conducted as a part of collaboration between NUS, NUH and University Eye Hospital Tübingen. The experiment was conducted to study the suitability of the designed implant, its positioning, surgical challenges and performance.

2.13 Effect of Coil parameters on the performance of the link

Detailed below in Table 2-3 are the effects of the various coil parameters of the square planar inductors on the performance of the link.

Parameter	Effects on variation
Trace Width	For a given area, an increase in trace width increases the quality factor of the coil until a threshold and then starts to decrease beyond the threshold. Hence an optimal trace width is obtainable
Inter trace spacing	For a given area, an increase in inter trace spacing increases the quality factor of the coil until a threshold and then starts to decrease beyond the threshold. Hence an optimal inter trace spacing is obtainable
Substrate thickness	Does not affect Inductance, minimal effect on resistance. Reduces the self-resonant frequency of the coil for small increments, but remain unaffected at large separations.

Table 2-3 Effects of coil parameters on link performance

2.14 Biosafety considerations

The scope of safety offered by the SAR is limited only to the electrical safety of the powering scheme. There are other aspects that need to be considered for clinical use namely biocompatibility of the material, conformity and tissue relaxation/fatigue effects due to chronic excitation. Since copper and most other metals are not bio-safe, only titanium can be used for making the coils. However due to lower conductivity of titanium when compared to copper, the quality factors of the coils are less leading to low power transfer efficiency. An alternative to using titanium as a bio-safe option is to coat the entire copper coils using bio-safe substances like polydimethylsiloxane (PDMS) or silicone. We currently use a thin layer (few hundred microns thick) of PDMS coating (biocompatible grade PDMS) to ensure biocompatibility of the powering system. However the study on chronic excitation needs to be carried out for specific end application to make it suitable for clinical needs.

2.15 Parasitics and Tissue losses

Lower frequencies have high tissue penetration depth than high frequencies and vice versa. Operating the power link at low frequencies hence helps to reduce tissue losses. In-fact the tissue losses are negligible compared to copper losses in power links up to an operational frequency of few tens of MHz. Hence models of tissue losses need not be included into the design of inductive power links for a frequency of up to 50 MHz. Since most inductive links operate at lower frequencies than 50 MHz it is safe to neglect tissue losses. The introduction of tissues hardly affects the inductance of the coils and hence the effects of parasitic coupling are minimal. However it is to be noted that the self-resonant frequency of the coils change with the introduction of tissues close to the coil. There is a change in quality factor and hence efficiency of the power transfer link. The modelling of the variation in self-resonant frequency of the link due to introduction of the tissues can be obtained from the stacked capacitance model described in [111].

2.16 Summary

Wireless power links using inductive coupling have been analysed thoroughly for maximum operating efficiency in the first part of this chapter. The analysis has been verified by using coils fabricated on PCB. The fact that the operating frequency determines the dominant topology for fixed loads has been analysed qualitatively and the boundary has been derived and verified experimentally. The limitation of resonant tuning has been identified and explanations have been provided for the anomaly both qualitatively and quantitatively. The possible use of series resonant method which can perform better at larger frequencies and smaller loads as is the case with RF circuits (50 ohm) has been proposed. Load and frequency optimization has been explained to improve the efficiency of wireless power links and can be adapted to existing links as well. Thus it is now possible from our extensive analysis to (improve or) design efficient wireless power transfer links operating under optimal conditions ensuring minimal loss in power transfer. Since the results were derived using an equivalent model of inductor, they can be applied to various inductor realizations irrespective of the manufacturing technology. The design of IPT links for neural implants using our approach is compared with latest optimization works. It is evident that there is clear improvement of PTE in IPT links that are built based on the concept of topology selection, load and frequency optimization presented in detail in this chapter.

Chapter 3: Overcoming coil misalignment and motion artifacts in inductive power transfer links

3.1 Introduction to IPT links and misalignment

The inductively coupled power link is one of the hot topics in the wireless power transfer (WPT) domain. There are a plethora of applications for WPT using inductive coupling as it provides a hassle free, aesthetic and wireless alternative to powering/charging devices and there are numerous literature that address the problems in such power transfer links. The applications of WPT using inductive coupling vary from bio-medical implants and electric vehicles to hand held devices such as electric shavers and tooth brush [53]-[55], [102]-[104] and [120]. Prior works have contributed significantly to improve power transfer efficiency (PTE) for specific applications. WPT using resonant inductive coupling is a very old concept first proposed by Tesla [1]. The concept was adopted for biomedical implants and analysis was conducted and reported in early works [39]-[40]. Today WPT using inductive coupling is being researched extensively for various applications including mid-range wireless power transfer for day to day applications [121].

The PTE is the main quality metric that is used to evaluate WPT links. Recent works have tried to improve the PTE of WPT link that employs inductive coupling using varied approaches. A generic study on low frequency WPT links for biomedical applications was conducted and PTE improvement using coil optimization techniques was reported in [110] & [111]. PTE improvement was also reported using a pair of high Q factor intermediate coils in which one intermediate coil is coupled strongly to the source coil and the other intermediate coil is coupled strongly to the receiving coil thereby decoupling the load and source resistances removing their effect on PTE [122]. The comparative study between three types of WPT links namely the traditional WPT link, WPT link with a high Q intermediate coil closely coupled to the

source alone and WPT link with two high Q intermediate coils one each coupled to the source coil and load coil respectively is well documented in very recent work [123]. The performance of the WPT link with an intermediate coil closely coupled to the receiving coil is analysed in [124]. WPT links for retinal implants, initially reported in [125] was bettered by introducing a pair of connected intermediate coils as has been shown in [101]. All the above mentioned works have contributed to PTE improvement using different approaches. Other approaches include early work [126] which analyses the optimal frequency of operation for the WPT links used in biomedical implants based on the tissue properties. This research on optimal frequency of operation was furthered by recent work [106]. PTE improvement using the right resonant topology and optimal load has been discussed in our earlier work [127]. WPT method for retinal implants presented in [100] was bettered using wired intermediate coils that increase the tolerance of PTE to eye motion in [101]. However two main challenges still remain to be addressed

1. Efficiently powering links with separation larger than the coil dimension.

2. Powering misaligned links where the transmitting and receiving coils are not aligned along a common axis.

We aim to address these challenges in this chapter. The use of WPT in many of the above mentioned applications places constraint on their mechanical design owing to the inductive coupling requirements such as alignment of coils, minimal separation between the coils, and absence of conductive substance like tissues between the coils. Overcoming these constraints causes either an increase in size of the end device or a change in the intended shape of the device, both of which act detrimental to the original aesthetic motive behind the use of the inductive coupling. In bio-medical implants, the coils are subject to motion artifacts leading to further complications in power transfer. We propose to address these issues using the concept of flux sharing in a system of three coils by extending our earlier work [128].

By introducing a passive low-loss tuned coil carefully into a traditional inductively coupled WPT system, the challenges mentioned earlier can be overcome. The positioning, size and tuning of the passive low-loss coil play a key role in the performance of the WPT system. Since the arbitrary placement of the passive coil can lead to reduction in the power transfer efficiency (PTE), the effect of the passive coil introduction needs careful assessment.

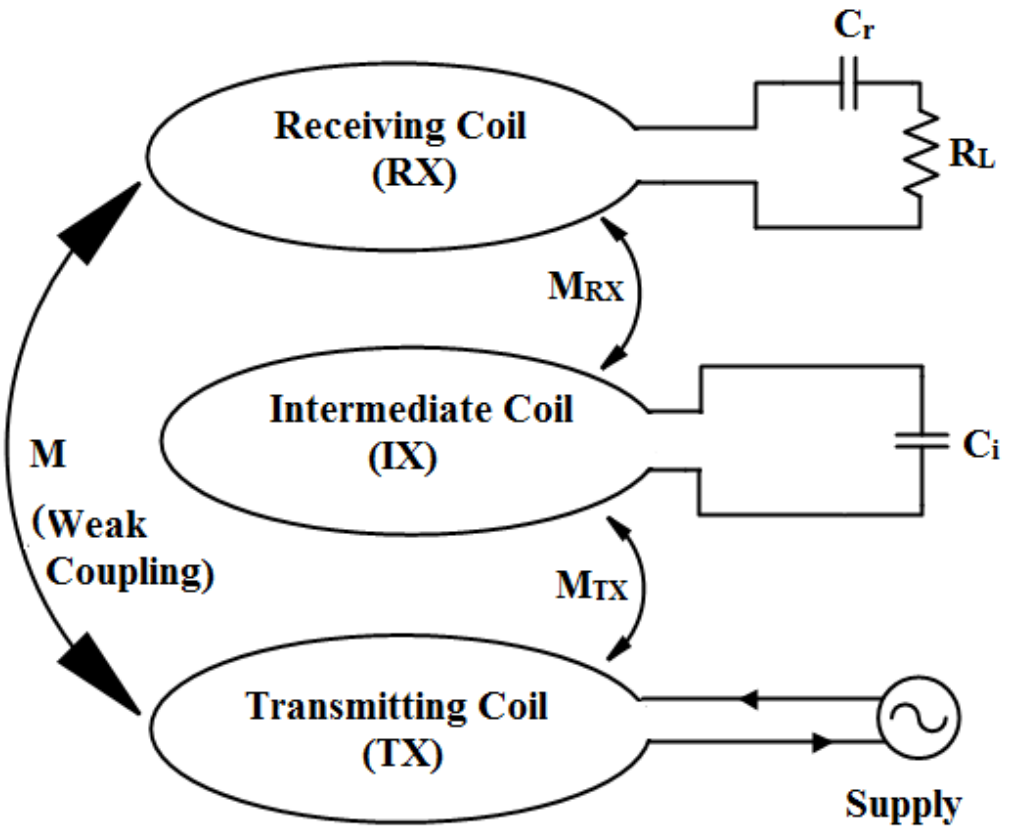

Figure 3-1.Flux linkage boosting using a passive intermediate coil

Consider the system shown in Figure 3-1, comprising of a transmitting coil TX and a receiving coil RX. We will show that the introduction of the passive intermediate coil IX can have both positive and negative impact on the PTE of the system and discuss how to choose the right position of the IX coil to improve PTE of the link. The TX coil is being excited (with a sinusoidal source), the power is bifurcated from TX to IX and RX coils. The power bifurcation ratio is a function of mutual inductances M_{TX}, M_{RX}, and M and can

be controlled by varying them [108]. The magnetic flux lines linked with RX coil are created by excitation current in TX coil and induced current in IX coil. Since currents flowing in A and B are not in phase (as the current in IX coil is in-fact induced due to the excitation current in TX coil), the total magnetic flux lines linked with RX coil depends on the position of IX coil. Thus if we can find positions for the IX coil which can improve the total magnetic flux linked with RX, then the power received by RX coil will be more in the presence of IX coil, than when it is absent. For such a positioning of the IX coil which enhances the power received by RX coil, there is an effective flux linkage boosting. We build on this basis of flux linkage boosting to come up with the passive intermediate tuned coil which can enhance the flux linkage between the transmitting (TX) and receiving (RX) coils in a traditional WPT setup and hence improve the power transfer capability of the system.

3.2 Motivation behind the use of IX coil

There are two main motivations that have inspired our work and are mentioned below.

A. Large Separation

The unacceptable performance of the inductively coupled wireless power links under large separations is one of the key issues not properly addressed. The efficiency of an inductively coupled WPT link falls sharply with the increase in distance between the TX and RX coils. Various optimization procedures as mentioned in [110]-[111], [122] and [123] exist to improve the PTE of traditional inductively coupled WPT links. However when the separation becomes larger than dimension of the coils used in the link, these techniques only provide minimal improvement as the coupling is very weak. To show the efficiency drop with distance in normal power transfer links, we consider square planar inductors (fabricated on a FR4 substrate) as shown in Figure 3-2 with W=0.2 mm, S= 0.4 mm, D_in = 7mm and trace thickness t of 0.035 mm (corresponding to thickness of one ounce copper). Six WPT links with

inductors (identical TX and RX coils) varying in number of turns (16 to 21) were considered and the PTE values were computed as a function of separation using experimentally verified expressions in [127] at 4 MHz for a 50- ohm load as shown in Figure 3-3.

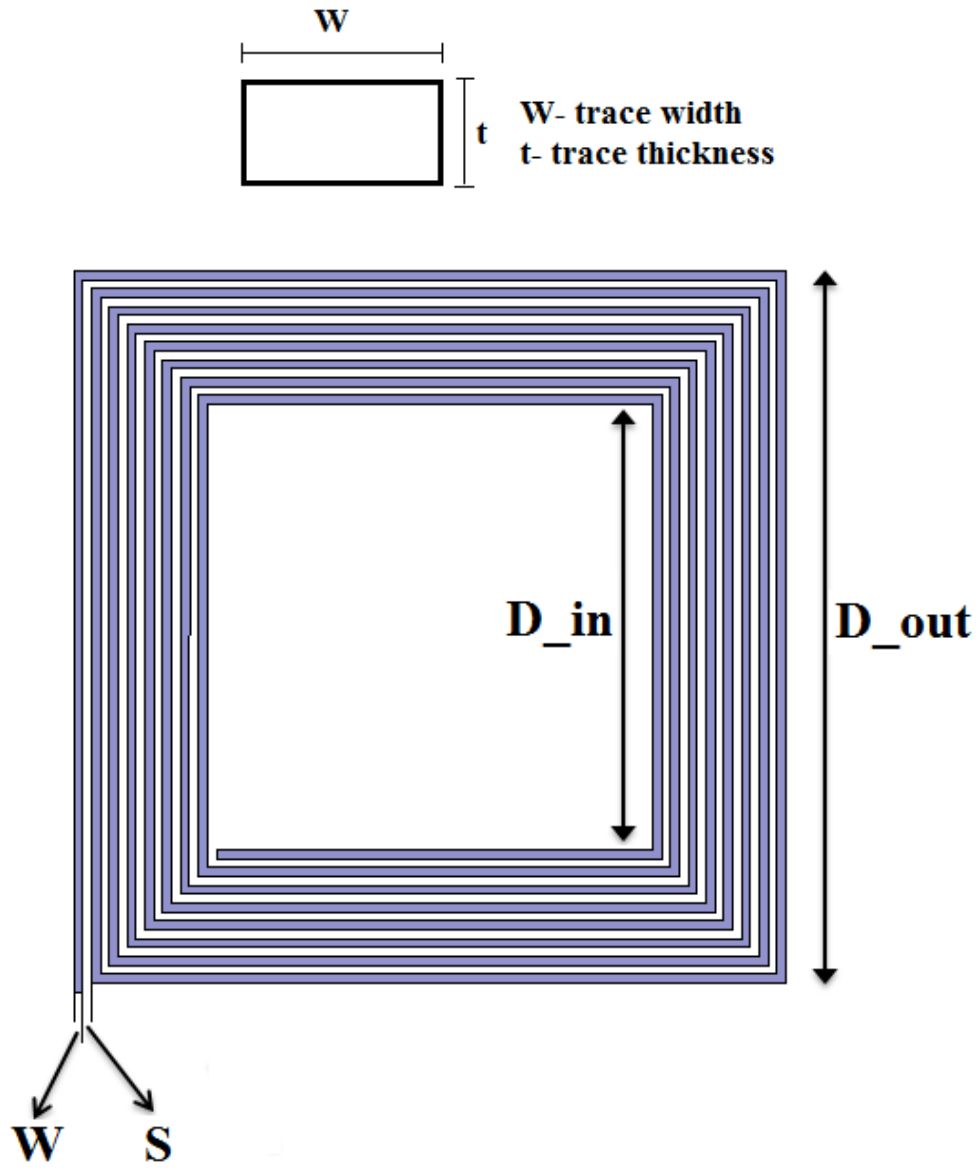

Figure 3-2 Square Planar Inductors

The efficiency of the WPT systems falls appreciably when the separation between the coils becomes comparable with the dimension of the coil irrespective of the size of the coil as shown in Figure 3-3.

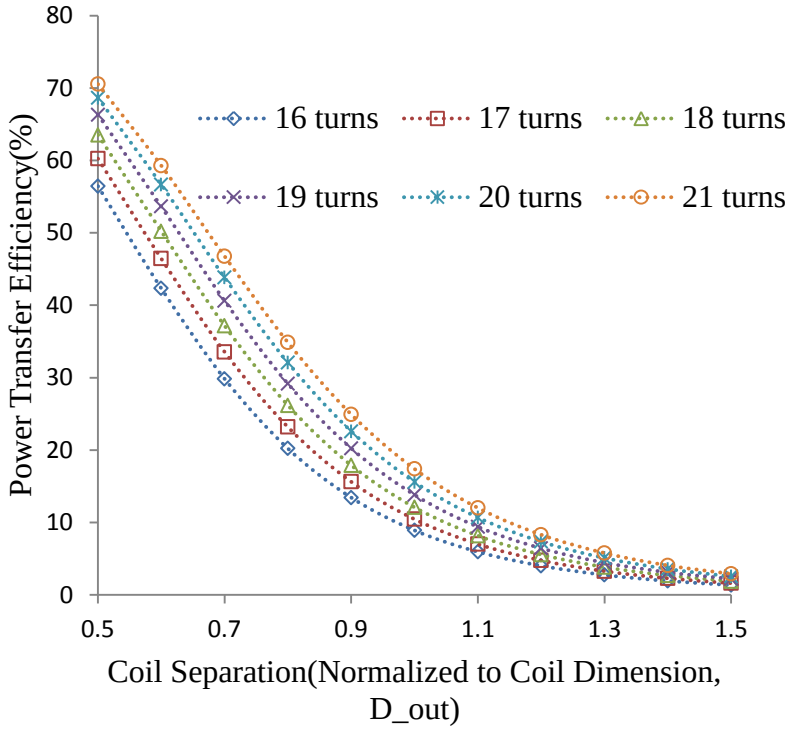

Figure 3-3 PTE vs. normalized coil separation for various coil turns

B. Coil Misalignment

Conventional wireless power links operate efficiently under coaxial alignment of primary and secondary coils. In fact some of the wireless power links are designed with alignment techniques such as magnetic core alignment ensuring proper operation. However many practical applications that use inductive coupling such as RFID and biomedical implants have coil misalignments that lead to poor performance of the power links and the degradation effects of misalignment in such applications have been documented in [129].

When the receiving coil is subject to change in position, the power transferred to the receiving coil reduces. To ensure that the required power level is delivered all the time, the input power is either adjusted to match the worst case orientation conditions or varied based on a feedback mechanism. The former causes unwanted heating in normal conditions and the latter requires

extra circuitry and additional transmit power for feedback. In many practical applications of biomedical implants the receiving coil is subject to change in position (both angular and lateral) as the implant is always in a moving frame. This causes intermittent drop in received power thereby performing poorly. In applications which use closely coupled coils (very short distance), coil misalignment and motion artifacts present less or no detrimental effects to its functioning. However with increase in separation between the TX and RX coils, the effects of coil misalignment and motion artifacts are pronounced and present a significant reduction in PTE.

Thus there is a real need to address the scenario of inductively powering coils that is not aligned with respect to each other. The wireless power transfer method is pushing its limits to transfer power over distances in the order of few centimetres. Very recent works on inductive coupling [130] have focused on using intermediate coils to improve power transfer efficiency. Though limited works have been published, a case for such links has been made. In this work we propose to use passive resonant tuned intermediate coils to power wireless links with either large separations or coil misalignments.

3.3 Theory of Intermediate Coil System

A traditional WPT system comprises of a TX and RX. Under normal operating conditions the current in TX creates a magnetic field that cuts through RX and the time variance of this magnetic field induces an electromagnetic field (EMF) in RX. However as coupling between the coils reduces to a negligible value due to misalignment of coils or large separation, there is a considerable drop in the induced EMF. This is a direct consequence of the reduction in magnetic flux linkage between the coils. Under such circumstances, if we can somehow make more magnetic flux lines to cross the RX coil without making any changes to the TX- RX set up, the PTE and power transfer capability of the WPT link can be improved. The trick is to introduce a low-loss intermediate (IX) coil alongside the TX & RX coils (resonant tuned with TX and RX coils) and position it properly so that it acts as a repeater, which relays

the power from TX to RX without affecting the existing setup. We propose to take advantage of using IX and its proper positioning to address applications that suffer from PTE drop due to large separation or misalignments. The added advantage of superior performance under motion artifacts will also be shown later. For purpose of proper depiction of the coil orientations, the square planar inductors will be represented as viewed into the YZ plane, along -X axis as shown in Figure 3-4.

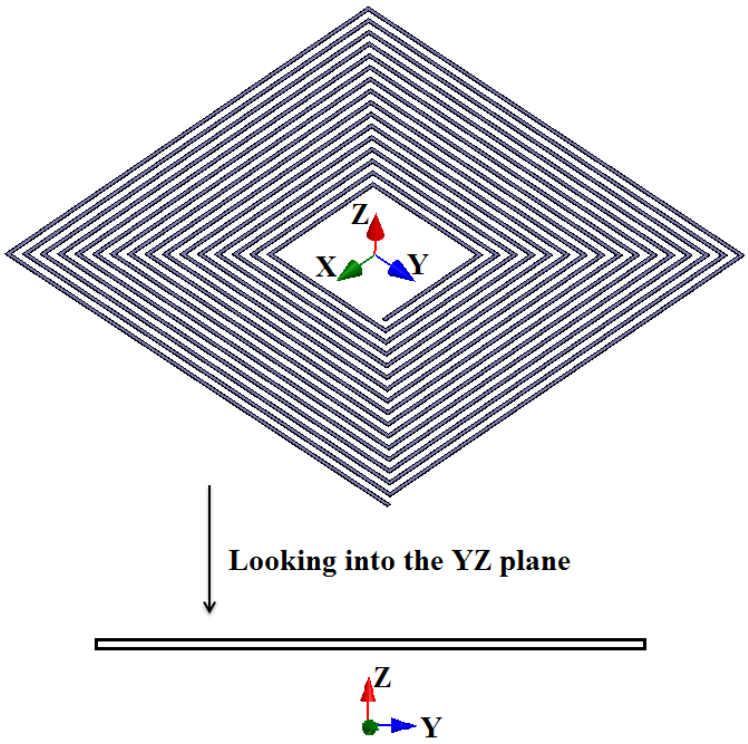

Figure 3-4 Square planar inductor representation

The importance of positioning IX coil properly has to be highlighted here. A simple illustration of the currents in each of the coils while the link is operational stresses the importance of IX coil positioning. Consider a stacked setup where the TX coil is excited using a current I^{EX} (clockwise at a given instant) as shown in Figure 3-5. The polarity of the induced electromotive force and hence the induced currents can be obtained for both the IX and RX coils using Lenz law. In the IX coil, the current induced by the excitation

current in TX coil will be counter clockwise as denoted by I^{TI}. In RX coil, there will be two induced currents, one (I^{TR}) induced by the excitation current in TX coil directly due to the weak linkage and the other (I^{IR}) due to the current in IX coil (I^{TI}).

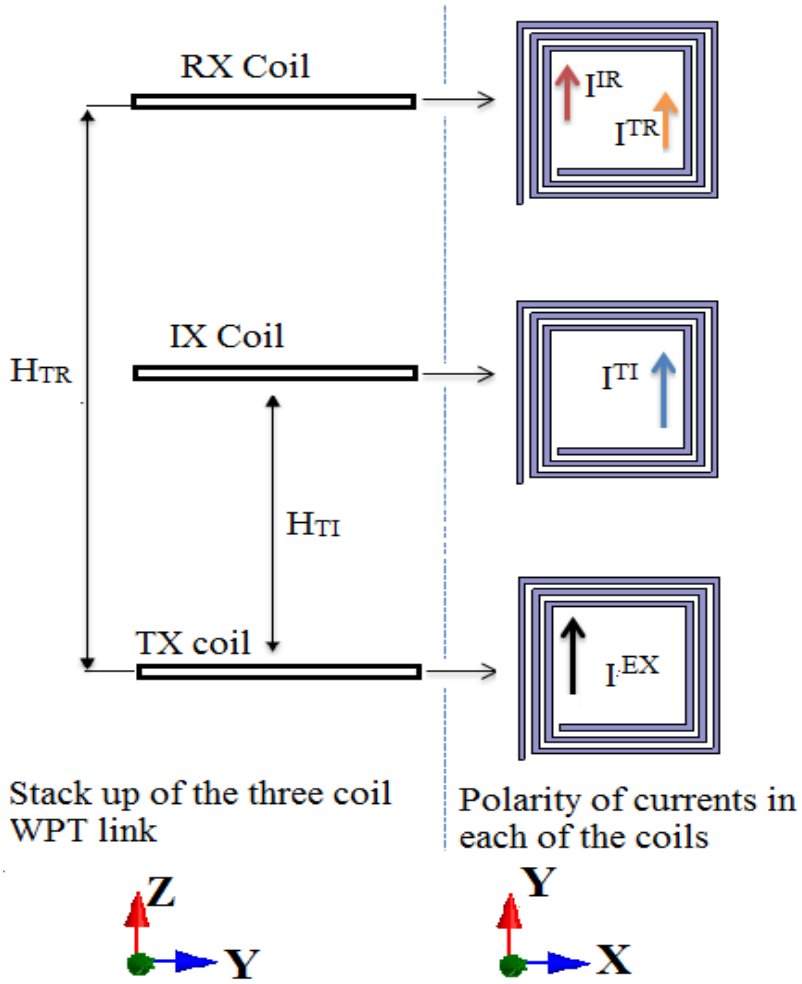

Figure 3-5 Polarity of currents in the WPT system with an IX

However these two currents will be in opposite directions based on Lenz law. The strength of these two currents (I^{TR} and I^{IR}) depends on coupling between the coils (TX-RX and IX-RX). For a fixed TX-RX set-up, varying the position of IX coil will hence determine the net current in RX coil. If the position of IX coil is such that the current I^{IR} is larger than twice the value of I^{TR}, then more power is transmitted to the receiver than when the IX coil is absent. Such positioning of IX coil can thus improve the PTE of a normal TX-

RX link. If the coupling between TX and RX coils is large, then the introduction of the IX coil will be detrimental to its operation as both the currents (I^{TR} and I^{IR}) are comparable and cancel each other. On the other hand if the coupling between TX and RX is very small, the current induced due to IX (I^{IR}) overpowers the current induced due to TX (I^{TR}) and improves the power delivered to the load connected to RX. Hence this method of introducing IX coil works only for loosely coupled links. It should be noted that even under weak coupling between TX-RX, the positioning of IX coil is vital. For example if IX coil is loosely coupled to TX, then both the currents in RX coil (I^{TR} and I^{IR}) are small and cancel each other. Hence proper positioning of IX is desired for loosely coupled TX-RX link to have any PTE improvement. From here on, we will call the WPT system with an intermediate coil as the IX-coil system.

3.4 PTE of an IX coil System

The setup of the proposed system with an intermediate coil looks like the one shown in the Figure 3-1. Let L_{TX}, L_{IX} and L_{RX} be the inductances, R_{TX}, R_{IX} and R_{RX} be the effective series resistances of the TX, IX and RX coils respectively. Let I_{TX}, I_{IX} and I_{RX} denote the currents flowing in TX, IX and RX coils respectively. Let us assume a sinusoidal voltage excitation V_{TX} is applied to the transmitting coil. The transmitting coil generates a time varying magnetic field due to the current flowing through the coil. The flux linked ϕ with each of the coils due to the excitation in the transmitting coil TX is given by

$$\phi_{TX} = L_{TX} I_{TX} + M_{TX} I_{IX} + M I_{RX} \quad \textbf{(3.1)}$$

$$\phi_{IX} = M_{TX} I_{TX} + L_{IX} I_{IX} + M_{RX} I_{RX} \quad \textbf{(3.2)}$$

$$\phi_{RX} = MI_{TX} + M_{RX}I_{IX} + L_{RX}I_{RX}$$

(3.3)

Differentiating both sides with respect to time and then applying Faraday's law by replacing rate change of flux with the open circuit electromotive force, the above expressions can be written as

$$V_{TX} = -j\omega(L_{TX}I_{TX} + M_{TX}I_{IX} + MI_{RX})$$

(3.4)

$$V_{IX} = -j\omega(M_{TX}I_{TX} + L_{IX}I_{IX} + M_{RX}I_{RX})$$

(3.5)

$$V_{RX} = -j\omega(MI_{TX} + M_{RX}I_{IX} + L_{RX}I_{RX})$$

(3.6)

V_{IX} and V_{RX} are the induced electromotive forces across IX and RX respectively. By inserting the coil losses and resonance conditions in the TX, RX and IX coils, we compute the efficiency of the power transfer from transmitter to receiver as shown below.

$$\eta = \frac{I_{RX}^2 R_L}{V_{TX}I_{TX}}$$

(3.7)

$$\eta_{IX} = \frac{R_L\omega^2(M_{TX}^2M_{RX}^2\omega^2 + M^2R_{IX}^2)}{(R_{IX}(R_{RX} + R_L) + M_{RX}^2\omega^2)\sqrt{A^2 + (2MM_{TX}M_{RX}\omega^3)^2}}$$

(3.8)

Where,

$$A = [R_{IX}(R_{RX} + R_L)(R_{TX} + R_s) + (M^2 R_{IX} + M_{TX}^2(R_{RX} + R_L) + M_{RX}^2(R_{TX} + R_S))\omega^2]$$

(3.9)

Without the presence of the intermediate coil the efficiency of the power transfer link can be computed as the limiting case of the above derived power transfer efficiency as

$$\eta_{NO\ IX} = \lim_{M_{RX}, M_{TX} \to 0} (\eta_I)$$

(3.10)

$$\eta_{NO\ IX} = \frac{1}{1 + \frac{R_{RX}}{R_L} + \frac{(R_{TX} + R_S)(R_L + R_{RX})^2}{M^2 R_L}}$$

(3.11)

Having derived the expressions for PTE with and without the IX, we can derive the boundary condition for a given M to find the locus of values of M_{TX} and M_{RX} that improve the PTE. Unfortunately, due to the numerous parameters involved, it is difficult to show a closed form expression (though available) for the boundary between IX method and the traditional method. We will however numerically show the boundaries using contour plots for our experimental setup later in later section of this chapter.

3.5 Theoretical model of inductive links

We will present the theoretical model for the coils that will be used in demonstrating the IX- coil method in this section. We will use square planar inductors built on an FR4 PCB for our experiments. The computation of self & mutual inductance, self-capacitance and coil resistance will be derived and the equivalent circuit model parameters will be abstracted from those computations. The geometrical representation of the square planar inductors is shown in Figure 3-2. Square planar inductors used in the experimental

verification of the proposed WPT method are built on an FR4 epoxy substrate with 1-Oz (35µm) copper traces.

A. Self- Inductance

The self-inductance is not essential in computing the WPT efficiency (using (3.8)) but is still needed to build the resonant tank. We use the most ubiquitous result for square planar inductors provided in [116].

$$L = \frac{1.27\mu_0 N^2 D_{AVG}}{2}\left[ln\left(\frac{2.07}{\varphi}\right) + 0.18\varphi + 0.13\varphi^2\right] \quad \textbf{(3.12)}$$

Where

$$D_{AVG} = \frac{D\_out + D\_in}{2} \quad \textbf{(3.13)}$$

$$\varphi = \frac{D\_out - D\_in}{D\_out + D\_in} \quad \textbf{(3.14)}$$

$$N = \frac{D\_out - D\_in + S}{2(W + S)} \quad \textbf{(3.15)}$$

B. Mutual Inductance

Currently lots of literature exists for the computation of the mutual inductance between coaxial coils. Since we address the problem of coil misalignment, mutual impedance computation for non-coaxial coils with angular misalignment is required and hence the derived closed form expressions [118] cannot be used. We hence propose a numerical computation of the mutual

inductance for our work. We use numerical approximations to the Neumann's integral to compute the mutual inductance between the coils.

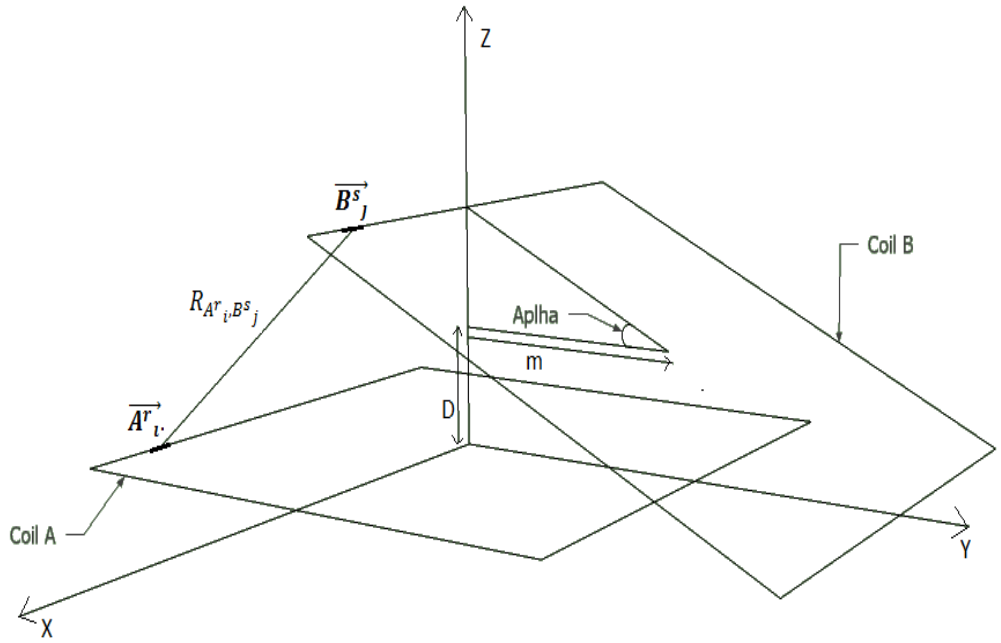

Figure 3-6 Geometrical representation of coils for Mutual Inductance computation

We present the procedure to compute the mutual inductance between two square planar inductors A and B as follows. Since the coils are not co-axial, evaluating the Neumann's integral is difficult. We approach this problem instead using the concept of partial mutual inductance. The partial mutual inductance between coil segments can be used to evaluate the mutual inductance between two loops though the converse is not true. We first divide the coils to straight line segments and then discretize these coil segments into sequential finer elements of length Δ_A and Δ_B respectively. By computing all the partial mutual inductance between any two such elements, one from the coil A and other from coil B and summing them up, we obtain the total mutual inductance between the two coils. By reducing the element size the accuracy of the method can be improved. The computational procedure is shown below. Consider the coils shown in Figure 3-6. Coil A and coil B are separated by a distance D and they are misaligned along the Y axis by a distance of m. The coil B also has an angular misalignment captured by the angle (α) the plane of

the coil B makes with the XY plane. Let $M_{A^r{}_i,B^s{}_j}$ is the mutual inductance between rth element in the ith segment of coil A and the sth element in the jth segment of coil B. For very small elements A_i^r and B_j^s, the mutual inductance can be approximated from Neumann's integral as

$$M_{A^r{}_i,B^s{}_j} = \frac{\mu_0}{4\pi} * \frac{\overrightarrow{\boldsymbol{A^r_i}}.\overrightarrow{\boldsymbol{B^s_J}}}{R_{A^r{}_i,B^s{}_j}}$$

(3.16)

The vectors $\overrightarrow{\boldsymbol{A^r_i}}$ and $\overrightarrow{\boldsymbol{B^s_j}}$ represent the current directional elements of A_i^r and B_j^s respectively and $R_{A^r{}_i,B^s{}_j}$ represents the distance between these two elements. The key assumption in converting the Neumann integral into summation is that the discretized current elements are small enough such that the distance between any two points, one from element A_i^r and the other from element B_j^s is the same for any such selection of points. Thus smaller the element, the more accurate the results are. The computational procedure is shown below.

Let $\overrightarrow{\boldsymbol{V(i)}}$, $\overrightarrow{\boldsymbol{W(j)}}$ denote the position vectors of ith vertex of coil A and jth vertex of coil B respectively. From basic geometry, the vertices of the primary coil turn edges can be computed as

$$\boldsymbol{V_x}(4i+k) = (-1)^{\left[\frac{k}{2}\right]}\left(\frac{D\_in_A}{2} + i(W_A + S_A) + \frac{W_A}{2}\right)$$

(3.17)

$$\boldsymbol{V_y}(4i+k) = (-1)^{\left[\frac{k-1}{2}\right]}\left(\frac{D\_in_A}{2} + i(W_A + S_A) + \frac{W_A}{2}\right)$$

(3.18)

$$\boldsymbol{V_z}(4*i+k) = 0$$

(3.19)

Where k =1 to 4, i = 0, 1, 2. . . (N_A -1) with N_A representing the number of turns in the coil A and [.] represents the greatest integer function. The suffix x, y and z denote the x, y and z component of the position vector $\overrightarrow{\boldsymbol{V}(\imath)}$ and $\overrightarrow{\boldsymbol{W}(\jmath)}$. To compute the co-ordinates of the vertices of the coil B, we proceed as follows. We first assume that the secondary coil is concentric and coplanar with the first coil and compute its vertices as

$$\boldsymbol{W'_x}(4*i+k) = (-1)^{\left[\frac{k}{2}\right]}\left(\frac{D\_in_B}{2} + i(W_B + S_B)\right) \tag{3.20}$$

$$\boldsymbol{W'_y}(4*i+k) = (-1)^{\left[\frac{k-1}{2}\right]}\left(\frac{D\_in_B}{2} + i(W_B + W_B)\right) \tag{3.21}$$

$$\boldsymbol{W'_z}(4*i+k) = 0 \tag{3.22}$$

Where k =1 to 4, i = 0, 1, 2. . . (N_B -1) with N_B representing the number of turns in coil B and [.] represents the greatest integer function. It should be noted that the vertices of the inner edge of the coil B were used to mark the boundary within which the total flux lines passing through would be computed (for that particular turn) using the Neumann's integral. The actual vertices are obtained by using the angular transformation followed by linear misalignment to represent the actual co-ordinates of the edges with respect to the centre of the coil A as shown below

$$\left[\boldsymbol{W_x}^{\boldsymbol{T}}\ \boldsymbol{W_y}^{\boldsymbol{T}}\ \boldsymbol{W_z}^{\boldsymbol{T}}\ \boldsymbol{X}\right] = \left[\boldsymbol{W'_x}^{\boldsymbol{T}}\ \boldsymbol{W'_y}^{\boldsymbol{T}}\ \boldsymbol{W'_z}^{\boldsymbol{T}}\ \mathbf{1}\right][\boldsymbol{R^1}(\alpha)] + [\boldsymbol{T}] \tag{3.23}$$

Where

$$\boldsymbol{R^1}(\alpha) = \begin{pmatrix} 1 & 0 & 0 & 0 \\ 0 & Cos\alpha & Sin\alpha & 0 \\ 0 & -Sin\alpha & Cos\alpha & 0 \\ 0 & 0 & 0 & 1 \end{pmatrix}$$

(3.24)

$$\boldsymbol{T} = \begin{pmatrix} 0 & m & D \\ \vdots & \vdots & \vdots \\ 0 & m & D \end{pmatrix}$$

(3.25)

It should be mentioned here that for the case of angular misalignment with all the co-ordinate axis, $\boldsymbol{R^1}(\alpha)$ needs to be replaced with the 3-axis rotational transformation matrix $\mathbf{R}^3(\alpha, \beta, \gamma)$. In-fact angular misalignment with respect to a line can also be accommodated with an appropriate transformation matrix. In this work, we will just limit ourselves to angular misalignment of coil caused by rotating it about one axis alone.

$$\overrightarrow{\boldsymbol{V}(\imath)} = [\boldsymbol{V_x}(i)\, \boldsymbol{V_y}(i)\, \boldsymbol{V_z}(i)]$$

(3.26)

$$\overrightarrow{\boldsymbol{W}(\jmath)} = [\boldsymbol{W_x}(j)\, \boldsymbol{W_y}(j)\, \boldsymbol{W_z}(j)]$$

(3.27)

The directional current elements are then computed as

$$\overrightarrow{\boldsymbol{A^r_\imath}} = \left(\overrightarrow{\boldsymbol{V}(\imath+1)} - \overrightarrow{\boldsymbol{V}(\imath)}\right) \Delta_A$$

(3.28)

$$\overrightarrow{\boldsymbol{B^s_\jmath}} = \left(\overrightarrow{\boldsymbol{W}(\jmath+1)} - \overrightarrow{\boldsymbol{W}(\jmath)}\right) \Delta_B$$

(3.29)

Where the $\wedge$ in ((3.32) & (3.33)) denotes unit vector and all the bold face quantities ((3.16) - (3.34)) represent arrays.

$$R_{A^r{}_i,B^s{}_j} = \left|(s-1)\overrightarrow{\boldsymbol{B^s_j}} - (r-1)\overrightarrow{\boldsymbol{A^r_\iota}} + \overrightarrow{\boldsymbol{W(\iota)}} - \overrightarrow{\boldsymbol{V(j)}}\right|$$

(3.30)

$$E_A(i) = \frac{\left|\overrightarrow{\boldsymbol{V(\iota+1)}} - \overrightarrow{\boldsymbol{V(\iota)}}\right|}{\Delta_A}$$

(3.31)

$$E_B(j) = \frac{\left|\overrightarrow{\boldsymbol{W(J+1)}} - \overrightarrow{\boldsymbol{W(J)}}\right|}{\Delta_B}$$

(3.32)

Where i = 1 to $4N_A$ and j = 1 to $4N_B$. The value of the mutual inductance is then computed as sum of all these partial inductances as

$$M_{AB} = \sum_{i=1}^{4N_A}\sum_{j=1}^{4N_B}\sum_{r=1}^{E_A(i)}\sum_{s=1}^{E_B(j)} M_{A^r{}_i,B^s{}_j}$$

(3.33)

And can be further modified using ((3.19) to

$$M_{AB} = \frac{\mu_0}{4\pi}\sum_{i=1}^{4N_A}\sum_{j=1}^{4N_B}\sum_{r=1}^{E_A(i)}\sum_{s=1}^{E_B(j)} \frac{\overrightarrow{\boldsymbol{A^r_\iota}}.\overrightarrow{\boldsymbol{B^s_J}}}{R_{A^r{}_i,B^s{}_j}}$$

(3.34)

Similar approach can be made to compute the mutual inductance between polygon shaped spiral coils by addressing the vertices $\boldsymbol{V}(i)$ and $\boldsymbol{W}(j)$ using the inner radius, pitch and the angle each side subtends at the centre and then following the procedure from ((3.23)- (3.34)) with slight modifications. For circular shaped coils, the procedure can be approximated to finding the mutual inductance between two n-sided polygonal spirals where n is large. From our

computations, we find that for n = 8, the mutual inductance computed was close to simulation results from HFSS for circular spirals with less than 10 turns. In this work, we will just stick to square planar inductors which are commonly used in many applications including biomedical implants.

C. Resistance

The AC resistance of the coil is affected by two important phenomena namely the skin effect and the proximity effect. Numerous works have derived the models for the planar traces in a PCB including either or both the effects. We use the principle presented in the classical work [131] to obtain the AC series resistance of the coil with rectangular cross section for our work.

D. Self-Resonant Frequency

The self-resonant frequency of the coil is the frequency at which the quality factor of the coil becomes zero. At this frequency the self-capacitance of the coil resonates with the inductance of the coil. The self-capacitance of the coil is obtained by using the work in [116]. The capacitance per unit length is given by

$$C = \frac{27.8}{\ln\left(1 + \frac{\pi S}{W+T}\right)} \left[\frac{pF}{m}\right]$$

(3.35)

Multiplying (3.35) by the length of the gap between the coil traces, we obtain the total self-capacitance of the coil. The self-resonant frequency of the coil is then computed from the self-capacitance and inductance as

$$f_r = \frac{1}{2\pi\sqrt{LC}} \; Hz$$

(3.36)

E. Effective Coil equivalent model

The square planar inductor built on an FR4 PCB with one ounce copper traces can be modelled as shown in Figure 3-7. The equivalent model of the coil is used to obtain the effective coil parameters as shown below in ((3.37- (3.38)).

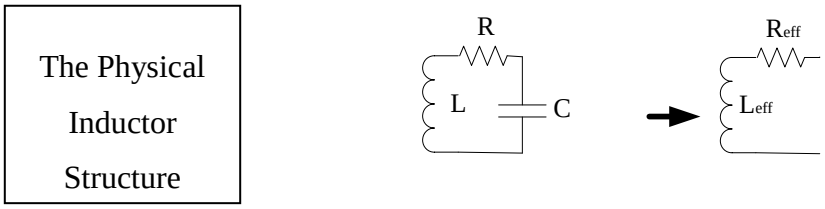

Figure 3-7 Equivalent circuit model of the square planar inductor

$$L_{eff} = \frac{L}{1 - \left(\frac{f}{f_r}\right)^2} \tag{3.37}$$

$$R_{eff} = \frac{R}{\left(1 - \left(\frac{f}{f_r}\right)^2\right)^2} \tag{3.38}$$

The values of R_{eff} and L_{eff} represent the effective resistance and inductance as can be measured from the terminals of the coil. The model described so far in this section for square planar inductors will be used alongside ((3.8)-(3.11)) to compute the PTE of the WPT link with and without IX theoretically.

3.6 Experimental Verification

To verify the PTE of the IX-coil method, we built 3 identical square planar coils as specified in Table 3-1.

Number of turns	16		
D_in	7 mm		
D_out	25.4 mm		
W	0.2 mm		
S	0.2 mm		
	Theory	Measurement	HFSS
L effective	4.90 µH	4.81 µH	4.73 µH
R effective	3.19 Ω	3.20 Ω	3.33 Ω
Self-Capacitance	4.7pF	5.1 pF	5.2 pF

Table 3-1 Coil geometry and parameters (Measured vs. theoretical vs. HFSS) at 4MHz (frequency of operation)

The orientation of the coils in the IX system is better explained through Figure 3-8. For all our experiments, the lateral misalignment of the coils refers to the misalignment along Y axis shown as D_{TR} and D_{TI} in Figure 3-8. The angular misalignment of the coils refers to the angle, the plane of the coil makes with the XY plane shown as θ_{RX} and θ_{IX} in Figure 3-8.

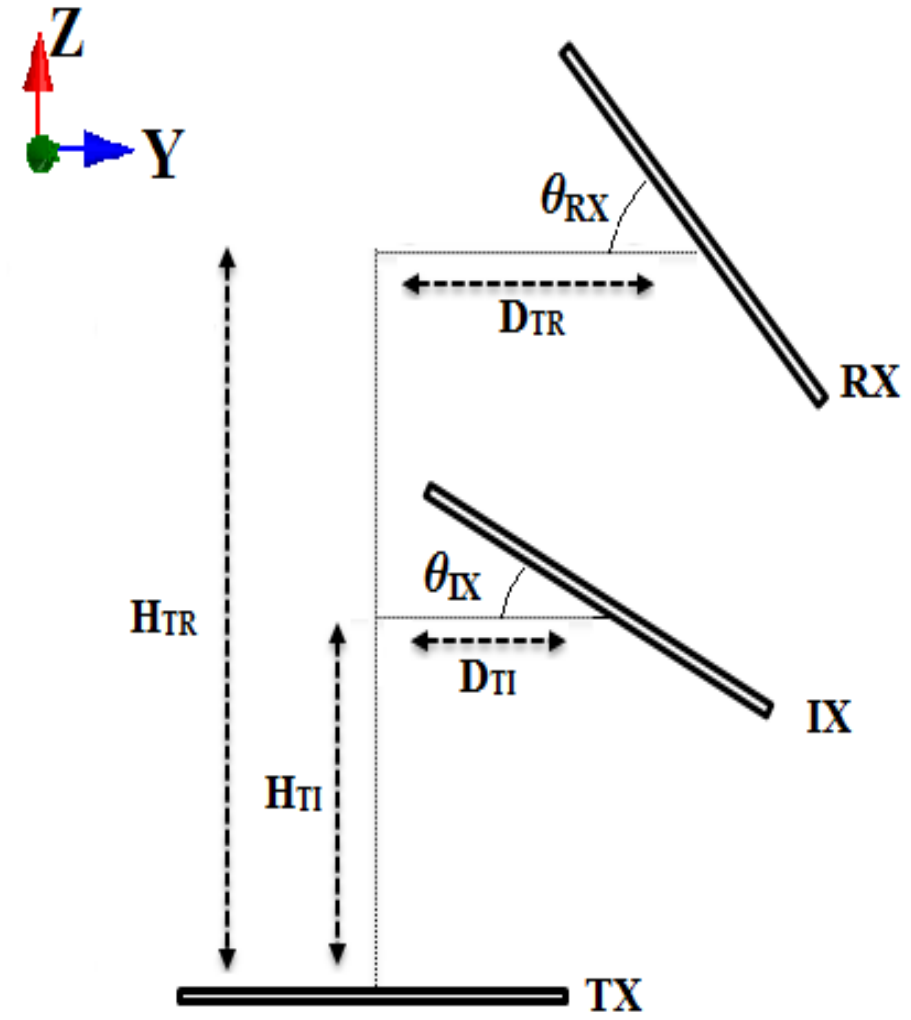

Figure 3-8 Orientation of the coils in the three coil system with notations for coil separations and coil orientations specified.

θ_{RX} *-Angular Misalignment of RX coil with respect to TX coil*

θ_{IX} *-Angular Misalignment of IX coil with respect to TX coil*

D_{TR} *-Lateral Misalignment of RX coil with respect to TX coil*

D_{TI} *-Lateral Misalignment of RX coil with respect to TX coil*

H_{TR} *-Separation between TX coil and RX coil*

H_{TI} *-Separation between TX coil and IX coil*

The TX, RX and IX are identical coils. We measured the PTE of WPT link using the setup pictorially represented in Figure 3-9. The TX coil was excited by a signal generator at 4 MHz (Agilent E8257D). The voltage across the load (50 ohm) connected to the receiving coil was measured using an Oscilloscope. Since the input is not matched to 50 ohm, the power input was computed after compensating for the return loss as shown in Figure 3-9. We first measure the PTE of the intermediate coil system in which the TX and RX are aligned to each other and IX is slowly moved along the Y axis creating lateral misalignment (D_{TI} = 0mm, 5mm, 10mm, 15mm). All the three coils have no angular misalignment and they all lie in planes parallel to the XY plane. We repeat this experiment for various separations of IX from TX

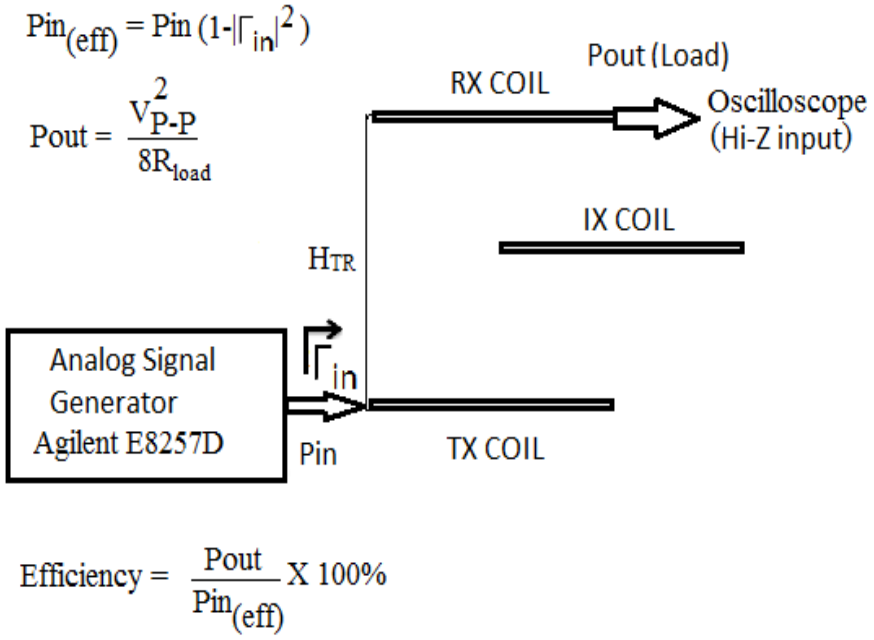

Figure 3-9 Pictorial representation of the measurement setup

The PTE was then theoretically computed using our models in previous section. The measurements were not done for all the positions due to the restrictions imposed by the fixtures. The measured results are compared with theoretical results and plotted in Figure 3-10. The experimental results agree

with the results predicted by the model. The difference between the results is acceptable and is due to the approximations done in computing the mutual inductance between the coils.

Since models have been developed to compute mutual inductance of square planar coils which have angular misalignment with respect to each other in previous section, it is possible to evaluate the 3-coil method for various angular orientations of IX as well. We now measure PTE of the intermediate coil system where TX and RX are perfectly aligned to each other having a separation H_{TR} = 30mm. The IX is positioned midway between TX and RX and has a separation H_{TI} = 15 mm.

The PTE values were measured for various angular misalignment (θ_{IX} = 0^o, 45^o, 90^o) of IX using the same procedure depicted in Figure 3-9. The experiment was repeated with various lateral misalignment of the IX (D_{TI} = 0mm, 5mm, 10mm). The corresponding PTE values were then computed using the models in V. The comparison between the computed and measured PTE values for the intermediate coil system with angular misalignment of IX is shown in *Figure* 3-11. The PTE was measured only for certain orientations that are possible using standard fixtures as mentioned in the caption of *Figure* 3-11.

From the PTE plots shown in Figure 3-10 and *Figure* 3-11, it is noted that there are positions and orientations of the IX coil that might lead to reduction in PTE. From Figure 3-10, we observe that the PTE reduces as the IX coil is moved away (increasing D_{TI}). The PTE is maximized when the IX coil is roughly midway between the TX and RX coils, irrespective of D_{TI} (lateral misalignment of IX coil from the TX and RX coils). From Figure 3-10 we also observe that for a 3-coil WPT link, the IX coil can have angular misalignment ($\theta_{IX} \neq 0^o$) with respect to the TX coil, but still can have better PTE than a traditional WPT link. The coils used in the experiment are shown in Figure 3-12.

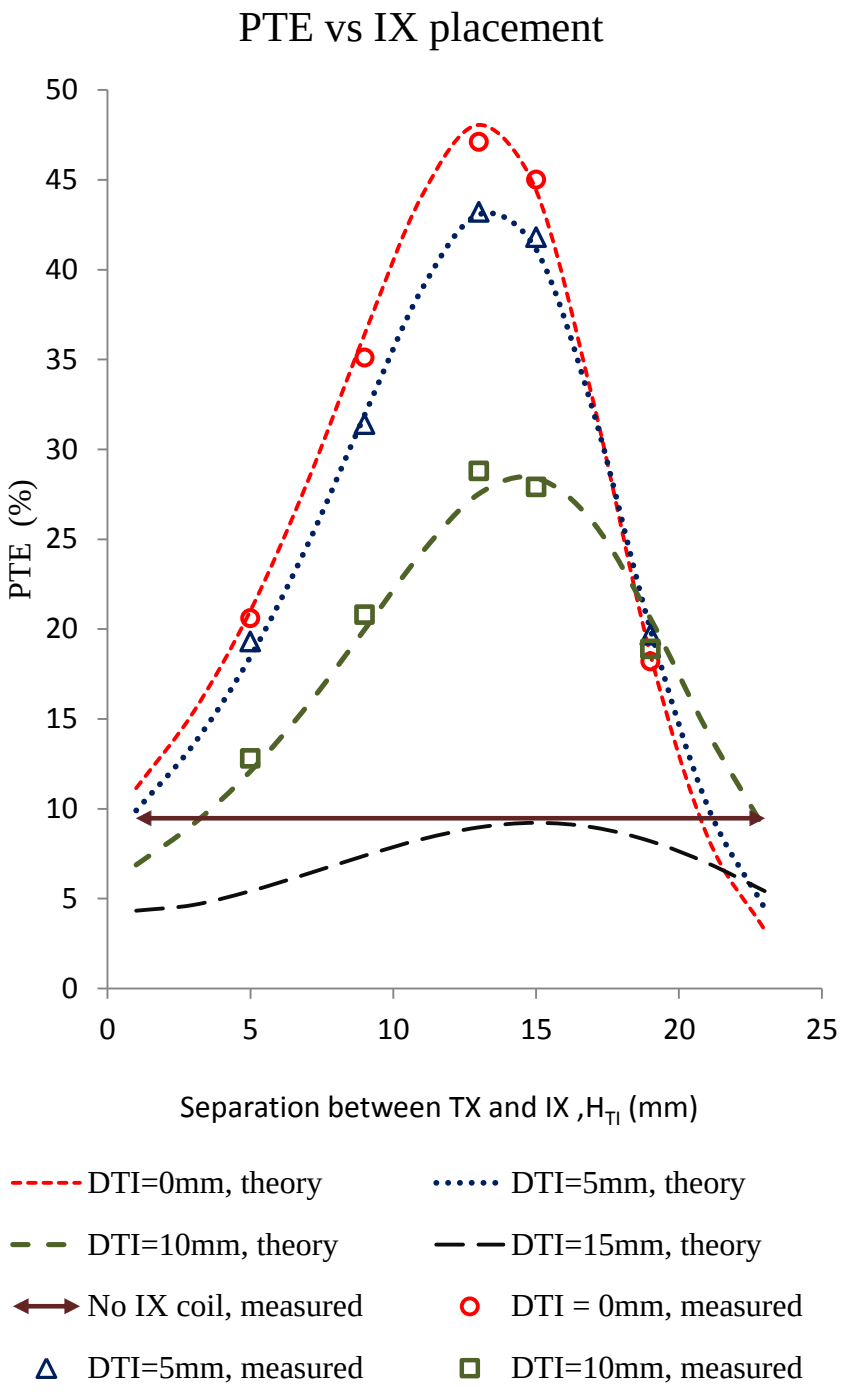

Figure 3-10 Plot of PTE vs. Efficiency for lateral misalignment of the IX, H_{TR}= 30 mm, D_{TR} = 0 mm, θ_{IX} = 0°, θ_{RX} = 0°, R_L=50 ohm.

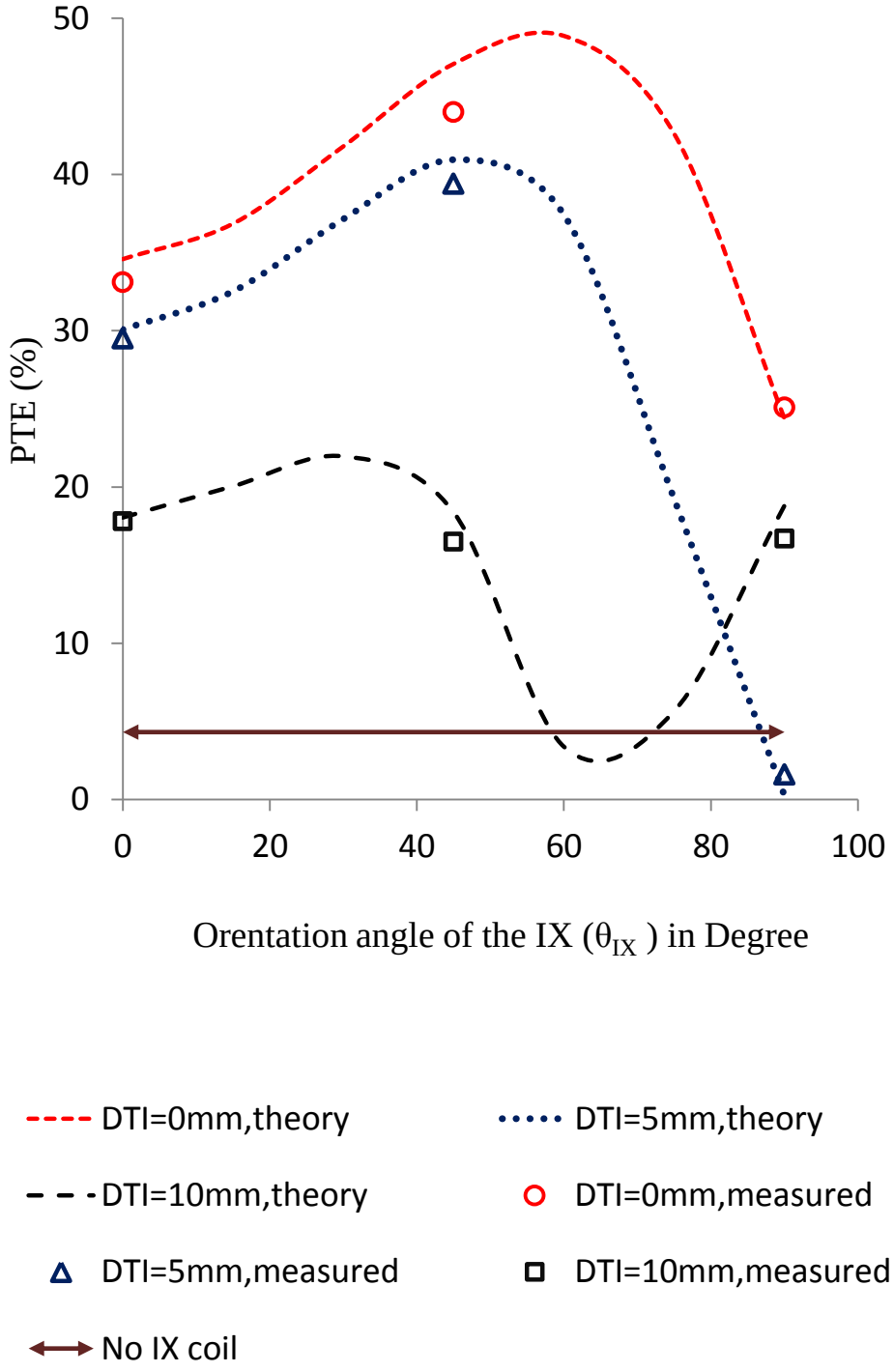

Figure 3-11 Plot of PTE vs. orientation at different misalignments of the IX, H_{TR}= 25.4 mm, HTI = 15 mm, θ_{RX} = 0^o, D_{TR} = 0 mm, R_L=50 ohm, θ_{IX} (experimental) = 0^0, 45^0, 90^0.

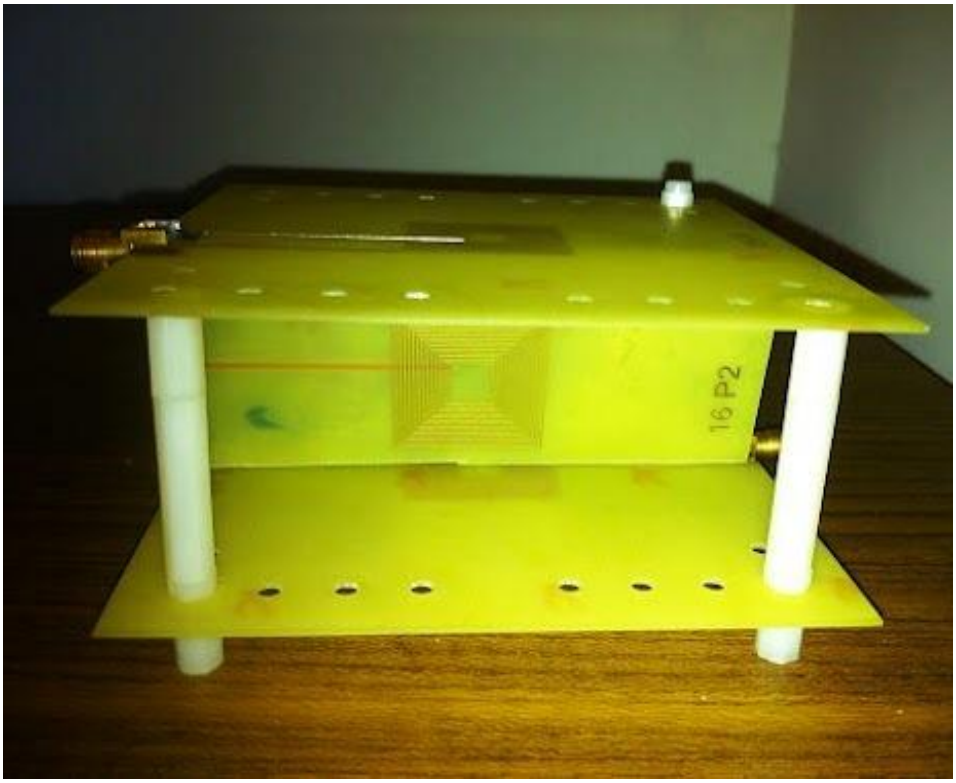

Figure 3-12 Experimental set-up used for verifying PTE of three coil topology

3.7 Using the magnetic fields of induced currents favourably:

For a traditional WPT link, introducing a resonant tuned passive coil can improve the PTE as has been proposed earlier and from the results shown in earlier section. However the passive structure needs to be properly positioned to harness the flux linkage boosting, failing which the effects can be detrimental. We look at IX coil placement for WPT links that use square planar inductors. The most general form of the WPT link used in biomedical implants, wireless chargers and RFID comprises of planar inductors as they have a thin form factor. A typical WPT link with planar inductors is shown in Figure 3-13

It is quite clear that introducing an intermediate coil in region between the coils alone can improve the PTE of the existing link. However positioning an IX in this region does not necessarily guarantee a PTE improvement of the existing link and needs careful assessment. We try to quantify the PTE

improvement for different positions of the IX coil using contour plots and identify positions of IX coil in region between the TX and RX coils, which can boost PTE. We will assume that the IX coil does not have any angular misalignments with the TX coil ($\theta_{IX} = 0^o$) and proceed with quantifying the PTE improvement. The same procedure can be extended for various orientations of the IX ($\theta_{IX} \neq 0^o$) as the models built are still valid, but will not be presented in this thesis for brevity.

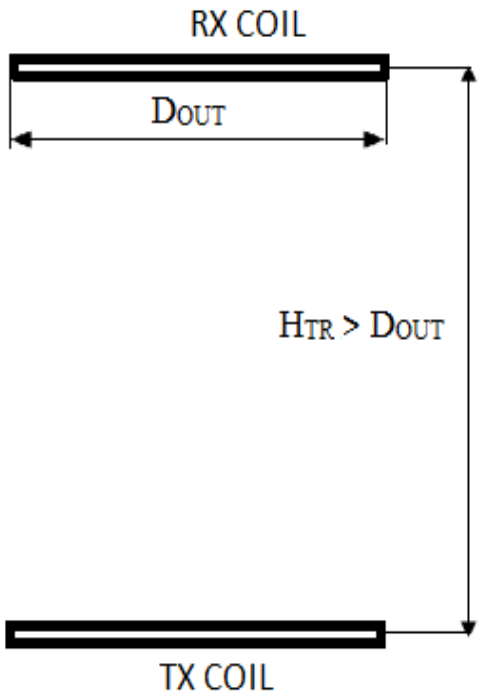

Figure 3-13 Traditional WPT link with large separation

We first consider a traditional WPT link with two coils TX and RX (as specified in Table 3-1 which are properly aligned to each other (D_{TR}=0 mm, H_{TR}=25.4 mm, $\theta_{RX} = 0^o$). We numerically compute the PTE of the link using the models presented in earlier section and (3.11). Now we numerically compare this PTE with the PTE of a 3-coil system by introducing an IX coil (which is identical to the TX and RX coils) for various positioning of the IX coil in the region between the TX and RX coils (Figure 3-13) and arrive at contour plots based on the mutual inductances (M_{TX} and M_{RX}), the newly

introduced IX coil has with TX and RX coils respectively as shown in Figure 3-14. If an IX Coil is introduced into a traditional WPT system, then based on the mutual inductances M_{TX} and M_{RX}, the PTE improvement can be easily quantified using the contour plot shown in Figure 3-14. Based on the location of the IX coil, we can compute the values of M_{TX} and M_{RX} and locate it in the plot to have an idea of how much additional efficiency can be obtained by placing the IX coil in that particular position.

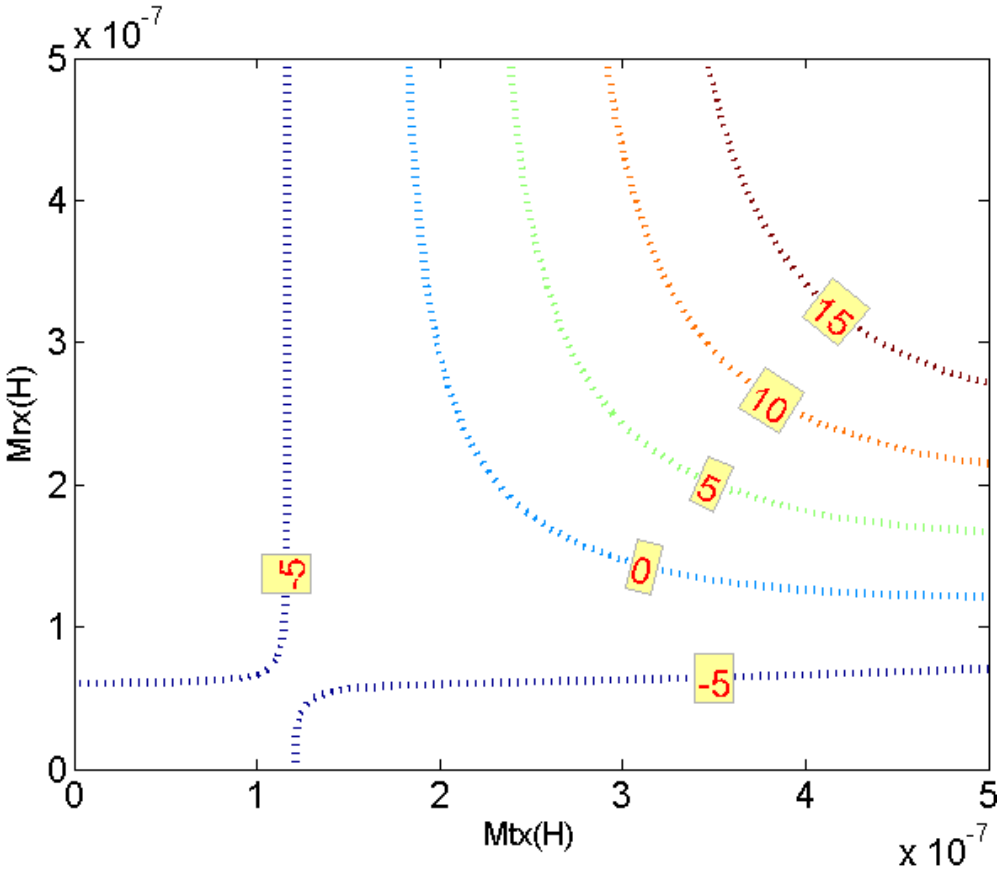

Figure 3-14 Efficiency improvement chart for various allowed values of Mtx and Mrx, H_{TR}= 30 mm, D_{TR} = 0 mm, θ_{IX} = 0°, θ_{RX} = 0°, R_L=50 ohm

The contour plot shown above has contours that represent the locus of M_{TX} and M_{RX} for equal efficiency improvement. For example, choosing the mutual inductance M_{TX} and M_{RX} associated with the IX coil, along the line marked as 10 will add another 10% to the PTE of the traditional two-coil WPT link. As

can be seen, for low values of either M_{TX} or M_{RX} the efficiency improvement is negative suggesting that there is a decrement in PTE if the IX coil is placed close to one coil (TX/RX) and far away from the other (RX/TX). Now going back to Figure 3-13, in the region between the TX and RX coils, if the IX coil is moved close to the TX coil, then M_{RX} reduces and hence change in PTE can be negative. If the IX coil is placed close to the RX coil, M_{TX} reduces and the again the change in PTE can be negative. Thus it is clear that the optimal location of the IX coil should be where both M_{TX} and M_{RX} are sufficiently large so that power can be relayed from TX coil to RX coil. From the contour plot, we observe that the contour lines roughly approximate rectangular hyperbolas with respect to M_{TX} and M_{RX}. Thus the position of the IX coil is optimal when the product of M_{TX} and M_{RX} is maximized. This corresponds to a position midway between the TX and RX coils as moving IX coil closer to either coil reduces the mutual inductance between IX coil and the farther coil. This argument is also supported by the results shown in Figure 3-10. We compute the mutual inductances M_{TX} and M_{RX} for each position of the IX by varying H_{TI} from 1mm to 23mm in steps of 2mm and repeat the same for different D_{TI} = 0 mm, 5 mm, 10 mm, 15 mm and 20 mm. We plot the computed mutual inductances alongside the contours (already shown in Figure 3-14) to see how each position of the IX coil fares in improving the PTE as shown in Figure 3-15.

As can be seen, when the IX coil is aligned with the TX and RX coils (D_{TI} = 0 mm), there is maximum PTE improvement. When the IX coil is placed at D_{TI} = 15 mm, the PTE improvement is negative which agrees with the PTE results shown in Figure 3-10.

Thus using the contour plot in Figure 3-15, we conclude that positioning the IX (for $\theta_{IX} = 0^o$) in the region bounded by 7mm<H_{TI}<17mm and |D_{TI}| < 15mm can alone improve the PTE and placing the IX outside this region does not provide any PTE improvement and can be detrimental to the functioning of the existing WPT link.

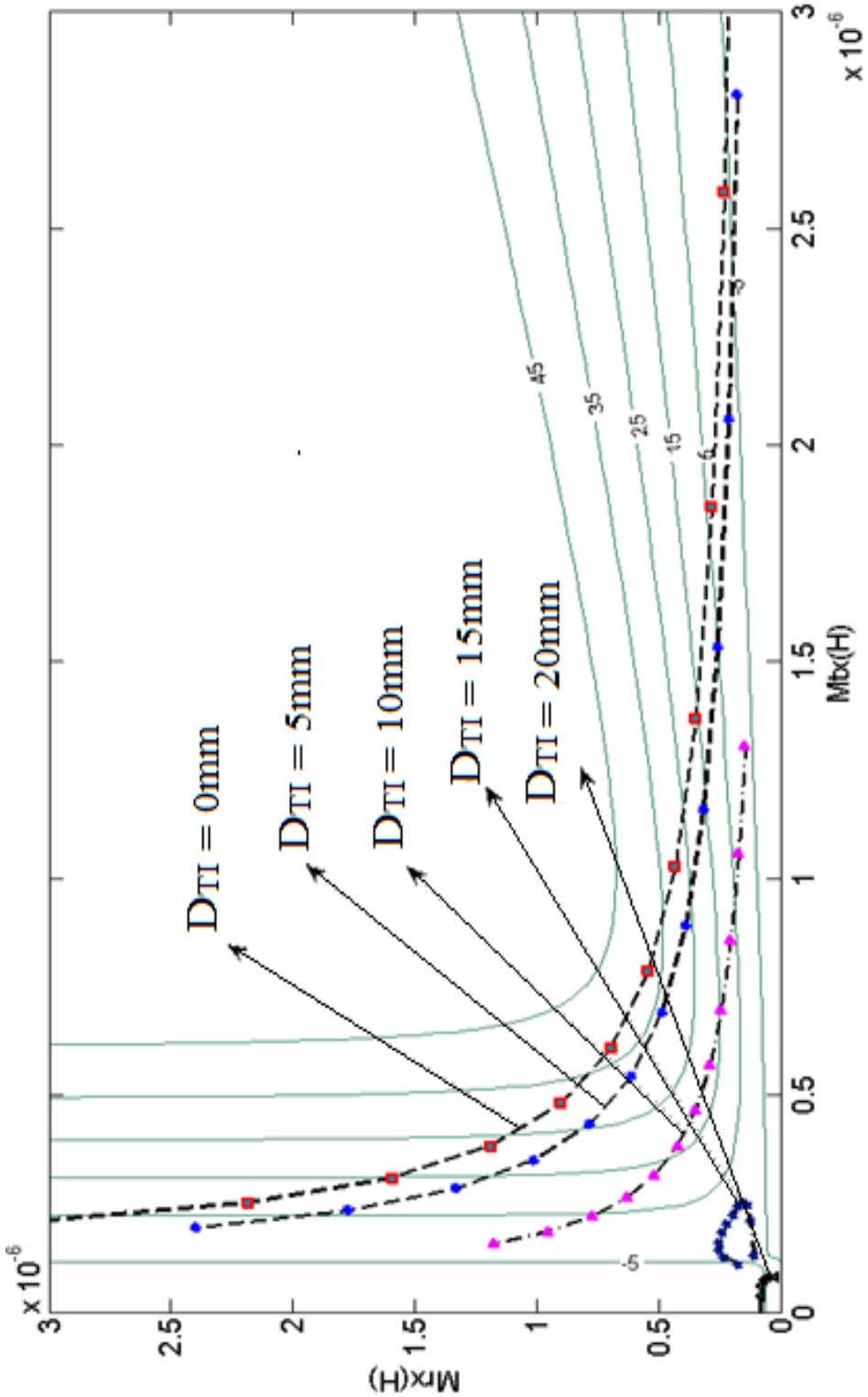

Figure 3-15 Position of the IX coil vs. efficiency improvement, by using the contour map for the WPT link, H_{TI} = 1mm, 3 mm... 23 mm; D_{TI} = 0 mm, 5 mm... 20 mm, H_{TR}= 30 mm, D_{TR} = 0 mm, $\theta_{IX} = 0^o$, $\theta_{RX} = 0^o$, R_L=50 ohm.

It should be noted that for a different IX, this region that favours PTE improvement will also be different and can be evaluated using the same method. Thus using the models in IV and the expression for PTE ((3.11) - (3.14)), we can localize the position of the IX coil to improve PTE of the link.

Thus it is shown that positioning the IX coil can be quantified based on PTE improvement using the contour plots built using the developed model for WPT link. With the model available for wireless power link with square planar inductors, the same procedure can be followed to evaluate the positioning of the IX coil in a specific area as allowed by the real application needs.

3.8 Overcoming motion artifacts:

The usage of an IX coil to improve the PTE of traditional WPT links with large separation has been proposed and discussed both quantitatively and qualitatively. The other main advantage of the IX-coil system is its inherent ability to perform robustly under small disturbances to the RX coil (due to motion artifacts as the RX coil can be in a moving frame). The inherency stems from the basis behind the functioning of the IX-coil method. When the IX coil is introduced, the RX coil has a better coupling with the IX coil than it earlier had with the TX coil as shown earlier. Most of the power delivered to the RX coil is due to the currents flowing in the IX coil. Since disturbances tend to affect loosely coupled coils more than strongly coupled coils, small disturbances to the RX coil caused possibly by motion artifacts tend to affect the traditional WPT link more in the absence of IX coil.

The introduction of IX coil can hence improve the robustness of the link to motion artifacts. To verify this qualitatively, the key metric we use is the percentage reduction in power that is delivered to the load due to small disturbance of the RX coil. We compare this metric for the case of a normal WPT link and a WPT link with IX coil by introducing small lateral misalignment ($D_{TR} \neq 0$) of the RX coil.

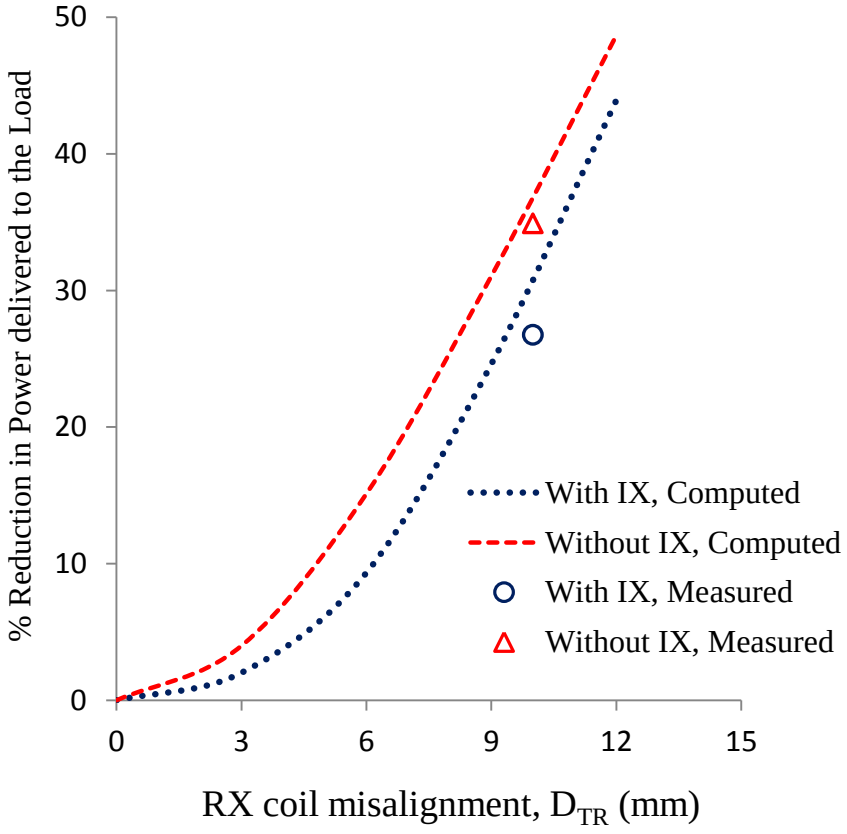

Figure 3-16 Comparison of power transfer drop with RX misalignment between traditional WPT method and WPT with IX coil, H_{TR}= 25.4mm, H_{TI} = 13mm, θ_{IX} = 0°, θ_{RX} = 0°, D_{TI} = 0 mm, R_L=50 ohm.

The experimental set-up consists of identical TX, RX and IX coils as described in Table 3-1with H_{TR}= 25.4mm, H_{TI} = 13mm, θ_{IX} = 0°, θ_{RX} = 0°, D_{TI} = 0 mm. We mimic small disturbance to RX by introducing lateral misalignment D_{TR} and compute the PTE for the two cases (normal WPT link and WPT link with IX coil) using ((3.8) - (3.11)). We then compute the drop in power delivered to the load due to misalignment ($D_{TR} \neq 0$) by subtracting the PTE of the aligned position (D_{TR} = 0) and normalizing it. The PTE values for one particular misalignment set-up (D_{TR} = 10 mm) was alone measured based on the availability of fixtures on the board. The corresponding percentage power drop was then computed and shown in Figure 3-16. It can be seen from the plot that the introduction of IX coil can mitigate the power drop due to motion artifacts in the RX coil. Having explained how the three-coil

topology can be robust to small RX coil disturbance that arise due to motion artifacts, we further the idea to power permanently misaligned RX coil, thus enabling misaligned WPT links with acceptable PTE. In this section, we will show how the WPT link with misaligned RX coil can operate more efficiently. The three practical scenarios which arise in the design of misaligned WPT links are as follows.

1. The RX coil has a lateral misalignment with the TX coil

2. The RX coil has an angular misalignment with the TX coil

3. The RX coil has both lateral and angular misalignment.

We discuss each of these scenarios separately as in the next few sections of this chapter.

3.9 Lateral Misalignment of RX Coil

Consider the case in which there is a requirement to transmit power to an RX coil which is laterally misaligned ($D_{TR} \neq 0$). We demonstrate the improvement of PTE due to the introduction of the resonant tuned passive IX coil and study the behaviour of PTE with various positions of the IX coil. For this study, we used new setups which have different RX coils and have similar TX and IX coils as shown in Table 3-2 and Table 3-3. The PTE of the WPT link at the tabulated positions was then evaluated theoretically using models in earlier section and ((3.8) - (3.11)). The corresponding values of PTE were measured using the same procedure depicted in Figure 3-9 at an operating frequency of 3MHz. The set-up used is shown in Figure 3-17. The comparison between the theoretical results and measured results are shown in the graphs in Figure 3-18-Figure 3-20. From the graphs we observe that misaligned coils can be powered more efficiently by introducing a resonant tuned passive IX coil and positioning it properly. In fact the PTE improvement is very significant.

	Coil A	Coil B
Number of turns	20	11
Internal diameter	10 mm	10 mm
External diameter	49 mm	20.4 mm
Width of trace	0.5 mm	0.2 mm
Pitch of the spiral	1 mm	0.5 mm
L effective	12.8 µH	2.84 µH
R effective	4.47 Ω	2.80 Ω

Table 3-2 Geometry and measured parameters (at 3MHz) of the coil used to validate the analysis

We infer the following from the results of the experiment. For a traditional WPT link, the power delivered to the load reduces by more than 50%, as the RX coil is moved away from the TX coil (H_{TR} = 22mm to 32 mm). For the same scenario, introducing an IX coil reduces the power drop as the PTE reduction is less (around 10% drop in PTE). This is due to the fact that for a traditional power link, the PTE reduces roughly as the square of distance and hence at larger separations, the PTE drop with distance is much higher. The other key advantage of the IX coil method as can be seen from Figure 3-18-Figure 3-20 is that for a fixed position of IX coil, the position of RX can vary without significantly altering the PTE. For a given position of RX, varying the IX coil does not significantly affect the PTE as shown in the graphs below.

Thus it provides the flexibility to position the IX coil at various locations as the end application requires.

	Set-up A1	Set-up A2	Set-up A3
TX	Coil A	Coil A	Coil A
IX Coil	Coil A	Coil A	Coil A
RX	Coil B	Coil B	Coil B
H_{TI}(Fixed)	11mm	11mm	11mm
D_{TR}	12mm	22mm	22mm
D_{TI}	12mm	22mm	12mm

Table 3-3 Description of Set-ups used in the experiment

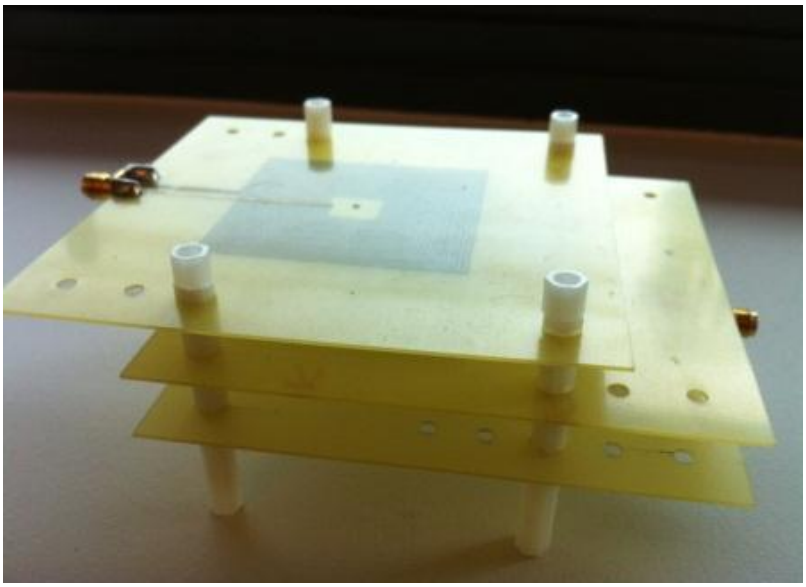

Figure 3-17 The experimental set-up used to verify PTE of misaligned links

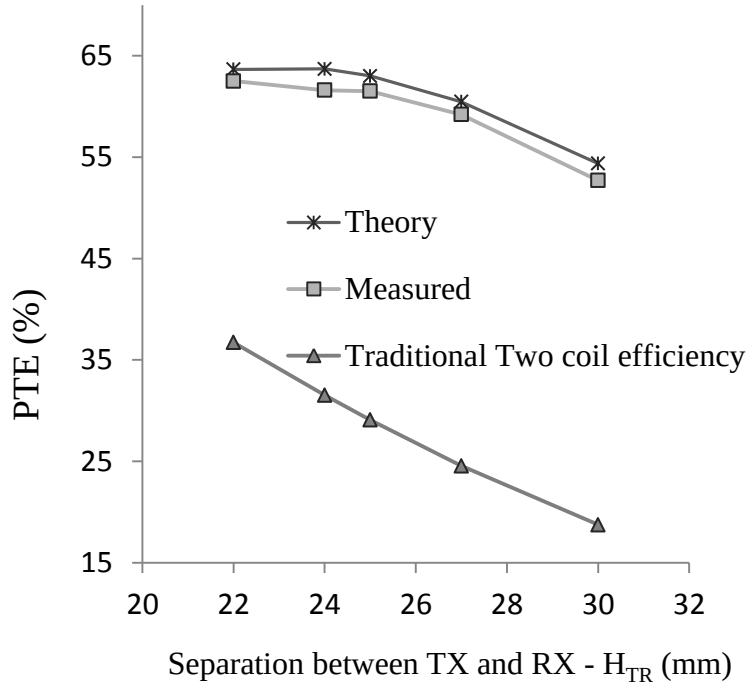

Figure 3-18 Set-up A1, H_{TI} = 11mm, D_{TI} = 12 mm, D_{TR} =12mm, $\theta_{IX} = 0^o$, $\theta_{RX} = 0^o$

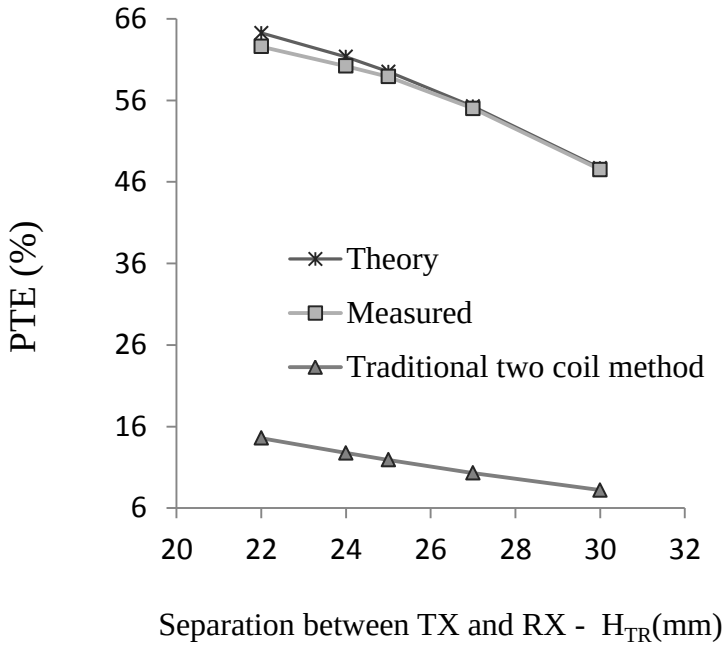

Figure 3-19 Set-up A2, H_{TI} = 11mm, D_{TI} = 22 mm, D_{TR} =22mm, $\theta_{IX} = 0^o$, $\theta_{RX} = 0^o$

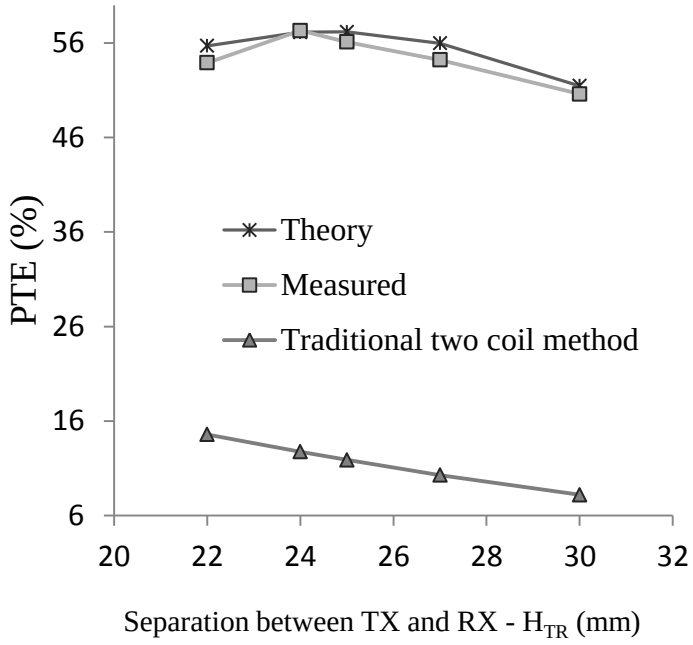

Figure 3-20 Set-up A3, H_{TI} = 11 mm, D_{TI} = 12 mm, D_{TR} = 22 mm, $\theta_{IX} = 0^o$, $\theta_{RX} = 0^o$

Experimental results of PTE using the IX coil method versus the traditional two coil WPT method, R_L=10 ohm.

3.10 Angular Misalignment

We now consider the case where the RX coil has an angular orientation with respect to the TX coil ($\theta_{RX} \neq 0$) however is aligned laterally ($D_{TR} = 0$ mm). For this, we consider a 3-coil WPT system with identical TX, IX and RX as given in Table 3-1. The set-up had H_{TR} = 30 mm, D_{TI} = 0 mm, D_{TR} = 0 mm, $\theta_{IX} = 0^o$. We compute the PTE of this 3-coil link for various angular misalignments of the RX coil ($\theta_{RX} = 0^o$ to 45^o) and repeat it for different separation of IX (H_{TI} = 12 mm to 18 mm).

By doing a sweep across H_{TI}, we can find the optimal H_{TI} for each angular orientation of the RX. The set-up to study the PTE of this scenario was completely computed as it is difficult to verify experimentally by making fixtures for all possible orientations. It is also possible to sweep the angular orientation (θ_{IX}) of the IX coil, to obtain the optimal value, as the models for

computing mutual inductance between coils with angular misalignment has been developed in earlier section. We will however not consider that case for brevity.

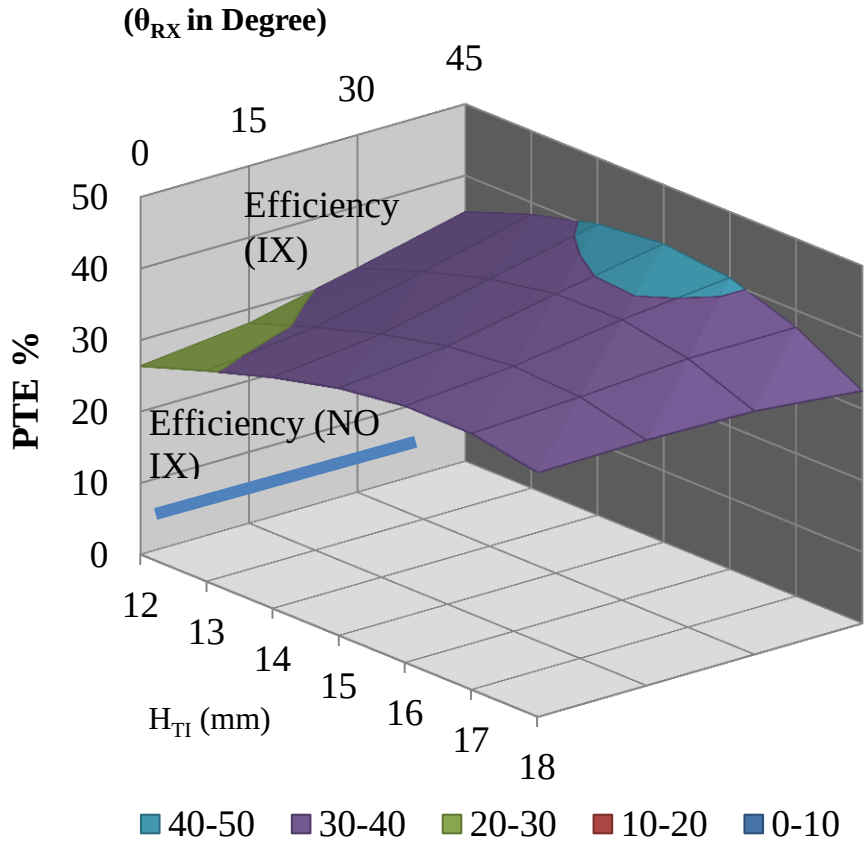

Figure 3-21. PTE vs position of IX Coil for different angular misalignment of RX, H_{TR} = 30 mm, D_{TI} = 0 mm, D_{TR} = 0 mm, θ_{IX} = 0°, R_L=50 ohm

The optimal positions of the IX coil (H_{TI}) for θ_{IX}=0° and D_{TI} = 0mm were found for various angular orientations of the RX coil to be between 13mm and 15mm. The corresponding value of PTE in the absence of IX coil was around the 5% mark. From the graph shown in Figure 3-21, we see that the 3-coil method can be used to efficiently power links where the TX and RX coils do not have angular alignment. It is also possible to find the optimal location of the IX coil for a given TX-RX set-up using the developed theory and models.

3.11 Both Angular and linear misalignment

We now consider the case where the RX coil has both lateral and angular misalignment ($\theta_{RX} \neq 0$, $D_{TR} \neq 0$). For this, we consider a 3-coil WPT system with identical TX, IX and RX as given in Table 3-1. The set-up had H_{TR} = 30 mm, H_{TI} = 15mm, D_{TR} = 0 mm, θ_{RX} = 45°, D_{TR} = 10 mm. For this set-up, we identify the optimal position (D_{TI}) and orientation (θ_{IX}) of IX by sweeping across the two variables. The optimal position of IX coil for H_{TI} = 15mm was found to be when IX coil has a lateral misalignment of 8mm and has no angular orientation with respect to TX (D_{TI} = 8mm, θ_{IX} = 0°).

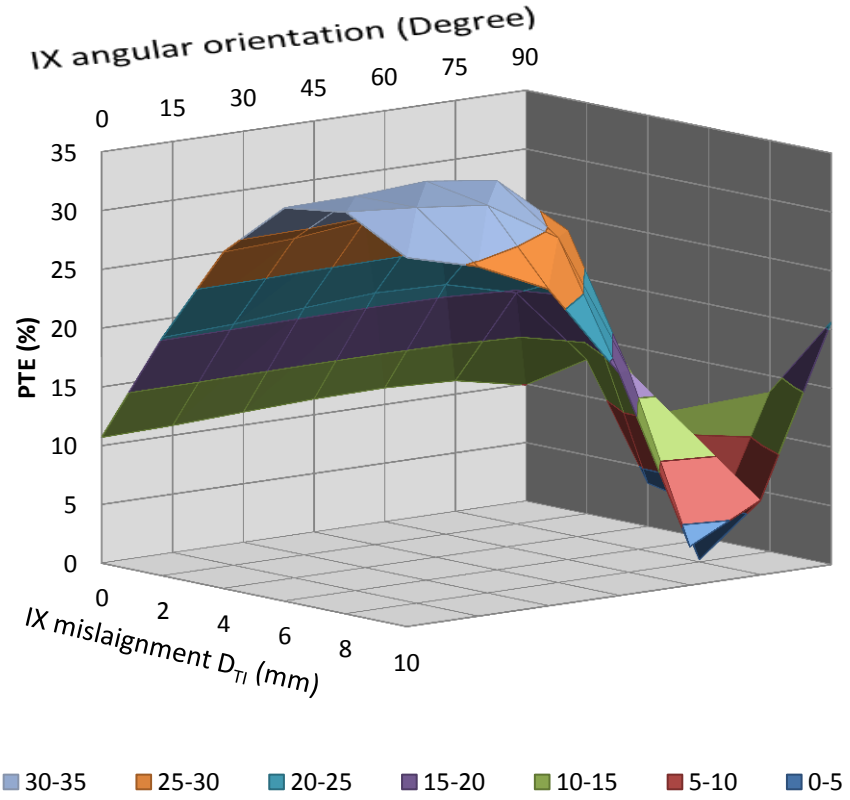

Figure 3-22 PTE vs. optimal position of the IX Coil, H_{TR} = 30 mm, H_{TI} = 15mm, D_{TR} = 0 mm, θ_{RX} = 45°, D_{TR} = 10 mm, R_L=50 ohm

The computed PTE sweep across the two variables is shown in Figure 3-22. The maximum PTE computed was 34%. The corresponding value of PTE in

the absence of the IX coil was less than 2%. The maximum PTE point was also verified experimentally and the efficiency measured was 36.5% which is close to the predicted value of 34%.

3.12 Discussion

We can infer the following from the work presented in this chapter as shown below

1. The PTE of WPT links with large separation can be improved by introducing a passive intermediate coil (IX coil) and positioning it aptly.
2. The positioning of the IX coil is vital in improving the PTE and can have detrimental effects if not properly positioned.
3. Using contour plots, a mapping between placement of the IX coil and PTE improvement can be obtained using the models provided in V and hence prediction of the apt positions of the IX coil is possible.
4. The IX coil can also be tilted (oriented with respect to the TX coil) to suit application needs. However it should be evaluated using the contour plots before being used.
5. The IX coil helps regulate the received power fluctuation which is generally caused by motion artifacts.
6. Misaligned power links can be operated much more efficiently by introducing a passive IX coil. The optimal positioning of IX coil can also be obtained using our model as has been shown.

Thus there are a plenty of advantages that can be obtained by introducing a passive intermediate coil in a traditional WPT link. The advantages have been stated both subjectively and objectively in this work. Experimental verifications for the same have been provided. Practical applications of this work are aplenty. First and foremost, it should be mentioned that there are some aspects of the IX coil that eases its practical usability.

1. The IX coil is passive with the capability of being completely planar (using distributed capacitance for resonance tuning) and coupled with a thin form factor, it can easily fit into an existing traditional WPT link.
2. Since the IX coil is a standalone system, it can be placed at various positions as allowed by the application without much dependence on the TX and RX coils. Since planar coils can be printed on many substrates including flexible ones [132], it can be integrated into the chassis of many systems without consuming additional space.

The use of this method can serve the following applications. Wireless charging in table-tops where the intermediate coils in the form of table mats can extend the charging range. Liver implants (flow sensor implant) where the separation between the coils is larger than the implant dimensions, can benefit from this method. Retinal implant where the implanted coil is constantly in motion due to the rotation of eye can benefit from this method. The eye socket provides an excellent space for housing the intermediate coil just outside the eye ball which has the implanted RX coil. RFID systems can extend their range of operation using passive intermediate coils acting as a relay for the reader.

3.13 Summary:

WPT over large separations can be made more efficient using a passive intermediate coil which is also tuned to the same frequency of operation. A detailed analysis on the theory behind this method has been provided in this work. The complete theoretical model for computing the PTE of a WPT link with an IX coil has been derived and verified experimentally for the most common square planar inductors. The proper use of the intermediate coil, it's positioning and advantages (PTE improvement over large separation, regulating the power fluctuation due to motion artifacts and powering misaligned links) have been explained with experimental results that correlate well with the results from theory.

Chapter 4: Capacitive power transfer links for biomedical implants

4.1 Introduction to capacitive wireless power transfer links

Wireless Power Transmission using inductive coupling has been the main method in use today for transferring power to implanted devices as have been shown in [39]-[99]. Good power transfer efficiency of the inductively coupled power link combined with resonant tuning and numerous optimization methods have made it the number one choice for the powering of biomedical implants. The IPT system uses the magnetic field coupling to transfer energy from TX to RX. This raises a question whether power transfer can be achieved by electric field coupling? The answer is yes and it is very much happening in capacitors. The added advantage is that the field lines are confined within the plates of the capacitor, thereby suggesting better coupling than what exists in an IPT link. However there is a catch. The field lines though confined within the plates reduce quickly as we move away from the plate. Hence it is advisable to transfer power wirelessly using capacitive coupling, provided the plates are very close.

Capacitive coupled links have been discussed for use in wireless chargers in [133]. However no work exists that proposes the use of CPT links for transcutaneous power transfer. There are two main reasons that stop CPT from being used in the powering of biomedical implants. The main deterrent is the fact that for small dimensions (<250 mm$^{\wedge 2}$) allowed by the implant device, the capacitance between the TX and RX plates is very less (few fF) even for a separation of few mm. Smaller the capacitance, larger the reflection at the input and more power needs to be input to the TX to maintain the power required at the RX. More input power generates large fields increasing tissue losses and heat dissipation. Also larger inductances are required to form resonant tanks to provide good matching at the TX input. The second deterrent is the fact that frequency detuning occurs even if there is a small misalignment between the TX and RX as the capacitance changes.

If we overcome these two challenges, CPT links can be used to power the biomedical implants. In this chapter we propose the use of CPT for specific applications in transcutaneous powering based on the following adaptations

1. Transcutaneous powering of implants is possible when the implanted RX is close to the skin surface as the distance between TX and RX is less, increasing capacitive coupling. The large capacitive impedance (large reflection) can be reduced significantly by the use of high frequency of operation thus enabling us to work with low input power, reducing the field strengths which in turn reduce tissue losses.

2. The frequency detuning affects the power handling of the CPT system. Increasing the size of the TX plates (TX plate alone is slightly increased and RX remains the same) easily decreases the variation in capacitance cased due to misalignments and hence reducing frequency detuning. It also needs to be mentioned that frequency detuning does not affect the power transfer efficiency much, but limits the total power handling capacity as safe SAR levels have to be met.

In this chapter, we circumvent the main issues in using CPT links by choosing higher frequency of operation, high enough to reduce the capacitive impedance and transfer power elegantly. Higher frequency of operation also reduces the inductor sizes required to form the resonant tank. The added advantage of the capacitive coupled link is that the compensation and tuning circuitry needed for proper operation can be retained at the transmitting side unlike the inductively coupled links and hence reduces the complexity of implanted electronics. The electric fields in capacitive link are well bounded by the capacitor plates unlike the magnetic fields in an inductive power link and hence have a better EMI performance and the effects of surrounding metallic elements are minimal [134] as the electric fields are mostly confined to the plates of the capacitor.

4.2 CPT links for biomedical implant application

The physical topology for the CPT link, where the implant RX is a small conducting plate is placed close to the skin as shown in Figure 4-1. It is assumed here that only one layer of tissue separates the Transmitting plate (TX) and Receiving plate (RX) (as in the case of neural implant). The analysis for case of stacked tissues (Skin, fat, muscle etc.) is not required as the CPT links can work only for smaller separations thereby eliminating its use in deep implant applications.

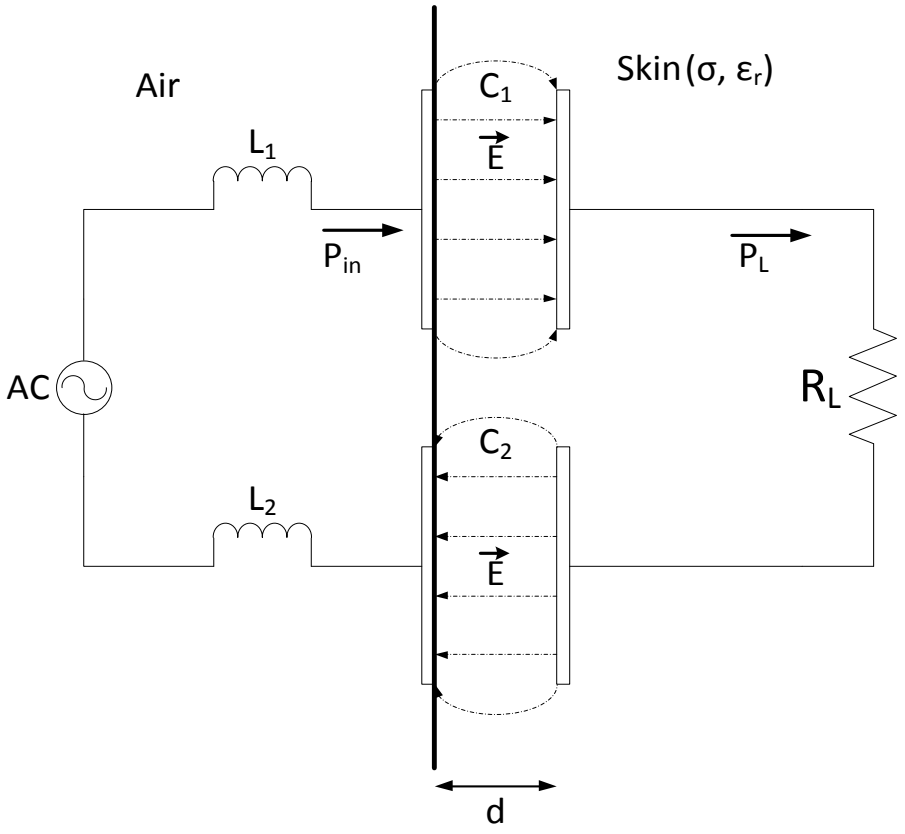

Figure 4-1Physical representation of a capacitive coupled power link

To analyse the capacitive coupled link shown in Figure 4-1, we make the following assumptions. The losses due to the thin lamination (for water-proofing and bio-compatibility) and losses in substrate of the plates can be ignored as they are less when compared to the tissue losses. The equivalent model of the link is built as shown in Figure 4-2. The main difference between

the normal capacitive coupled links and the ones used in implant application at high frequency is that the loss in the tissue is dominated by the dielectric relaxation mechanism while it is the conduction loss that dominates the low frequencies.

Both the conduction loss and relaxation loss need to be considered for the power link. The conduction loss which is the dominant loss at lower frequencies is generally modelled as a series resistor in other works [133-134]. In our work we will model the power link as lossless capacitors with loss resistances R_{T1} and R_{T2} as shown in the Figure 4-2 taking into account both the loss mechanisms. This is chosen to easily derive the model parameters using the input admittance of the capacitor with a lossy dielectric. The Power Transfer Efficiency (PTE) is the main quality metric that is required to evaluate the capacitive coupled link used for biomedical implant, as it determines the SAR level in tissues. Better PTE translates to lower losses in tissues and a lower SAR.

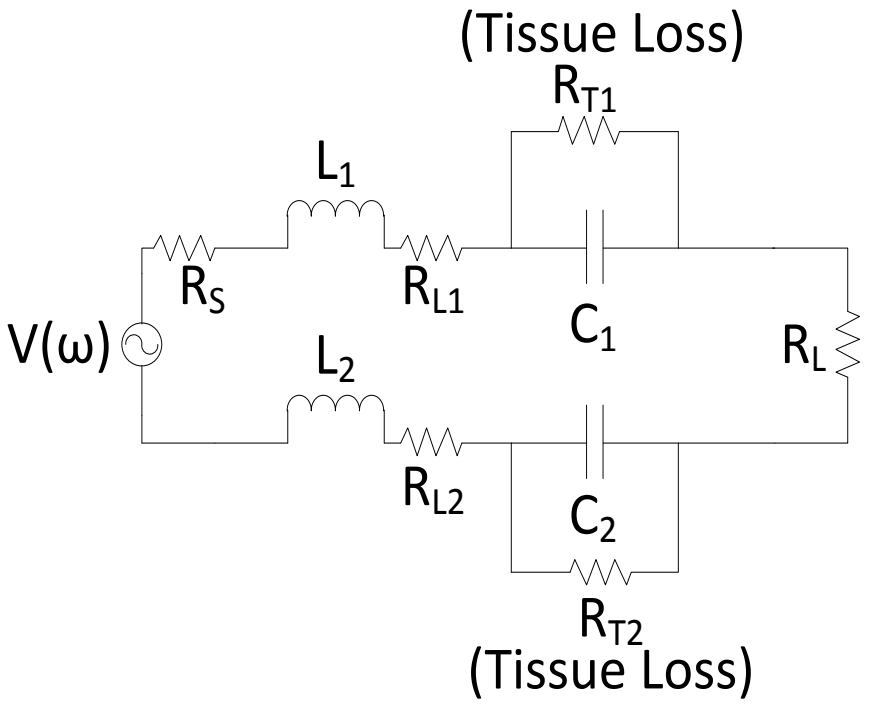

Figure 4-2 A simple loss model for of a capacitive coupled power link

The frequency dependency of permittivity of the tissue can be best demonstrated using the Debye-relaxation model and many tissues have been characterized and correlated to this model in [135].

$$\varepsilon_r(\omega) = \varepsilon_\alpha + j\frac{\sigma}{\omega\varepsilon_0} + \frac{\varepsilon_{r0} - \varepsilon_\alpha}{1 + j\omega\tau}$$

(4.1)

Where ε_{r0} is the static relative permittivity, σ is the conductivity and τ is the relaxation time of the tissue and ε_α is the relative permittivity of the tissue at frequencies where $\omega\tau$ >1. This model has also been put to use in [106] for inductive links in biomedical implants. The power transfer efficiency of the link is derived directly in terms of the capacitor plate dimensions, separation between the plates and tissue properties and is shown in (4.24.2).

$$\eta = \left\{1 + \frac{R_S}{R_L} + \frac{d}{R_L}\left(\frac{(\sigma + \varepsilon_0(\varepsilon_{r0} - \varepsilon_\alpha)\,\omega^2\tau)}{(\varepsilon_0^2\varepsilon_{r0}^2\omega^2) + (\sigma + \varepsilon_0(\varepsilon_{r0} - \varepsilon_\alpha)\,\omega^2\tau)^2}\left(\frac{1}{A_1} + \frac{1}{A_2}\right) + \frac{1}{\varepsilon_0\varepsilon_{r0}\omega}\left(\frac{1}{A_2 Q_{L2}} + \frac{1}{A_2 Q_{L2}}\right)\right)\right\}^{-1}$$

(4.2)

It is to be noticed that the power transfer efficiency is directly given in terms of the physical link parameters and hence can be optimized for various parameters as needed by the application.

4.3 Experimental Set-up

Capacitive power links are ideal for transcutaneous power transfer, where the implant device is just beneath the skin. When the separation between the two power transfer plates is less than 0.5 cm, the capacitive power link operates seamlessly with a good power transfer capability.

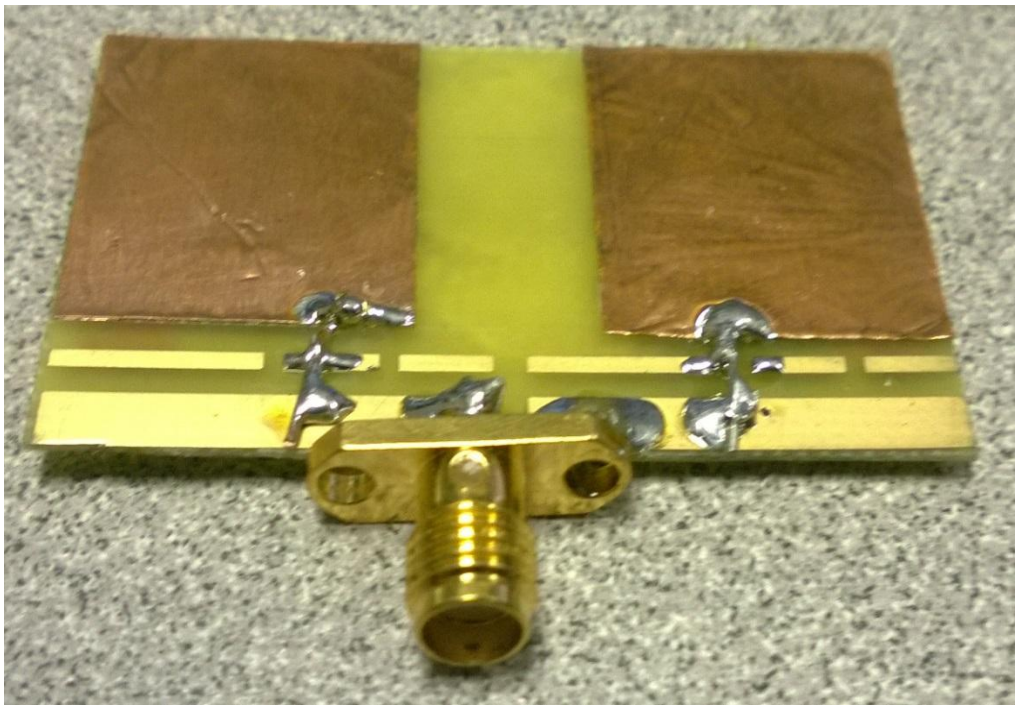

Figure 4-3 The TX/RX of a CPT system built on FR4 using copper patches.

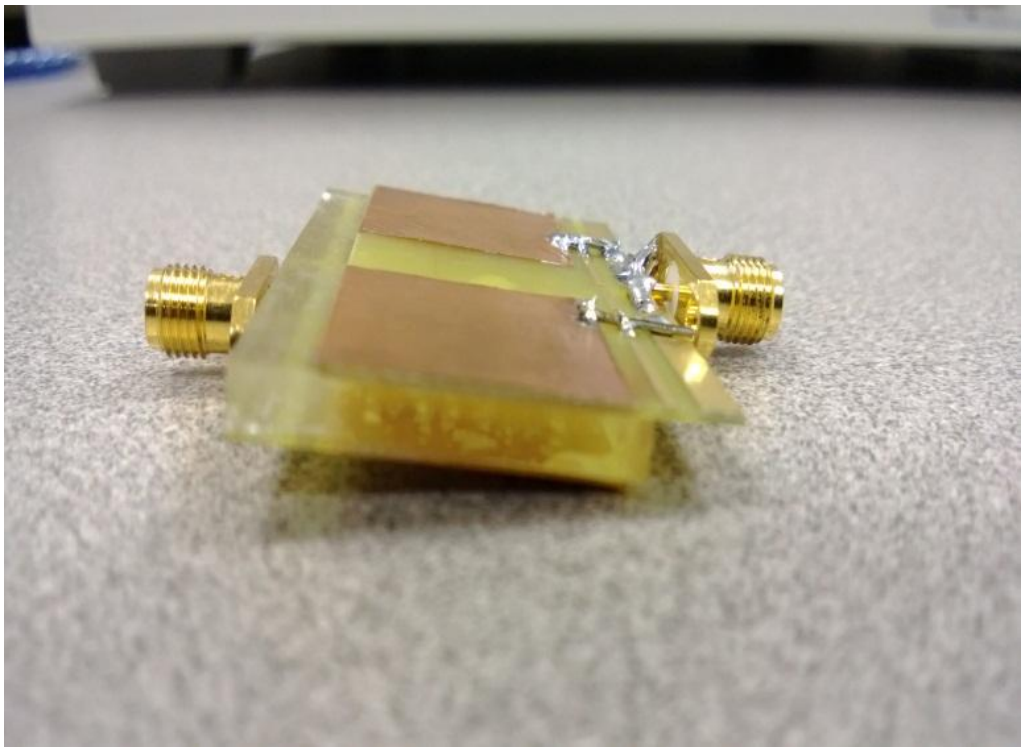

Figure 4-4 The Capacitive Power Transfer Link with the skin mimicking gel (colourless) sandwiched in between the two boards (TX and RX).

To demonstrate this, we set to build a set of two capacitive power transfer links(varying implant plate (RX) dimensions 100 mm^2, 380 mm^2) for beneath the skin applications and test them at three different separations (distance between TX and RX is 3mm, 4mm and 5mm). The power link was designed using 0.8 mm thick FR4 substrates as shown in Figure 4-3. The capacitances C1 and C2 shown in Figure 4-1 are formed using the copper patches shown in Figure 4-3. The TX and RX systems are separated by skin mimicking gel that approximates the skin at 402 MHz. The inductors L1 and L2 are combined into one inductor of 12nH, 47nH correspondingly for the two links. The load was chosen as 50 ohms for the 380mm^2 patches as it had a higher power transfer capacity and 1000 ohm for the 100mm^2 patches which have a lower power transfer capability. The CPT link was thus built to closely resemble the actual implant application as shown in Figure 4-4.

4.4 Preparation of Skin Mimicking Gel

The implantable board is placed beneath the skin in the actual application and power is transmitted to it by the external board from outside the skin. To mimic the exact application, we created skin like gel with equivalent dielectric properties (at the frequency of operation, 402 MHz) based on proven work [136] and was sandwiched in between the transmitting and receiving boards as shown in Figure 4-4.

The tissue mimicking gel was created by mixing distilled water with calculated amount of sugar and salt (Na^+, Cl^-). The common salt has free ions which can vary the conductivity of the solution and sugar is used to adjust the permittivity of the solution. The solution was made into a solid gel as shown in Figure 4-5 by heating the mixture with 1 gram of Agarose for 30 minutes and allowed to cool into a container which acts as a mould.

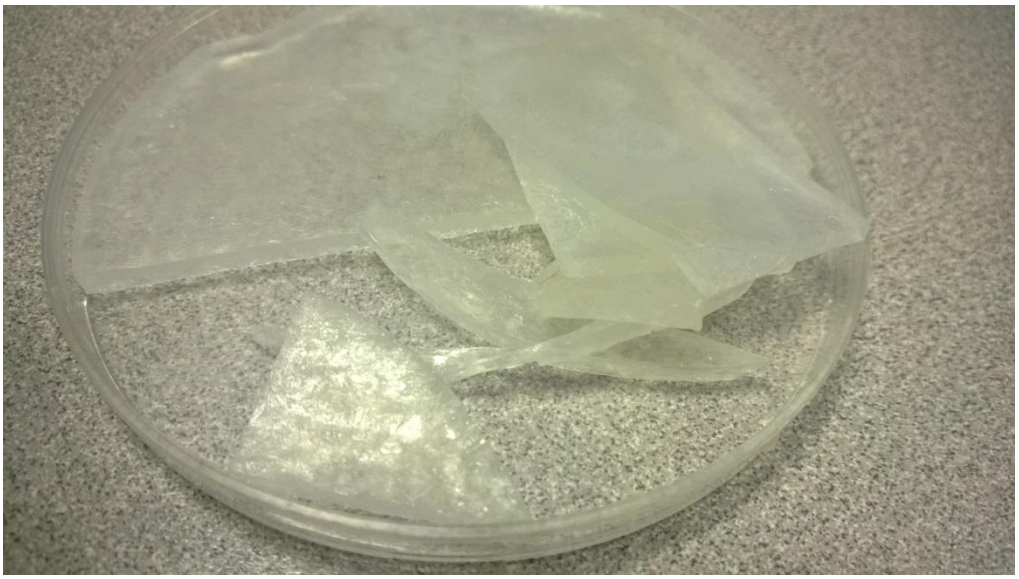

Figure 4-5 Preparation of skin mimicking gels using sugar, salt, distilled water and agarose

Three different thickness of skin mimicking gels were made (2mm, 3mm,4mm) using the above said process for 402 MHz operation. The gel was made from 2 gram of salt, 56 gram of sugar and 42 gram of distilled water and poured into various containers to obtain skin of different thickness (relative permittivity = 46.7, conductivity = 0.69 S/m).

4.5 Experimental results using tissue mimicking gel

We experimentally determine the power transfer efficiency of the CPT links which were built as discussed in earlier sections by powering it using a signal generator and measuring the output power at RX using an oscilloscope as shown in Figure 4-6. Since the input of the TX board was not matched to 50 ohm, the input reflection was measured to aid in computing the power transfer efficiency. The power transfer efficiency was calculated as the ratio of power delivered to the load (as measured from the oscilloscope) to the power fed to the transmit board. The experiment was repeated with different skin thickness for all the two CPT links. The power transfer efficiency was then computed theoretically using (4.2) with the assumption that the entire volume between the patches is homogenously filled with skin mimicking gel, rather than using

a stacked model of the patch substrate and gel. This is valid as the losses in the substrate are much lesser than the losses in the tissues. The comparisons between the results are shown in Table 4-1.

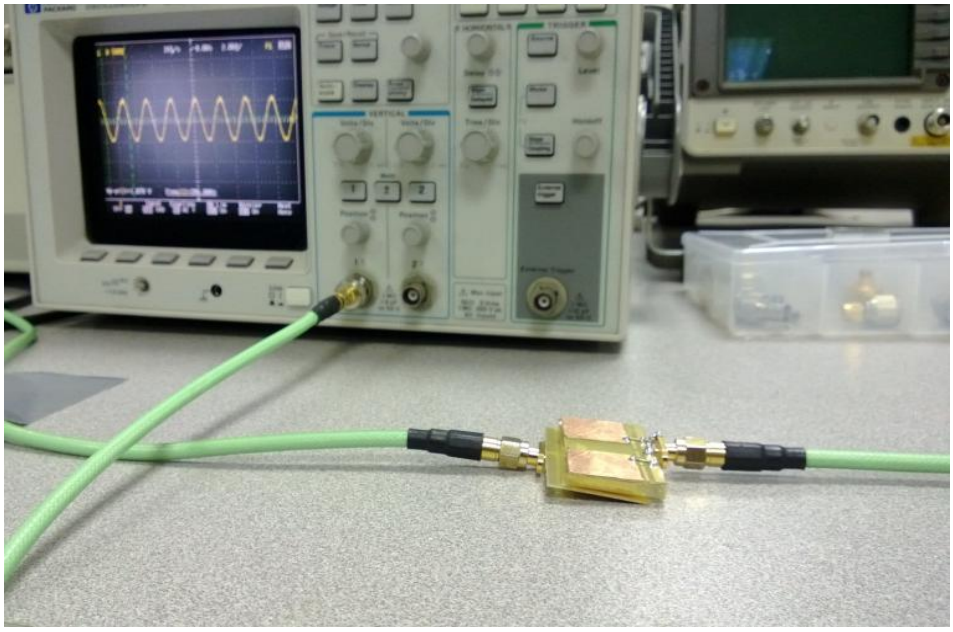

Figure 4-6 The measurement setup for evaluating the power transfer efficiency

Link I Performance			
	3 mm	***4 mm***	***5mm***
Separation between copper patches ‘d’	4.6mm	5.6mm	6.6mm
Area of implanted patches	380 mm^2	380 mm^2	380 mm^2
Load	50 ohm	50 ohm	50 ohm
Power transfer efficiency at 402 MHz (Measured)	68.3%	67.2%	67.0%
Power transfer efficiency at 402 MHz (Computed)	72.85%	72.78%	72.63%

Link II Performance	**Values**		
	3 mm	***4 mm***	***5mm***
Separation between copper patches ‘d’	4.6mm	5.6mm	6.6mm
Area of implanted patches	100 mm^2	100 mm^2	100 mm^2
Load	1000 ohm	1000 ohm	1000 ohm
Power transfer efficiency at 402 MHz (Measured)	91.4%	87.3%	76.2%
Power transfer efficiency at 402 MHz (Computed)	89.6%	82%	76.5%

Table 4-1 CPT link description with power transfer efficiency data

We can see from the table that the measured efficiency values are lower than the computed values. This is due to the fact that the substrate losses are ignored in our computation and the not-so perfect alignment of the copper patches reduces the capacitive coupling.

It is also to be noted that the power transfer efficiency does not vary much with the thickness of the skin. Thus placement of the implant board can be chosen as per the application need. However it is to be mentioned here that large separations reduces the effective capacitive coupling between the conducting patches and demands higher frequency of operation to maintain the power transfer capability and can increase the losses. The quality factors of the compensating inductors also reduce at higher frequencies thereby reducing the overall efficiency of the system. Hence it is preferred to use the capacitive power transfer link for applications with small separations at an optimal frequency of operation.

The power transfer efficiency for the experimental set up with smaller plate dimensions is higher than the values obtained for the larger CPT link, which sounds strange. This is due to the choice of load used in the experiment. The smaller link used a large load so that less power is drawn at the receiver (15 mW). If the load was reduced, then the capacitance was not sufficient to provide enough coupling at 402 MHz to supply that amount of power and consequently loading occurs reducing the PTE. Hence the power handling capability of the link has a definite say in the PTE. Smaller links operate efficiently only for smaller power transferred and larger links operate efficiently even when higher power is transmitted to the load. The frequency of operation chosen for this experiment was 402 MHz and the system was simulated in HFSS to make sure that the radiation at this frequency is minimal and most of the energy is in the near field of the capacitor plate. Thus it can be shown that power can be transferred in a transcutaneous fashion using electric near field coupling in an efficient manner. The implanted board need not have any matching network as all the compensations can be added to the transmitter side and hence facilitates the ease of implanting the device.

4.6 Experimental results in rats

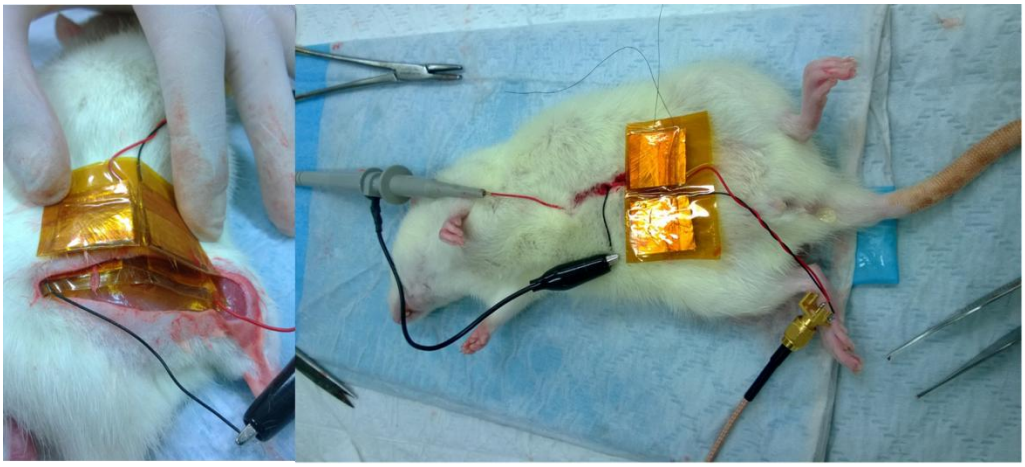

Figure 4-7Capacitive power transfer link tested in rat

The 19mm X 20mm capacitive patches were built using copper tapes and enclosed using polyamide. The patches were then inserted into the abdomen of the rat just beneath the skin and were powered externally using similar sized patches as shown in Figure 4-7 . The optimal frequency of operation for this small separation of 2mm between the patches is found to be 175 MHz. As expected, for deeper implant the optimal frequency of operation reduced. Power of up to 25mW was able to be received at the terminals of the implanted patches. The power transfer efficiency was measured to be above 40%.

4.7 Substrate losses in CPT links

Capacitive Power transfer links operate at few hundreds of MHz and hence substrate losses need to be considered. Though much smaller than the losses in tissues, they present degradation in efficiency if not properly accounted for. One significant way to reduce the losses is to reduce the thickness of the substrate which also is required for providing better flexibility of the patches. The choice of material is also vital as substrates with low loss tangents perform well when compared to the normal FR4 substrates.

4.8 Summary:

Capacitive coupling for transcutaneous power transmission to biomedical implants has been proposed with appropriate models to estimate the losses. Wireless power transfer systems using electric near field coupling was built and power was transferred to a receiving system which is placed beneath a skin mimicking gel to showcase the feasibility of safely powering implantable devices wirelessly with minimal electronics required on the implant side. The CPT scheme is also tested in rats to demonstrate its feasibility for powering implant devices. This method paves way for an attractive alternative to the traditional IPT links to power biomedical implants. The method however is restricted to the implant just being placed beneath the skin and does not work efficiently for deep seated implants.

Chapter 5: Conclusion and future work

5.1 Conclusion

Wireless power transfer links have been analysed thoroughly and methods to design, improve and optimize such links more specifically to adapt to the biomedical implant application have been presented in detail in this dissertation.

The series and parallel resonant topologies used in inductively coupled power transfer links for transcutaneous powering of biomedical implants have been studied comparatively. The suitability of the topology to a particular application has to be decided based on the frequency of operation and the type of load and the analytical way to do it has been presented in this thesis. The method to maximize the power transfer efficiency of IPT links based on the optimal choice of load and frequency of operation has been shown and verified in this work. The limitation of resonant tuning has been identified and explanations have been provided for the anomaly in parallel resonant topology both qualitatively and quantitatively. The possible use of series resonant method which can perform better at larger frequencies and smaller loads has been proposed. It is now possible from the extensive analysis presented in this thesis to (improve or) design efficient wireless power transfer links operating under optimal conditions ensuring minimal loss in power transfer, irrespective of the manufacturing technology.

The major problem of coil misalignment and motion artifacts in IPT links used for biomedical implants has been addressed in this dissertation based on the usage of passive intermediate coil which acts as a flux linkage booster. A complete theoretical model for WPT link with an IX coil has been presented with closed form expressions for PTE which have been verified experimentally. Numerical procedure to compute the mutual inductance of misaligned coils (both lateral and angular misalignment) has been developed

for a completely theoretical model of IX coil method based on the coil dimensions and positioning. The proper use of the intermediate coil, it's positioning and advantages namely PTE improvement over large separation, regulating the power fluctuation due to motion artifacts and overcoming misalignments have been explained with experimental results that correlate well with the results from theory.

Capacitive coupling for transcutaneous power transmission to biomedical implants has been proposed in this dissertation under the condition that the implant device is placed just beneath the skin (like in the case of neural implants). A theoretical model was developed for the loss mechanism in CPT links and was verified experimentally. The skin mimicking gel was made using sugar and salt solutions and was used as a dielectric phantom in CPT system. The designed CPT system was able to transfer power wirelessly across the tissue mimicking gel with no matching elements required at the implant side. The CPT system is also verified in rats where 20mW of power was transmitted into copper patches placed beneath the skin. The proposed CPT method presents itself as an attractive alternative to traditional IPT links with better EMI performance.

5.2 Future Work

Flexible electronics has been around for some time. Adapting IPT links into flexible electronics is no easy task as the coil parameters such as inductance and coupling vary with bending. However, using broadband matching techniques, the variations can be handled with an agreeable degree of PTE deterioration with the added benefits of a conformal system that help easy implantation. Hence it can be one possible area where further research can help transcutaneous powering of implantable devices.

The range of capacitive coupled links can be extended by the use of stacked plates and an initial analysis on such type of links showed lot of promise. The implanted plates used in the CPT links can also be easily used for data transfer

using modulation techniques. The most important aspect is that, since the CPT links operate at a few 100 MHz of frequency, large data rates can be achieved alongside transcutaneous powering in a single system. Hence there is definite scope for further work in this area that can bring forth excellent transcutaneous power and data links.

Bibliography

[1] N. Tesla, "Apparatus for transmitting electrical energy," *US patent number 1,119,732*" issued in December 1914.

[2] W.C. Brown, "Free-space transmission," *IEEE Spectrum,* vol.1, no.10, pp.86- 91, Oct. 1964.

[3] R. Dickinson, W. Brown, "Radiated Microwave Power Transmission System Efficiency Measurements", *TM 33-727, Jet Propulsion Lab*, Pasadena, California, May 15, 1975.

[4] R.M. Dickinson, "Performance of a High-Power, 2.388-GHz Receiving Array in Wireless Power Transmission over 1.54 km," *IEEE-Microwave Theory and Techniques Society International Microwave Symposium, 1976*, vol., no., pp.139-141, 14-16 June 1976.

[5] A. S. Marincic, "Nikola Tesla and the Wireless Transmission of Energy," *IEEE Transactions on Power Apparatus and Systems*, vol.PAS-101, no.10, pp.4064-4068, Oct. 1982.

[6] R. Andryczyk, P. Foldes, J. Chestek, B. M. Kaupang, "Power/energy: Solar Power Satellite ground stations: The ground systems for microwave beaming from the SPS would require a rectifying antenna with over 13 billion elements," *IEEE Spectrum*, vol.16, no.7, pp.51, 55, July 1979.

[7] R.V. Gelsthorpe, P. Q. Collins, "Increasing power input to a single solar power satellite rectenna by using a pair of satellites," *Electronics Letters* , vol.16, no.9, pp.311,313, April 24 1980

[8] J. I. Vuckovic, "Nikola Tesla: the man time forgot," *IEEE Potentials*, vol.9, no.3, pp.53-54, Oct. 1990.

[9] T. W. YOO, K. CHANG, "35 GHz integrated circuit rectifying antenna with 33% efficiency," *Electronics Letters*, vol.27, no.23, pp.2117,, 7 Nov. 1991.

[10] T. W. R. East, "A self-steering array for the SHARP microwave-powered aircraft," *IEEE Transactions on Antennas and Propagation*, vol.40, no.12, pp.1565, 1567, Dec 1992.

[11] T. W. Yoo, K. Chang, "Theoretical and experimental development of 10 and 35 GHz rectennas," *IEEE Transactions on Microwave Theory and Techniques*, vol.40, no.6, pp.1259, 1266, Jun 1992.

[12] J. O. McSpadden, T. W. Yoo, K. Chang, "Theoretical and experimental investigation of a rectenna element for microwave power transmission," *IEEE Transactions on Microwave Theory and Techniques*, vol.40, no.12, pp.2359, 2366, Dec 1992.

[13] A. Alden, T. Ohno, "Single foreplane high power rectenna," *Electronics Letters* , vol.28, no.11, pp.1072,1073, 21 May 1992.

[14] P. Koert, J. T. Cha, "Millimeter wave technology for space power beaming," *Microwave Theory and Techniques, IEEE Transactions on* , vol.40, no.6, pp.1251,1258, Jun 1992

[15] J. C. McCleary, T. W. Yoo, K. Chang, "Optimizing the rectifying antenna performance of wireless power transmission systems," *International Symposium of Antennas and Propagation Society Digest*, vol., no., pp.1050, 1053 vol.2, June 28 1993-July 2 1993.

[16] R. H. Nansen, "Wireless power transmission: the key to solar power satellites," *IEEE Aerospace and Electronic Systems Magazine*, vol.11, no.1, pp.33, 39, Jan 1996.

[17] A. P. Smakhtin and V. V. Rybakov "Comparative analysis of wireless systems as alternative to high-voltage power lines for global terrestrial power transmission," *Proceedings of the 31st Intersociety Energy Conversion Engineering Conference, IECEC 96.*, vol.1, no., pp.485,488 vol.1, 11-16 Aug 1996.

[18] R. M. Dickinson, "Power in the sky: Requirements for microwave wireless power beamers for powering high-altitude

platforms," *IEEE Microwave Magazine*, vol.14, no.2, pp.36, 47, March-April 2013.

[19] J. C. Lin, "Space solar-power stations, wireless power transmissions, and biological implications," *IEEE Microwave Magazine*, vol.3, no.1, pp.36, 42, Mar 2002.

[20] N. Shinohara, H. Matsumoto, "Experimental study of large rectenna array for microwave energy transmission," *IEEE Transactions on Microwave Theory and Techniques*, vol.46, no.3, pp.261, 268, Mar 1998.

[21] J. O, McSpadden, J. C. Mankins, "Space solar power programs and microwave wireless power transmission technology," *IEEE Microwave Magazine*, vol.3, no.4, pp.46, 57, Dec 2002.

[22] B. Strassner, K. Chang, "Microwave Power Transmission: Historical Milestones and System Components," *Proceedings of the IEEE* , vol.101, no.6, pp.1379,1396, June 2013.

[23] J. O. McSpadden, F. Lu, K. Chang, "Design and experiments of a high-conversion-efficiency 5.8-GHz rectenna," *IEEE Transactions on Microwave Theory and Techniques*, vol.46, no.12, pp.2053, 2060, Dec 1998.

[24] R. H. Rasshofer, M. O. Thieme, E. M. Biebl, "Circularly polarized millimeter-wave rectenna on silicon substrate," *IEEE Transactions on Microwave Theory and Techniques*, vol.46, no.5, pp.715, 718, May 1998.

[25] L. W. Epp, A. R. Khan, H. K. Smith, R. P. Smith, "A compact dual-polarized 8.51-GHz rectenna for high-voltage (50 V) actuator applications," *IEEE Transactions on Microwave Theory and Techniques*, vol.48, no.1, pp.111,120, Jan 2000.

[26] Y. H. Suh, C. Wang, K. Chang, "Circularly polarised truncated-corner square patch microstrip rectenna for wireless power transmission," *Electronics Letters* , vol.36, no.7, pp.600,602, 30 Mar 2000.

[27] Y. H. Suh, K. Chang, "A high-efficiency dual-frequency rectenna for 2.45- and 5.8-GHz wireless power transmission," *IEEE Transactions on Microwave Theory and Techniques*, vol.50, no.7, pp.1784, 1789, Jul 2002.

[28] J. Heikkinen, M. Kivikoski, "A novel dual-frequency circularly polarized rectenna," *IEEE Antennas and Wireless Propagation Letters*, vol.2, no.1, pp.330, 333, 2003.

[29] J. A. Hagerty, F. B. Helmbrecht, W. H. McCalpin, R. Zane, Z. B. Popovic, "Recycling ambient microwave energy with broad-band rectenna arrays," *IEEE Transactions on Microwave Theory and Techniques*, vol.52, no.3, pp.1014, 1024, March 2004.

[30] J. A. G. Akkermans, M. C. van Beurden, G. J. N. Doodeman, H. J. Visser, "Analytical models for low-power rectenna design," *IEEE Antennas and Wireless Propagation Letters*, vol.4, no., pp.187, 190, 2005.

[31] Y. J. Ren; K. Chang, "5.8-GHz circularly polarized dual-diode rectenna and rectenna array for microwave power transmission," *IEEE Transactions on Microwave Theory and Techniques*, vol.54, no.4, pp.1495, 1502, June 2006.

[32] H. K. Chiou, I. S. Chen, "High-Efficiency Dual-Band On-Chip Rectenna for 35- and 94-GHz Wireless Power Transmission in 0.13- CMOS Technology," *IEEE Transactions on Microwave Theory and Techniques*, , vol.58, no.12, pp.3598,3606, Dec. 2010.

[33] A. Georgiadis, G. Andia, A. Collado, "Rectenna design and optimization using reciprocity theory and harmonic balance analysis for electromagnetic (EM) energy harvesting," *Antennas and Wireless Propagation Letters, IEEE* , vol.9, no., pp.444,446, 2010.

[34] U. Olgun, C. C. Chen, J. L. Volakis, "Investigation of Rectenna Array Configurations for Enhanced RF Power Harvesting," *IEEE Antennas and Wireless Propagation Letters*, vol.10, no., pp.262,265, 2011.

[35] H. Sun, Y. X. Guo, M. He, Z. Zhong, "Design of a High-Efficiency 2.45-GHz Rectenna for Low-Input-Power Energy Harvesting," *IEEE Antennas and Wireless Propagation Letters*, vol.11, no., pp.929,932, 2012.

[36] A. Collado, A. Georgiadis, "Conformal Hybrid Solar and Electromagnetic (EM) Energy Harvesting Rectenna," *IEEE Transactions on Circuits and Systems I: Regular Papers*, vol.60, no.8, pp.2225, 2234, Aug. 2013.

[37] F. J. Huang, C. M. Lee, C. L. Chang, L. K. Chen, T. C. Yo, C. H. Luo, "Rectenna Application of Miniaturized Implantable Antenna Design for Triple-Band Biotelemetry Communication," *IEEE Transactions on Antennas and Propagation*, vol.59, no.7, pp.2646, 2653, July 2011.

[38] IEEE Standard for Safety Levels With Respect to Human Exposure to Radio Frequency Electromagnetic Fields, 3 KHz to 300 GHz, IEEE Standard C95.1-1999, 1999.

[39] J. C. Schuder, H. E. Stephenson, Jr., "Energy transport to a coil which circumscribes a ferrite core and is implanted within the body," *IEEE Transactions on Biomedical Engineering*, vol. BME-12, pp. 154-163, July-October 1965.

[40] J. W. Fuller, "Apparatus for efficient power transfer through a tissue barrier," *IEEE Transactions on Biomedical Engineering*, vol. BME- 1, pp.63-65, 1968.

[41] C. F. Andren, M. A. Fadali, V. L. Gott, S. R. Topaz, "The skin tunnel transformer: A new system that permits both high efficiency transfer of power and telemetry of data through the intact skin," *IEEE Transactions on Biomedical Engineering*, vol. BME-15, no. 4, pp. 278-285,1968.

[42] R. Kadefors, E. Kaiser, I. Petersen, "Energizing implantable transmitters by means of coupled inductance coils," *IEEE Transactions on Biomedical Engineering*, vol. BME-16, no. 3, pp. 177-183, 1969.

[43] J. C. Schuder, H. Gold, H. E. Stephenson, "An Inductively Coupled RF System for the Transmission of 1 kW of Power Through the Skin," *IEEE Transactions on Biomedical Engineering*, vol.BME-18, no.4, pp.265, 273, July 1971.

[44] F. C. Flack, E. D. James, and D. M. Schlapp, "Mutual inductance of air-cored coils: effect on design of rf-coupled implants," *Medical and Biological Engineering.*, vol. 9, pp. 79-85, 1971.

[45] R. Kadefors, "Controlled external powering of miniaturized chronically implanted biotelemetry devices, "*IEEE Transactions on Biomedical Engineering*, vol. BME-23, no. 2, pp. 124-129, 1976.

[46] W. H. Ko, S. P. Liang, C.D.F. Fung, "Design of rf-powered coils for implant instruments," *Medical & Biological Engineering and Computing*, vol. 15, pp. 634-640, 1977.

[47] W. H. Ko, J. Hynecek, J. Homa, "Single frequency rf powered ECG telemetry system," *IEEE Transactions on Biomedical Engineering*, vol. BME-26, no. 2, pp. 105-109, 1979.

[48] D. C. Jeutter, "A transcutaneous implanted battery recharging and bio-telemeter power switching system," *IEEE Transactions on Biomedical Engineering*, vol. BME-29, no.5, pp. 314-321, 1982.

[49] N. de N. Donaldson, T. A. Perkins, "Analysis of resonant coupled coils in the design of radio-frequency transcutaneous links," *Medical & Biological Engineering and Computing*, vol. 21, pp. 612-627, 1983.

[50] D. C. Galbraith, M. Soma, R. L. White, "A wide-band efficient inductive transdermal power and data link with coupling insensitive gain," *IEEE Transactions on Biomedical Engineering*, vol. BME-34, pp. 265-275, Apr. 1987.

[51] C. M. Zierhofer, E. S. Hochmair, "High-efficiency coupling-insensitive transcutaneous power and data transmission via an inductive link," *IEEE Transactions on Biomedical Engineering*, vol.37, no.7, pp.716-722, July 1990.

[52] F. W. Fraim, F. N. Huffman, "Performance of a Tuned Ferrite Core Transcutaneous Transformer," *IEEE Transactions on Biomedical Engineering*, vol.BME-18, no.5, pp.352, 359, Sept. 1971.

[53] Y. Kouya (Yaskawa Electric Company), "Contactless power supply," Japanese Patent. 1184108, 1983.

[54] A. Esser, H. C. Skudelny, "A new approach to power supply for robots," *IEEE Transactions on Industrial Applications*, vol. 27, pp. 872–875, Sept./Oct.1991.

[55] J. Hirai, T.W. Kim, A. Kawamura, "Practical study on wireless transmission of power and information for autonomous decentralized manufacturing system," *IEEE Transactions on Industrial Electronics*, vol.46, no.2, pp.349-359, Apr 1999.

[56] M. Eghtesadi, "Inductive power transfer to an electric vehicle-analytical model," *IEEE 40th Vehicular Technology Conference, 1990*, vol., no., pp.100-104, 6-9 May 1990.

[57] Y. Hiraga, J. Hirai, Y. Kaku, Y. Nitta, A. Kawamura, K. Ishioka, "Decentralized control of machines with the use of inductive transmission of power and signal," *Record of the 1994 IEEE Conference on Industry Applications, Society Annual Meeting, 1994.*, , vol., no., pp.875,881 vol.2, 2-6 Oct 1994.

[58] W. J. Weiss, G. Rosenberg, A. J. Snyder, T. J. Cleary, R. P. Gaumond, D. B. Geselowitz, W. S. Pierce, "Permanent circulatory support systems at the Pennsylvania State University," *IEEE Transactions on Biomedical Engineering*, vol.37, no.2, pp.138, 145, Feb. 1990.

[59] Y. Mitamura, E. Okamoto, A. Hirano, T. Mikami, "Development of an implantable motor-driven assist pump system," *IEEE Transactions on Biomedical Engineering*, vol.37, no.2, pp.146, 156, Feb. 1990.

[60] A. Ghahary, B. H. Cho, "Design of transcutaneous energy transmission system using a series resonant converter," *IEEE*

Transactions on Power Electronics, vol.7, no.2, pp.261, 269, Apr 1992.

[61] H. Matsuki, M. Shiiki, K. Murakami, T. Yamamoto, "Investigation of coil geometry for transcutaneous energy transmission for artificial heart," *IEEE Transactions on Magnetics*, vol.28, no.5, pp.2406, 2408, Sep 1992.

[62] D. B. Geselowtiz, Q. T. N. Hoang, R. P. Gaumond, "The effects of metals on a transcutaneous energy transmission system," *IEEE Transactions on Biomedical Engineering*, vol.39, no.9, pp.928, 934, Sept. 1992.

[63] H. Matsuki, "Energy transfer system utilizing amorphous wires for implantable medical devices," *IEEE Transactions on Magnetics*, vol.31, no.2, pp.1276, 1282, March 1995.

[64] H. Matsuki, K. Ofuji, N. Chubachi, S. Nitta, "Signal transmission for implantable medical devices using figure-of-eight coils," *IEEE Transactions on Magnetics*, vol.32, no.5, pp.5121, 5123, Sep 1996.

[65] G. B. Joun; B. H. Cho, "An energy transmission system for an artificial heart using leakage inductance compensation of transcutaneous transformer," *IEEE Transactions on Power Electronics*, vol.13, no.6, pp.1013, 1022, Nov 1998.

[66] F. C. Fok; T. K. Jet, Z. L. Yin, "New structure transcutaneous transformer for totally implantable artificial heart system," *Electronics Letters* , vol.35, no.2, pp.107,108, 21 Jan 1999

[67] A. Shinsuke; M. Hidekazu; S. Fumihiro; H. Matsuki, S. Tadakuni, "Examination of circuit parameters for stable high efficiency TETS for artificial hearts," *IEEE Transactions on Magnetics*, vol.41, no.10, pp.4170, 4172, Oct. 2005.

[68] H. Miura, A. Shinsuke, Y. Kakubari, S. Fumihiro, H. Matsuki, S. Tadakuni, "Improvement of the Transcutaneous Energy Transmission System Utilizing Ferrite Cored Coils for Artificial Hearts," *IEEE Transactions on Magnetics*, vol.42, no.10, pp.3578,3580, Oct. 2006.

[69] K. Shiba, M. Nukaya, T. Tsuji, K. Kohji, "Analysis of Current Density and Specific Absorption Rate in Biological Tissue Surrounding Transcutaneous Transformer for an Artificial Heart," *IEEE Transactions on Biomedical Engineering*, vol.55, no.1, pp.205,213, Jan. 2008.

[70] J. Ma, Q. Yang, H. Chen, "Transcutaneous Energy and Information Transmission System With Optimized Transformer Parameters for the Artificial Heart," *IEEE Transactions on Applied Superconductivity*, , vol.20, no.3, pp.798,801, June 2010

[71] B. H. Waters, A. P. Sample, P. Bonde, J. R. Smith, J.R., "Powering a Ventricular Assist Device (VAD) With the Free-Range Resonant Electrical Energy Delivery (FREE-D) System," *Proceedings of the IEEE* , vol.100, no.1, pp.138,149, Jan. 2012.

[72] E. S. Hochmair, I. J. Hochmair-Desoyer, "An implanted auditory eight-channel stimulator for the deaf," *Medical & Biological Engineering and Computing*, vol. 19, pp. 141-148, Mar. 1981.

[73] E. S. Hochmair, "System optimization for improved accuracy in transcutaneous signal and power transmission," *IEEE Transactions on Biomedical Engineering*, vol. BME-31, pp. 177-186, Feb. 1984.

[74] H. McDermott, "An advanced multiple channel cochlear implant," *IEEE Transactions on Biomedical Engineering*, vol.36, no.7, pp.789, 797, July 1989.

[75] C. M. Zierhofer, I. J. Hochmair-Desoyer, E. S. Hochmair, "Electronic design of a cochlear implant for multichannel high-rate pulsatile stimulation strategies," *IEEE Transactions on Rehabilitation Engineering*, vol.3, no.1, pp.112,116, Mar 1995.

[76] K. D. Wise, K. Najafi, "Fully-implantable auditory prostheses: restoring hearing to the profoundly deaf," *International Electron Devices Meeting, 2002. IEDM '02*, vol., no., pp.499, 502, 8-11 Dec. 2002.

[77] S. Guo, H. Lee, "An Efficiency-Enhanced CMOS Rectifier With Unbalanced-Biased Comparators for Transcutaneous-Powered High-Current Implants," *IEEE Journal of Solid-State Circuits*, , vol.44, no.6, pp.1796,1804, June 2009.

[78] E. Goll, H. P. Zenner, E. Dalhoff, "Upper Bounds for Energy Harvesting in the Region of the Human Head," *IEEE Transactions on Biomedical Engineering*, vol.58, no.11, pp.3097, 3103, Nov. 2011.

[79] S. K. Arfin, R. Sarpeshkar, "An Energy-Efficient, Adiabatic Electrode Stimulator with Inductive Energy Recycling and Feedback Current Regulation," *IEEE Transactions on Biomedical Circuits and Systems*, vol.6, no.1, pp.1, 14, Feb. 2012.

[80] H. Taghavi, B. Hkansson, S. Reinfeldt, "Analysis and Design of RF Power and Data Link Using Amplitude Modulation of Class-E for a Novel Bone Conduction Implant," *IEEE Transactions on Biomedical Engineering*, vol.59, no.11, pp.3050,3059, Nov. 2012.

[81] P. R. Troyk, R. J. Jaeger, M. Haklin, J. Poyezdala, B. Thomas, "Design and Implementation of an Implantable Goniometer," *IEEE Transactions on Biomedical Engineering*, vol.BME-33, no.2, pp.215, 222, Feb. 1986.

[82] W. J. Heetderks, "RF powering of millimeter- and submillimeter-sized neural prosthetic implants," *IEEE Transactions on Biomedical Engineering*, , vol.35, no.5, pp.323,327, May 1988.

[83] M. Mojarradi, D. Binkley, B. Blalock, R. Andersen, N. Ulshoefer, T. Johnson, L. Del Castillo, "A miniaturized neuro-prosthesis suitable for implantation into the brain," *IEEE Transactions on Neural Systems and Rehabilitation Engineering*, vol.11, no.1, pp.38,42, March 2003.

[84] M. Ghovanloo, K. Najafi, "A wideband frequency-shift keying wireless link for inductively powered biomedical implants," *IEEE Transactions on Circuits and Systems I: Regular Papers*, , vol.51, no.12, pp.2374, 2383, Dec. 2004.

[85] C. Sauer, M. Stanacevic, G. Cauwenberghs, N. Thakor, "Power harvesting and telemetry in CMOS for implanted devices," *IEEE Transactions on Circuits and Systems I: Regular Papers*, vol.52, no.12, pp.2605, 2613, Dec. 2005.

[86] P. P. Irazoqui, I. Mody, J. W. Judy, "Recording brain activity wirelessly," *IEEE Engineering in Medicine and Biology Magazine*, vol.24, no.6, pp.48,54, Nov.-Dec. 2005

[87] S. Mingui, G. A. Justin, P. A. Roche, J. Zhao, B. L. Wessel, Y. Zhang, R. J. Sclabassi, "Passing data and supplying power to neural implants," *IEEE Engineering in Medicine and Biology Magazine,* , vol.25, no.5, pp.39,46, Sept.-Oct. 2006

[88] M. Ghovanloo, K. Najafi, "A Wireless Implantable Multichannel Microstimulating System-on-a-Chip With Modular Architecture," *IEEE Transactions on Neural Systems and Rehabilitation Engineering,* , vol.15, no.3, pp.449,457, Sept. 2007

[89] R. Sarpeshkar, W. Wattanapanitch, S. K. Arfin, B. I. Rapoport, S. Mandal, M. W. BakerM. S. Fee, S. Musallam, R. A. Andersen, "Low-Power Circuits for Brain–Machine Interfaces," *IEEE Transactions on Biomedical Circuits and Systems*, vol.2, no.3, pp.173,183, Sept. 2008.

[90] A. M. Sodagar, G. E. Perlin, Y. Yao, K. Najafi, K. D. Wise, "An Implantable 64-Channel Wireless Microsystem for Single-Unit Neural Recording," *IEEE Journal of Solid-State Circuits*, vol.44, no.9, pp.2591,2604, Sept. 2009.

[91] Kim, S.; Harrison, R.R.; Solzbacher, F., "Influence of System Integration and Packaging on Its Inductive Power Link for an Integrated Wireless Neural Interface," *IEEE Transactions on Biomedical Engineering*, vol.56, no.12, pp.2927,2936, Dec. 2009.

[92] C. C. Peng, Z. Xiao, R. Bashirullah, "Toward Energy Efficient Neural Interfaces," *IEEE Transactions on Biomedical Engineering* , vol.56, no.11, pp.2697,2700, Nov. 2009.

[93] A. Sharma, L. Rieth, P. Tathireddy, R. Harrison, F. Solzbacher, "Long term in vitro stability of fully integrated wireless neural interfaces based on Utah slant electrode array," *Applied Physics Letters*, vol.96, no.7, pp.073702, 073702-3, Feb 2010.

[94] T. Bjorninen, R. Muller, P. Ledochowitsch, L. Sydanheimo, L. Ukkonen, M.M. Maharbiz, J.M. Rabaey, "Design of Wireless Links to Implanted Brain–Machine Interface Microelectronic Systems," *IEEE Antennas and Wireless Propagation Letters*, vol.11, no., pp.1663,1666, 2012.

[95] H. N. Schwerdt, F. A. Miranda, J. Chae, "A Fully Passive Wireless Backscattering Neurorecording Microsystem Embedded in Dispersive Human-Head Phantom Medium," *IEEE Electron Device Letters*, vol.33, no.6, pp.908,910, June 2012.

[96] M. Chae, Z. Yang, M. Yuce, L. Hoang, W. Liu, "A 128-Channel 6 mW wireless neural recording IC with spike feature extraction and UWB transmitter," *IEEE Trans. Neural Syst. Rehabil. Eng*., vol. 17, no. 4, pp. 312–321, Aug. 2009.

[97] M. Clements et al., "An implantable neuro-stimulator device for a retinal prosthesis," *IEEE International Solid-State Circuits Conference, 1999*, vol., no., pp.216-217, 1999.

[98] W. Li, D. Rodger, J. Weiland, M. Humayun, and Y. Tai, "Integrated flexible ocular coil for power and data transfer in retinal prostheses," in *Proc. 27th Annual International Conference IEEE Engineering Medicine Biology Society*, Shanghai, China, 2005, pp. 1028–1031.

[99] C. Koch, W. Mokwa, M. Goertz, P. Walter, "First Results of a Study on a completely implanted retinal prosthesis in blind humans," *IEEE Sensors 2008*, Oct 2008, pp. 1237 - 1240.

[100] D.C. Ng, G. Felic, E. Skafidas, Shun Bai, "Closed-loop inductive link for wireless powering of a high density electrode array retinal

prosthesis," *Electromagnetic Compatibility Symposium Adelaide*, 2009. , vol., no., pp.92-97, Sep. 2 2009-Sept. 6 2009.

[101] D. C. Ng et al., "Wireless power delivery for retinal prostheses," *Annual International Conference of the IEEE Engineering in Medicine and Biology Society*, EMBC, 2011 , vol., no., pp.8356-8360, Aug. 30 2011-Sept. 3 2011.

[102] G. A. J. Elliott, J. T. Boys, A. W. Green, "Magnetically coupled systems for power transfer to electric vehicles," *Proceedings International Conference on Power Electronics and Drive Systems*, Singapore, 1995, pp. 797-801.

[103] J. T. Boys, G. A. Covic, A. W. Green, "Stability and control of inductively coupled power transfer systems," *IEE Proceedings Electric Power Applications*, vol. 147, no. 1, pp. 37-43, 2000.

[104] J. T. Boys and A. W. Green, "Intelligent road-studs – lighting the paths of the future," *IPENZ Transactions*, vol. 24, 1997.

[105] A.S.Y Poon, S. O'Driscoll, T.H. Meng, "Optimal Operating Frequency in Wireless Power Transmission for Implantable Devices," *29th Annual International Conference of the IEEE Engineering in Medicine and Biology Society* 2007, pp.5673-5678, 22-26 Aug. 2007.

[106] A.S.Y Poon, S. O'Driscoll, T.H. Meng, "Optimal Frequency for Wireless Power Transmission Into Dispersive Tissue," *IEEE Transactions on Antennas and Propagation*, vol.58, no.5, pp.1739-1750, May 2010.

[107] X. Liu, W.M. Ng, C.K. Lee, S.Y. (Ron) Hui, "Optimal operation of contactless transformers with resonance in secondary circuits", *Twenty-Third Annual IEEE Applied Power Electronics Conference and Exposition* 2008 (APEC 2008), 24-28 Feb. 2008, pp. 645 – 650.

[108] C.-S. Wang, G.A. Covic, "Power transfer capability and bifurcation phenomena of loosely coupled inductive power transfer systems", *IEEE Transactions on Industrial Electronics*, vol. 51, no. 1, Feb. 2004, pp. 148 – 157.

[109] K.M. Silay, C. Dehollain, M.Declercq, "Improvement of power efficiency of inductive links for implantable devices," *Research in Microelectronics and Electronics*, 2008. PRIME 2008. pp.229-232, June 22-25 2008.

[110] U.M. Jow and M. Ghovanloo, "Design and Optimization of Printed Spiral Coils for Efficient Transcutaneous Inductive Power Transmission," *IEEE Transactions on Biomedical Circuits and Systems*, vol.1, no.3, pp.193-202, Sept. 2007.

[111] U.M. Jow and M. Ghovanloo, "Modeling and Optimization of Printed Spiral Coils in Air, Saline, and Muscle Tissue Environments," *IEEE Transactions on Biomedical Circuits and Systems*, vol.3, no.5, pp.339-347, Oct. 2009.

[112] W.Z. Fu, B. Zhang, D.Y. Qiu. "Study on frequency-tracking wireless power transfer system by resonant coupling," *IEEE 6th International Power Electronics and Motion Control Conference* 2009 (IPEMC '09), pp.2658-2663, 17-20 May 2009.

[113] B.L. Cannon, J.F. Hoburg, D.D. Stancil, S.C.Goldstein, "Magnetic Resonant Coupling As a Potential Means for Wireless Power Transfer to Multiple Small Receivers," *IEEE Transactions on Power Electronics*, vol.24, no.7, pp.1819-1825, July 2009.

[114] R. Jegadeesan, Y.X. Guo, "A Study on the Inductive Power Links for Implantable Biomedical Devices," *IEEE International symposium on Antennas and Propagation 2010*, Toronto, July 2010.

[115] S.S. Mohan, M. del Mar Hershenson, S.P. Boyd and T.H. Lee, "Simple accurate expressions for planar spiral inductances," *IEEE Journal of Solid-State Circuits*, vol.34, no.10, pp.1419-1424, Oct 1999.

[116] M. Zolog, D. Pitica, O. Pop, "Characterization of Spiral Planar Inductors Built on Printed Circuit Boards," *30th International Spring Seminar on Electronics Technology*, pp.308-313, 9-13 May 2007.

[117] B.L. Ooi, D. X. Xu, P. S. Kooi, F. J. Lin, "An improved prediction of series resistance in spiral inductor modelling with eddy-current effect,"

IEEE Transactions on Microwave Theory and Techniques, vol.50, no.9, pp. 2202- 2206, Sep 2002.

[118] Paul, C., "Loop and Partial," Inductance , p.220.

[119] R. Jegadeesan, Y. X. Guo, "Evaluation and Optimization of High Frequency Wireless Power links", *IEEE International Symposium on Antennas and Propagation (APS)*, Spokane, WA, July 2011.

[120] K. Oguri, "Power supply coupler for battery charger", US patent 6356049, 2000.

[121] A. Karalis, J. Joannopoulos, M. Soljacic, "Efficient wireless non-radiative mid-range energy transfer," *Annals of Physics*, vol. 323, pp. 34–48, Apr. 2007.

[122] A.K. RamRakhyani, S. Mirabbasi, C. Mu, "Design and Optimization of Resonance-Based Efficient Wireless Power Delivery Systems for Biomedical Implants," *IEEE Transactions on Biomedical Circuits and Systems*, vol.5, no.1, pp.48-63, Feb. 2011.

[123] A. K. RamRakhyani, G. Lazzi, "On the Design of Efficient Multi-Coil Telemetry System for Biomedical Implants," *IEEE Transactions on Biomedical Circuits and Systems,* vol.7, no.1, pp.11,23, Feb. 2013.

[124] M. Kiani, U. M. Jow, M. Ghovanloo, "Design and Optimization of a 3-Coil Inductive Link for Efficient Wireless Power Transmission," *IEEE Transactions on Biomedical Circuits and Systems,* vol.5, no.6, pp.579-591, Dec. 2011.

[125] G.Wang, W. Liu, M. Sivaprakasam, M. Zhou, J. D.Weiland, M. S. Humayun, "A dual band wireless power and data telemetry for retinal prosthesis," *Proceedings of IEEE conference on Engineering in Medicine Biology Society*, Aug. 30–Sep. 3, 2006, pp. 28–38.

[126] P. Vaillancourt, A. Djemouai, J.F. Harvey, M. Sawan, "EM radiation behavior upon biological tissues in a radio-frequency power transfer link for a cortical visual implant," *Proceedings of the 19th Annual International IEEE Conference on Engineering in Medicine and*

Biology Society, 1997., vol.6, no., pp.2499-2502 vol.6, 30 Oct-2 Nov 1997.

[127] R. Jegadeesan, Y.X. Guo, "Topology Selection and Efficiency Improvement of Inductive Power Links," *IEEE Transactions on Antennas and Propagation*, vol.60, no.10, pp.4846-4854, Oct. 2012.

[128] R. Jegadeesan, Y. X. Guo, M. Je, "Overcoming coil misalignment using magnetic fields of induced currents in wireless power transmission," *IEEE MTT-S International Microwave Symposium Digest* (IMS2012),17-22 June 2012.

[129] K. Fotopoulou, B.W. Flynn, "Wireless Power Transfer in Loosely Coupled Links: Coil Misalignment Model," IEEE Transactions on Magnetics, vol.47, no.2, pp.416-430, Feb. 2011.

[130] J. Kim, H.C. Son, K.H. Kim, Y.J. Park, "Efficiency Analysis of Magnetic Resonance Wireless Power Transfer with Intermediate Resonant Coil," IEEE Antennas and Wireless Propagation Letters, vol.10, pp.389-392, 2011.

[131] H.A. Wheeler, "Formulas for the Skin Effect," Proceedings of the IRE , vol.30, no.9, pp. 412- 424, Sept. 1942.

[132] C. Ionescu, P. Svasta, D. Bonfert, G. Klink, "Analysis of planar inductors on flexible substrates for RFID antennas," 33rd International Spring Seminar on Electronics Technology (ISSE) 2010, pp.338-343, 12-16 May 2010.

[133] M.P. Theodoridis, "Effective Capacitive Power Transfer," IEEE Transactions on Power Electronics, , vol.27, no.12, pp.4906-4913, Dec. 2012.

[134] M. Kline, I. Izyumin, B. Boser, S. Sanders, "Capacitive power transfer for contactless charging," Twenty-Sixth Annual IEEE Applied Power Electronics Conference and Exposition (APEC), 2011, vol., no., pp.1398-1404, 6-11 March 2011.

[135] S. Gabriel, R. W. Lau, C. Gabriel, "The dielectric properties of biological tissues: III. Parametric models for the dielectric spectrum of

tissues" *Physics in Medicine and Biology*, vol. 41, no. 11, pp. 2271-2293, Nov 1996.